Doctoral Dissertations (All Dissertations, All Years)   Electronic Theses and Dissertations

2018-7

Modeling & Analysis of Design Parameters for Portable Hand Orthoses to Assist Upper Motor Neuron Syndrome Impairments and Prototype Design

Christopher Julius Nycz
Worcester Polytechnic Institute

Follow this and additional works at: https://digitalcommons.wpi.edu/etd-dissertations

Modeling & Analysis of Design Parameters for Portable Hand Orthoses to Assist Upper Motor Neuron Syndrome Impairments and Prototype Development

by

Christopher J Nycz

A dissertation submitted to The Worcester Polytechnic Institute in conformity with the requirements for the degree of Doctor of Philosophy.

Worcester, Massachusetts
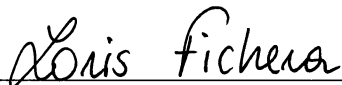
August, 2018
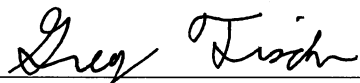
Approved by:

Greg Fischer
Dr. Gregory S. Fischer, Advisor
Worcester Polytechnic Institute

Karen Troy
Dr. Karen Troy, Committee Member
Worcester Polytechnic Institute

Zhi Li
Dr. Zhi Li, Committee Member
Worcester Polytechnic Institute

Loris Fichera
Dr. Loris Fichera,
Worcester Polytechnic Institute

Abstract

Wearable assistive robotics have the potential to address an unmet medical need of reducing disability in individuals with chronic hand impairments due to neurological trauma. Despite myriad prior works, few patients have seen the benefits of such devices. Following application experience with tendon-actuated soft robotic gloves and a collaborator's orthosis with novel flat-spring actuators, we identified two common assumptions regarding hand orthosis design. The first was reliance on incomplete studies of grasping forces during activities of daily living as a basis for design criteria, leading to poor optimization. The second was a neglect of increases in muscle tone following neurological trauma, rendering most devices non-applicable to a large subset of the population. To address these gaps, we measured joint torques during activities of daily living with able-bodied subjects using dexterity representative of orthosis-aided motion. Next, we measured assistive torques needed to extend the fingers of individuals with increased flexor tone following TBI. Finally, we applied this knowledge to design a cable actuated orthosis for assisting finger extension, providing a basis for future work focused on an under-represented subgroup of patients.

Acknowledgments

This work would not have been possible without the support, time, and feedback of many individuals, research groups, and organizations. While it's a bit cliché to say, it's true that the amount of people I've worked with over the last five years is too numerous to name all of them individually. I would, however, like to especially acknowledge the help of a few individuals who have made a real impact on my work in the AIM lab.

To my peers in the AIM lab, especially Gang, Nirav, Paulo, Katie, and Marek, for lending a hand, working with me through my programming errors, and providing a source of engaging conversations on a variety of topics, this work would not have been as successful or enjoyable without all of you. I would also like to say a special thanks to the two members of the lab who contributed the most to this project. Firstly, Mike Delph, for showing me the ropes and getting me started on the project, you were largely responsible for sparking my interest in hand orthoses. Secondly, Tess, for re-motivating my interest in this project and devoting so much time and effort to it, I will be forever grateful.

Outside of WPI, I would like to thank some of our collaborators including the

researchers at ETH Zurich, Roger, Olivier, and Tobi, and the clinicians who gave input, especially Gretchen Meier and Deborah Latour, your feedback and guidance was invaluable in elevating the impact and relevance of my work.

I would also like to acknowledge the funding agencies who supported myself and/or this work over the last few years, the NSF (IGERT DGE 1144804), DoD (SBIR W81XWH-15-C-0030), and NIH (R01 CA166379). Without investment in research and researchers, progress in areas such as this would be much harder to come by.

And finally, I would like to acknowledge my advisor, Greg Fischer, for supporting me through this work. You always made things work behind the scenes so I never had to experience the typical grad student funding anxiety. You gave me the freedom to work on any project that caught my interest, and trusted me to get everything done in the end. I feel that I've had a somewhat unique experience for a graduate student, but it was this experience that I was hoping for when applying to programs. I'm grateful that you brought me into this lab and advised me through my work.

Dedication

I would like to dedicate this work to my parents, Michael and Lisa Nycz, who have been nothing but understanding and supportive throughout nearly a decade of my being a college student. I owe it all to you!

Contents

List of Tables

List of Figures

Disclaimer: certain materials are included under the fair use exemption of the U.S. Copyright Law and have been prepared according to the fair use guidelines and are restricted from further use.

Acronyms

AA Abduction and Adduction

ABP Abductor Pollicis Brevis

ADL Activity of Daily Living

AHA American Heart Association

CP Cerebral Palsy

CMC Carpometacarpal

DIP Distal Inter-Phalangeal

DOF Degree of Freedom

EDC Extensor Digitorum Communis

EMG Electromyography

FDI First Dorsal Interosseous

FDM Fused Deposition Modeling

FDP Flexor Digitorum Profundus

FDS Flexor Digitorum Superficialis

FE Flexion and Extension

FIM Functional Independence Measures

FMA Fugl-Meyer Assessment

FPL Flexor Pollicis Longus

IP Inter-Phalangeal

ISB International Society of Biomechanics

MCP Metacarpo-Phalangeal

NIH National Institutes of Health

PIP Proximal Inter-Phanlangeal

PLA Polylactic Acid

PS Pronation and Supination

PWM Pulse Width Modulation

QOL Quality of Life

RMS Root Mean Square

SCI Spinal Chord Injury

SNR Signal-to-Noise Ratio

TBI Traumatic Brain Injury

UHMWPE Ultra High Molecular Weight Polyethelyne

UMN Upper Motor Neuron

CHAPTER 1

Introduction

> "To invent your own life's meaning
>
> is not easy, but it's still allowed,
>
> and I think you'll be happier for the
>
> trouble."

Bill Watterson

A review of neurological traumas and diseases which result in chronically impaired motor function of the hand reveals a large population of people who remain disabled for years or decades, with negative impacts to their independence and quality of life. Ultimately, lasting disability persists in some patients due to an inability to fully treat the underlying causes, or assist the resulting impairments, of the disorders. For decades now, the robotics community has attempted to help address this unmet need through many varied approaches. Two primary philosophies of treating through

rehabilitation robotics and assisting through wearable robotics have emerged from the numerous works. Several groups employing rehabilitation robotics have shown statistically significant improvements in patients on functional assessment scales, improvements which for most devices are similar to those achieved with the same intensity of conventional, non-robotic, therapy [1, 2]. The prognosis for recovery through rehabilitation, however, is very much patient dependent and many individuals will retain some degree of impairment regardless of the duration and intensity of treatment. Difficulty in achieving complete recovery of relevant motor function through rehabilitation robotics has lead to the more direct approach of mechanically assisting the patient's movements using wearable devices. The goal of assistive technologies is to normalize the patient's movements in a manner which provides relevant function for the user, reducing their disability without directly treating the impairment. Improvements in the design of these devices has slowly progressed over the past ten to twenty years with powered hand orthoses becoming lighter and smaller. The field, however, still faces major hurdles which must be addressed before the use of assistive devices becomes ubiquitous among those with motor impairments in the hand. A handful of commercially available devices have made their way into the market-space but clinician and patient enthusiasm over their capabilities has been somewhat tepid. The added function provided by such devices rarely justifies the difficulty of donning them or their obtrusiveness while being worn. Furthermore, currently available commercial devices are tailored towards specific subsets of impairments, specifically

moderate weakness with minimal to no hypertonicity, leaving most individuals as un-suitable candidates for their use [3,4]. Improvements in device function, or reduction in their burden of use, are needed for user acceptance to rise. Finally, a fusion of the two philosophies using assistive wearable devices as a means of improved rehabilita-tive therapy has been considered by some [5–8]. These exoskeletons are intended to re-train motor function by repetitively assisting in functional tasks. Some of these devices have increased complexity over their purely assistive counterparts which in-creases their size and weight and restricts their portability. It's unclear, however, whether the added dexterity over simpler rehabilitation robots results in improved patient outcomes [2].

Throughout our work, we have pursued most seriously the path of wearable as-sistive devices in the form of powered hand orthoses. This decision was the result of a thorough review of prior work, informal interviews with numerous clinicians and patients, and preliminary work with prototype devices. Entering the field required a thorough examination of past approaches and the benefits and limitations of each. Highly articulated fully actuated devices [9], simple single DOF mechanisms [10], under-actuated soft robotics [11–14], dc motor driven [10–16], hydraulically pow-ered [6,17], pneumatically powered [18–20], shape memory actuators [21], and more have all been explored in search of some performance gain. While each of these ap-proaches has their strengths and weaknesses, none has provided a cure-all for the problems facing the field. Ultimately, limitations come from the energy density of

current actuators, power storage, and the properties of materials from which devices are constructed. Designing around current actuator and battery technology, these are limitations which cannot simply be overcome by a single clever mechanism, rather, detailed evaluation of device requirements and refinement of components is required with a systems-based approach. In a field as mature as this one, proof of concept works rarely are sufficient for meaningful progression of knowledge. Surprisingly, while the field is mature, quantitative characterizations of design specifications are somewhat limited. Reliance by orthotic engineers on tangentially-related studies of grasping is common when designing and evaluating device performance. To improve upon the design process and contribute to a better understanding of the outstanding problems in the field, we sought to address gaps in critical design criteria through targeted biomechanics studies with measurements directly applicable to orthosis design.

While it was logically our desire to define and quantify specifications prior to constructing a device, in practice, addressing gaps in the knowledge needed for design optimization is often difficult without prior application experience. Understanding what the constraining components are often becomes clear only after going through the design steps and working with hardware. As such, we started our work by building prototypes of cable-actuated soft robotic gloves [11, 22] and working with collaborators on their novel exoskeleton using compliant flat-spring actuators [23]. Working on these two diverse designs helped us build an understanding of the systems as a whole, what components were needed, and how they needed to interact with each

other. In general, we found benefits in remotely locating the bulk of the hardware away from the hand. Placing actuators, electronics, and power storage in a more proximal location on the body eased some of the weight and size constraints with little loss of efficiency. Through this process we also gained a better understanding of underlying assumptions being made during the design phase. Two primary gaps in prior knowledge were identified. The first gap was the common assumption that the user's hand is transparent to the forces provided by the exoskeleton, that is, if the exoskeleton pushes on the back of a finger with a certain amount of force, it is assumed that this force is also applied to the object being grasped. This assumption turns out to be especially poor for individuals with the upper motor neuron (**UMN**) syndrome, as they can exhibit a resting state of increased muscle tension and hyper-excitable reflexes [24–26]. These conditions lead to flexed postures in the upper limb which can require substantial force to counteract [27]. This syndrome is characteristic of stroke [28], taumatic brain injury (**TBI**) [25], and cerebral palsy [29], conditions which are commonly cited as the application of assistive devices. The second assumption was related to the amount of gripping force needed to successfully complete activities of daily living. Prior work in this area was found difficult to apply directly to the design of orthoses due to incomplete information regarding hand pose and the relative locations of the measured forces. Furthermore, previous studies were designed as general studies of able-bodied grasping which did not consider the limited dexterity an individual using an orthosis would possess nor the type of activities which an

orthosis would be beneficial in assisting. With most individuals facing impairment on only one side of their body, devices which assist with bimanual activities of daily living has been the primary need indicated through discussions with occupational therapists.

The lessons learned in our early design experience provided the motivation for what are the primary contributions of this work. These contributions can be summarized as reducing the gaps in knowledge needed for optimization of assistive hand orthoses for individuals with upper motor neuron syndrome and exploration of design concepts for assisting finger extension of individuals with increased flexor muscle tone. To fill these gaps in knowledge, we implemented a protocol for accurate tracking of the joints in the thumb, index, and middle fingers using optical tracking of surface markers. With this protocol, we conducted two biomechanics studies. The first study recruited 10 able bodied subjects on whom we measured fingertip forces in nine activities of daily living using specially instrumented household objects. From this data we were able to determine torques at each of the finger's joints which an orthosis would need to produce, information that could not be discerned from data that had previously been presented. Our study was also designed with orthosis use in mind by constraining subjects to basic grasps achievable with a hypothetical simple orthosis. The second study applied the same motion capture protocol to subjects who had suffered a TBI [27]. Again, measuring load cell vectors with respect to the subjects joints, we were able to characterize the joint torques needed by an orthosis

to assist full finger extension. Understanding the relationship between applied torque at each of the joints and motion of the fingers is critical in defining criteria such as actuator power, torque, and moment arms.

The impact of this work, arising from the research contributions, is in enhancing the understanding of how an orthosis should be designed if it is to assist an individual suffering from UMN in completing activities of daily living. Focusing attention not just on augmenting grip strength, but also on assisting extension deficits arising from increases in flexor tone, co-contraction of antagonist muscles, contractures, and abnormal joint synergies was found to be a necessary aspect of an orthosis design if it is to benefit a larger portion of this population. The bimoechanic studies conducted to support this understanding were done so from a robotics engineering perspective, with a focus on measuring forces in a way which lends itself to defining design criteria. The process of doing this has also uncovered new questions providing guidance for future work in the area. For example, observations and measurements of how TBI patients responded when asked to attempt volitional extension of their hands has lead to questions regarding the design of user interfaces based on EMG intent recognition. While this work has not completely solved the problems brought on by hand impairments associated with these disorders, expansion and refinement of the ideas presented here may one day bring an improved quality of life to many individuals.

CHAPTER 2

Background

The development of devices for restoring or assisting function in a hand with limited or impaired movement has been explored in great depth by engineers, orthotists, clinicians, and entrepreneurs alike due to a seemingly apparent value in their application. The prior work in this area is extensive with numerous concepts having been previously explored by research groups and commercial ventures. Different actuation mechanisms, linkages, and overall philosophies have been covered in great detail. The result of all these efforts have, however, been somewhat underwhelming and few patients see the intended benefits. Entering a field as mature as this one requires a deep evaluation of these past works, an understanding of their limitations, and a concerted effort to systematically address them. In this chapter, the potential users of such a device are explored and characterized in detail with a focus on how motor deficits in the hand manifest themselves as a result of various traumas or diseases. Following this, methods and devices previously developed for the application

are reviewed, and current limitations identified. The focus of this work is on hand orthoses, however, dedicated robotic systems for rehabilitation of the upper limb are also reviewed. Chapter 3 will explore in more detail the limitations of different approaches with applied work on physical devices while Chapter 4 will address gaps in previously published data needed for optimization of designs. Finally, in Chapter 5, we apply the lessons learned to the design of an orthosis for assisting finger extension of individuals with increased flexor tone.

2.1 Device Need and Patient Populations

In establishing the need for hand exoskeletons, the often cited justifications include an aging population [14,30,31] along with a high occurrence of stroke [6,10,14,17,31–33] and other neurological injuries resulting in motor deficits. Occasionally, disorders such such as multiple sclerosis (**MS**) or muscular dystrophy are cited as potential applications as in the work of Rotella et al. [34]. Non-medical applications of hand exoskeletons are limited almost exclusively to haptic feedback devices such as the commercially available CyberGrasp (CyberGlove Systems Inc., San Jose, CA). Very rarely are hand exoskeletons designed for "superhuman" strength or endurance, which is in contrast to lower limb, torso, and arm exoskeletons where it is not uncommon for military or industrial uses to be explored [35, 36]. The scarcity of non-medical applications in hand orthoses is likely due to factors specific to the hand such as re-

strictive size constraints, a need to replicate the hand's dexterity, and the importance of maintaing the user's tactile feedback. Applying super-human loads through a user without damaging their soft tissues, joints, or bones would prove difficult without enveloping the hand in mechanical structures to bare the excess load. A "superhuman" exoskeleton of this type would obscure the user's sense of touch and compensating for this lack of sensory input with artificial sensors would prove exceedingly difficult with current technology. Similarly problematic, assisting or preserving the entirety of the hand's dexterity would require dozens of independent actuators and complex articulation resulting in large and complex devices. Loss of tactile feedback and loss of dexterity would rob healthy individuals of their ability to perform dexterous manipulation which is typically of more value than is absolute strength. Medical applications, however, present engineers with a group of people who have severely impaired hand function where the performance crossover from hindrance to helpful is much lower. When the alternative for an individual is no hand function at all, a properly developed device with just a couple independent degrees of freedom could improve a person's quality of life [3].

Medical applications of hand orthoses do seem warranted and the classic justification of an aging population with a high prevalence of stroke related motor deficits is well documented. The portion of the United States population over the age of 65 is currently 15% and is projected to grow to one fifth by 2030 [37]. Related to this aging population, around 795,000 incidences of stroke occur in the United States

each year [38]. This number has continued to slowly increase against a decline over the past 50 years in the prevalence of stroke at age 65 from 19.5% to 14.5% in men and 18% to 16.1% in women [38, 39]. Following stroke, initial motor impairment is nearly ubiquitous [40, 41], however, the majority of those surviving at six months will recover to have no or only mild deficits [40]. Even when considering this prognosis for recovery, stroke is still the most prevalent cause of upper limb impairment. The total number of individuals in the United States who have had a stroke is 6.6 million [38], or about 2% of the total population. Of these, approximately 25% will have lasting moderate to severe upper limb motor deficits [40]. These deficits arise due to damage in the upper motor neurons of the corticospinal tract and are characterized by the upper motor neuron (**UMN**) syndrome [28]. In addition to stroke, the symptoms of UMN can arise from most traumas or diseases which effect the brain and its descending pathways such as traumatic brain injury (**TBI**) [25], cerebral palsy (**CP**) [29], and certain cases of spinal cord injury (**SCI**) [42]. These disorders further justify the need for advanced orthoses as CP effects 2-3 out of every 1000 children [43, 44]. Likewise, TBI is common with a yearly occurrence of about 1.4-2 million in the United States [45, 46], although resulting chronic impairment is much more varied than in stroke and CP. 70-90% of TBIs can be classified as mild [47], where confusion or loss of consciousness lasts less than 30 minutes. Of all TBIs occurring in the United States each year, 80,0000-125,000 result in long term disability [46, 48]. In total, approximately 3.2 million people in the United states are living with long term disability as

11

a result of TBI [49] with arm paresis seen in approximately 17% [50].

Another, less cited but still present, focus of hand orthoses is for assisting MS related motor disorders. MS is an autoimmune disease characterized by demyelination of nerve fibers in the central nervous system and, unlike stoke, TBI, CP, and SCI, MS is a progressive degenerative disease [51]. The prevalence of MS is about 1.5 per 1000 people in the United States [52] with mild to complete hand impairment self-reported in 20-60% of patients and the impairment becoming more common and more severe the further patients are from initial diagnosis [53]. Due to the progressive nature of MS, however, the period of time in which hand function is of primary concern may be relatively short as other, more serious, symptoms develop.

The symptoms of UMN and MS both arise from damage to the central nervous system. Distinct from these conditions, peripheral neuropathy, which is damage or disease to the pathways connecting the spinal cord to the skeletal muscle in the limbs, is another cause of persistent motor deficits. For the upper limbs, damage to the brachial plexus, a nerve bundle which traverses the shoulder and innervates muscles of the shoulder, upper arm, forearm, and hand, is the most common cause of the disorder. This damage can occur during child birth with a prevalence of 1.5 per 1000 births in the United States [54], is due typically to shoulder dystocia [55], and results in deficits lasting longer than 1 year in 10-18% of cases [56]. In adults, trauma, such as that resulting from motor vehicle accidents or sports injuries, can also cause damage to the brachial plexus resulting in lost motor function in the upper

limbs. Reporting on 1068 adult brachial plexus trauma cases referred to him over a period of 18 years, Narakas et al. found 70% were attributed to motor vehicle accidents, with 70% of those specific to motorcycle accidents [57]. Depending on which spinal roots are affected, spontaneous recovery of function can be seen in up to 80% of cases [58] with surgical and rehabilitation options remaining for those without spontaneous recovery [58, 59].

The prevalence and characteristics of these diseases and traumas are summarized in Table 2.1. Summary of these conditions indicate that the total prevalence of hand impairment in the United States is on the order of about 2 million individuals. Upper motor neuron injuries appear to be the most common cause, although data on the prevalence of brachial plexus trauma in non-infant populations is limited. It should be noted that these numbers are rough estimates based on review of the literature and not based on a rigorous meta-analysis of the data. Inconsistencies in how research groups define their populations can make direct comparison of results across studies prone to error. A number of other rare disorders, such as muscular dystrophy, were not covered here in depth but may also result in hand impairment. Even given the limitations of this review, the market and need for a clinically relevant assistive hand orthosis is clearly present.

Table 2.1: Summary of diseases and traumas which commonly cause motor deficits in the hand. Overall, potential beneficiaries from an assistive hand orthosis in the US total 2 million people with the majority due to an upper motor neuron lesion. *Rough estimate from prevalence per 1000 among children and current US population of 323 million. †Only individuals with long term disability as a result of TBI included.

Disease or Trauma	Prevalence (Lifetime US)	Chronic Upper Limb Impairment (%)	Injury Type
Stroke	6,600,000 [38]	24.6 [40]	Upper Motor Neuron Injury
Cerebral Palsy	640,000* [29, 44]	60 [60]	Upper Motor Neuron Injury
Traumatic Brain Injury	3,170,000-5,300,000† [46, 49]	17.6 [50]	Upper Motor Neuron Injury
Multiple Sclerosis	250,000-350,000 [51]	20-60 [53]	Autoimmune Demylination in CNS
Brachial Plexus Palsy	484,000* [54]	10-18 [56]	Peripheral Nerve Trauma

2.1.1 The Upper Motor Neuron Syndrome

The upper motor neuron syndrome (**UMN**) is a condition which arises due to injury of the "motor cortex or its descending projections" [28]. As established in Section 2.1, the majority of individuals with chronic upper limb motor deficits can be classified as having upper motor neuron disorders. A similar set of motor deficits arising from UMN are shared across the diseases and traumas of stroke, CP, SCI, and TBI making their lumped classification beneficial in discussions related to the design of hand orthoses. These deficits can be broadly classified as either "negative" or "pos-

itive" in which negative symptoms are characterized by lost function due to muscle weakness and positive symptoms are characterized by involuntary hyperactivity of reflexes or resting muscle tone [24]. Having a complete understanding of the various manifestations of UMN is critical to a practical orthosis design as some of the motor deficits may be unintuitive to engineers who are likely to have limited interaction with patients. Correctly interpreting descriptions of motor deficits related to UMN can prove difficult, however, as commonly used terms can simultaneously describe vastly different hand function. For example, although its formal definition is that of a velocity-dependent increase in tonic stretch reflexes [61], the term spasticity is frequently used as generally referring to all positive symptoms of UMN. While velocity dependent features can be present among this population, a resting state of increased muscle tone is commonly observed as well [24] which is arguably imperfectly described by generalizing patients as either spastic or flaccid. The meaning of paralysis is also often difficult to discern as it describes a lack of volitional movement due either to negative or positive features [62], leaving ambiguity which may lead to assumptions of flaccidity when a resting flexed posture is being described. Symptoms classified as "positive" may include spasticity, tendon hyper-reflexia, clonus, the clasp knife phenomenon, a Babinski sign, rigidity, and dystonia [24,63]. It should again be noted that these terms are not necessarily used consistently among different researchers or publications. For the sake of clarity, the definitions of terms used to describe UMN symptoms as adopted by this work are as follows:

- **Tone**: "The property of a muscle whereby a steady state of partial contraction is maintained, varying only in degree" [64]. Tone is the tension maintained by a muscle, tension that is not due to volitional contraction.

- **Hypertonia**: "A condition in which there is too much muscle tone so that arms or legs, for example, are stiff and difficult to move" [65]. Hypertonia is the general term which encompasses the "positive" symptoms of UMN such as spasticity, dystonia, and clonus [66].

- **Spasticity**: "A motor disorder characterized by a velocity-dependent increase in tonic stretch reflexes (muscle tone) with exaggerated tendon jerks, resulting from hyperexcitability of the stretch reflex as one component of the upper motor neuron syndrome" [66]

- **Weakness**: A reduction in muscle strength characterized by a decreased ability to volitionally elicit muscle contractions.

- **Hemiparesis**: A partial loss of volitional movement affecting one side of the body. People who are described as hemparetic typically exhibit both weakness and hypertonia which each contribute to the lack of volitional motion.

- **Hemiplegia**: Complete paralysis of one side of the body characterized by an inability to elicit any volitional motion in the limbs. In the upper limbs, hemiplegia can either describe a rigidly flexed posture or a flaccid limb.

- **Rigidity**: "Continuous resistance to passive stretching. Muscle tone is increased in agonist and antagonist muscles." [24]

- **Tendon hyper-reflexia**: "An exaggerated muscle response to an externally applied tap of deep tendons." [42]

- **Clonus**: Rhythmic distal joint oscillation. [67]

- **The clasp knife phenomenon**: "A sudden reduction of resistance during stretch" [68].

- **Dystonia**: "An involuntary alteration in the pattern of muscle activation during voluntary movement or maintenance of posture. In general, dystonia is diagnosed by the observation of abnormal twisted postures or repetitive movements." [66]

We adopt our own definitions of weakness, hemiparesis, and hemiplegia that we feel better reflect how they are colloquially used. We want to clarify that hemiparesis and hemiplegia describe a lack of volitional motion that does not preclude the presence of muscle contractions associated with increases in muscle tone. A more typical definition of hemiparesis as "a weakness effecting one side of the body" we feel can too easily be interpreted as describing a flail or flaccid limb which may not be the case. Also, as previously stated, many individuals who are described as spastic also have irregular resting flexed postures. These flexed postures seemingly fit the definition of dystonia, however, dystonia typically is not associated with stroke, TBI, and MS

while spasticity and hypertonia are. In general, care needs to be taken when reading publications to accurately determine the conditions being described. To avoid further confusion, where possible, we explicitly describe the characteristics of an individual's muscle weakness and muscle tone while straying away from using terms like spasticity, rigidity, and dystonia. While it does not lend itself to brevity, it removes the ambiguity that has arisen from the inconsistent use of the terms. For additional clarity, the joint names, segment names, and anatomical directions used for describing the hand are shown in Fig. 2.1.
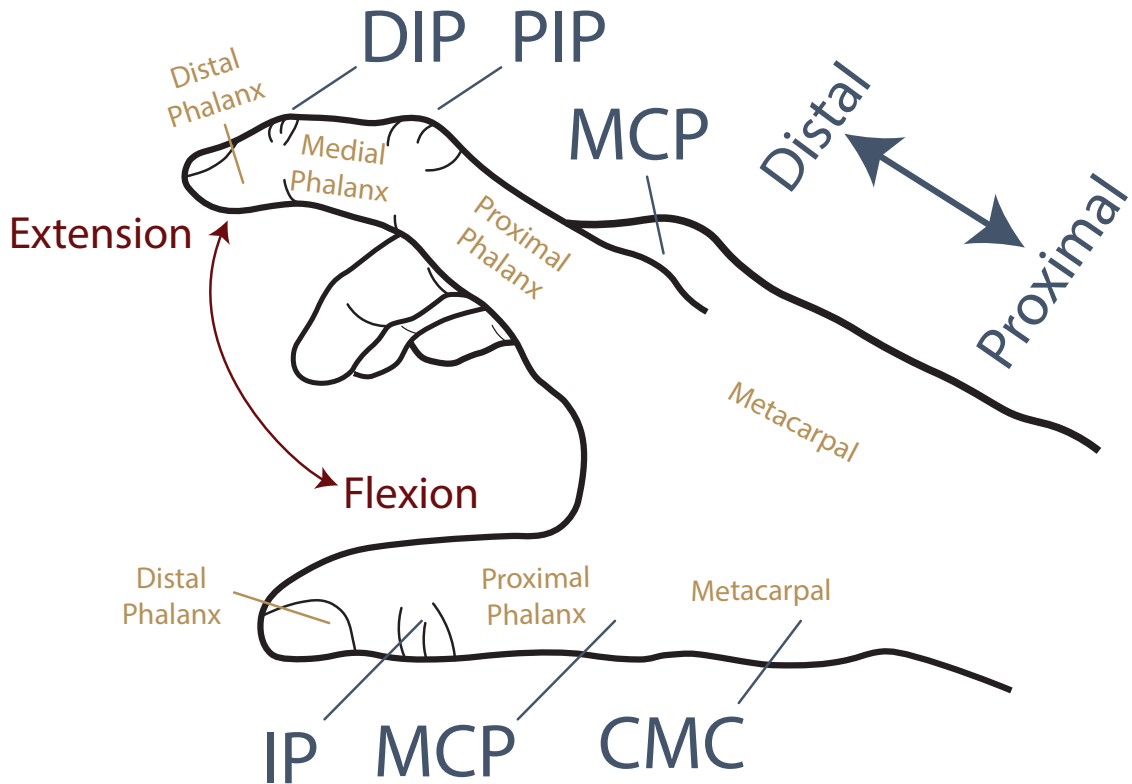
Figure 2.1: Diagram of the hand specifying joint names, segment names, and anatomical directions.

The "positive" features of UMN, increased tone and hyper-excitable reflexes, can at first be counter-intuitive outcomes of damage to the motor neurons. While the mechanisms responsible for these features may be multifaceted, in general they are believed to be caused by decreased inhibitory input to reflexes occuring in the spinal cord [24]. A more detailed description of the underlying neural mechanisms is outside the scope of this work, as an understanding of the how these impairments manifest in an individual's joint mechanics is of primary concern when considering orthosis design. Accounting for these "positive" symptoms would appear to be important for an orthosis to be able to provide relevant function for a large portion of individuals with hand impairments. Increased or irregular muscle tone (spasticity) is prevalent in 17-38% of chronic stoke patients [69–71] and of children with CP approximately 85% are classified as spasitic [44] with about 70% having increased flexor tone in their hands [60].

Our discussions with physical and occupational therapists, as well as patients, has also indicated a need for assisting with movement deficits arising from the "positive" UMN features, which is contrary to the primary intent of most developed devices. Due to the resulting flexed postures, many patients will struggle with finger extension making pre-shaping of the hand prior to grasp difficult or impossible. Concisely describing the impairments faced by the population as a whole, however, is challenging. The amount of resistance in each of the joints is typically dependent on a number of factors such as the speed of the movement, the posture of other joints,

stress, and physical activity. Motion synergies may be observed where movement of the proximal joints causes additional flexion in the distal joints. To illustrate the effects of these movement impairments, the resting hand posture of an individual with increased flexor tone following a TBI is shown in Fig. 2.2. A depiction of how this increased flexor tone, coupled with muscle weakness, effects the individual's ability to use their hand is shown in Fig. 2.3. Use of the impaired hand for grasping requires external assistance to extend the fingers and a concerted effort to shape the fingers around objects. The tasks shown, grasping a jar and grasping a cup, each took several attempts and over half a minute before the individual was able to successfully hold the objects. In Chapter 4 we add to these observations with measurements of the external assistance required to achieve finger extension of hands with increased flexor tone.

Though spasticity and increases in muscle tone are common, they are typically present in concert with muscle weakness. When reviewing how the "positive" and "negative" symptoms contribute to disability multiple well-cited works find weakness as the primary cause of impairment [26, 28, 71, 72]. The work of Kamper et al., for example, finds that weakness, "is the primary contributor to finger impairment in chronic stroke" [26]. Sommerfeld found that weakness was more prevalent than spasticity 3 months post stroke with 67% of subjects hemiparetic and only 19% having increased muscle tone as measured on the Modified Ashworth Scale [71]. However, while Kamper's study found that extensor weakness was a prominent indicator of

impairment, static stiffness, spastic reflexes, and an imbalance in flexor co-activation during voluntary extension were all simultaneously present in severely impaired patients. The resting posture of the subjects' hands were described as flexed and the results indicated that extension of one impaired subject's metacarpophalangeal ($\boldsymbol{MCP}$) joint required an externally applied torque of $0.5Nm$. Similarly, Sommerfeld found that though weakness was more prevelant, an equal number of spastic and non-spastic patients had severe motor and activity problems [71]. Given these qualifiers, it is clear that increased flexor tone coexisting with muscle weakness is a common manifestation of UMN in these studies. As stated earlier, for orthotic engineers it is typically more important to consider the resulting joint mechanics than the details of the underlying mechanisms and their relative contributions. While cursory review of these papers would suggest a need to aid finger flexion, a more thorough read reveals the need for both flexion and extension assistance.

Understanding these various impairments is critical to designing an orthosis which has relevance to a larger portion of individuals who need assistance with hand motion. From an engineering perspective, providing actuation to a hand which is flaccid is more approachable than normalizing the function of a hand suffering from the "positive" symptoms of UMN. In the later case, the torques at each of the joints are unknown, hard to measure in real time, and constantly changing. Furthermore, assisting in extension without obscuring the palmar surface of the hand presents challenges which are difficult to address in a manner which makes the device easy to don and dof.
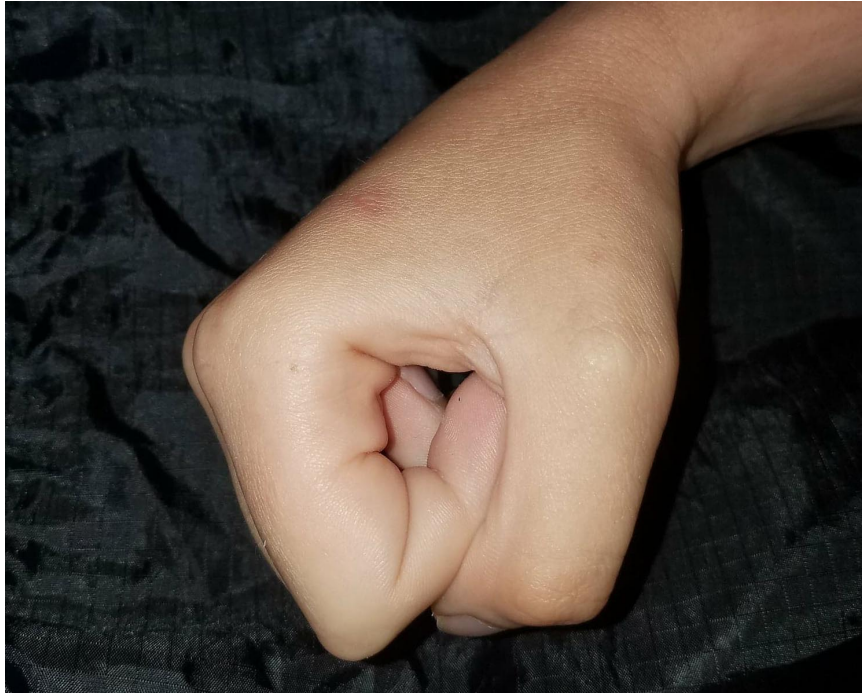
Figure 2.2: The resting hand posture of an individual with chronic motor deficits as the result of a traumatic brain injury (TBI). An increase in muscle tone keeps the hand in a resting flexed posture. The degree of resting tone is highly variable and is dependent on factors such as posture, stress, and recent physical activity.

Focusing exclusively on augmenting grip strength, however, would clearly limit the number of people who would benefit from an orthosis. The individual shown in Fig. 2.3 would not be able to use the augmented strength as they would be incapable of positioning their hand around objects. Though there are people who have weakness without increases in muscle tone, they don't represent an overwhelming majority of people who have disabilities related to UMN.
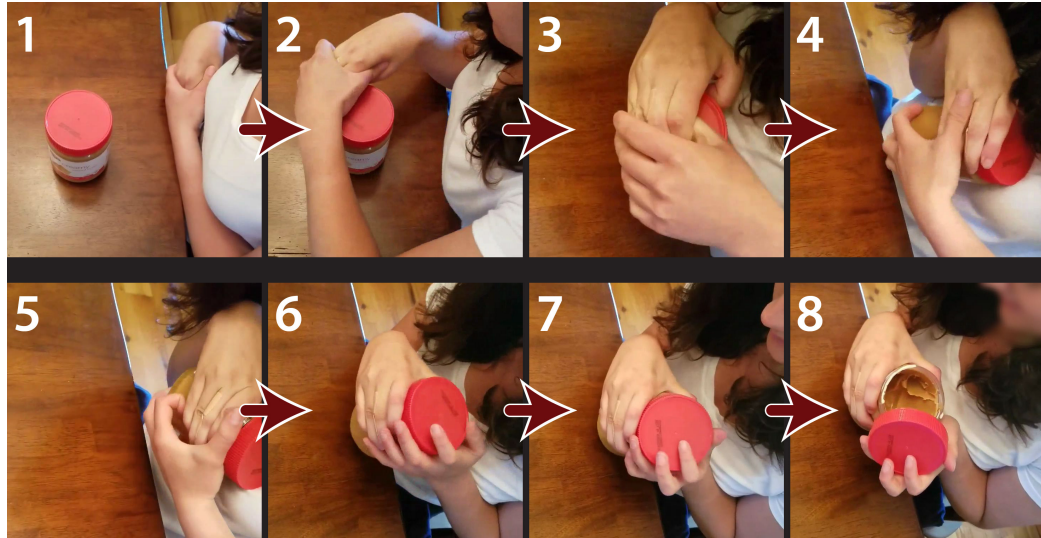
(a) Removing a jar lid
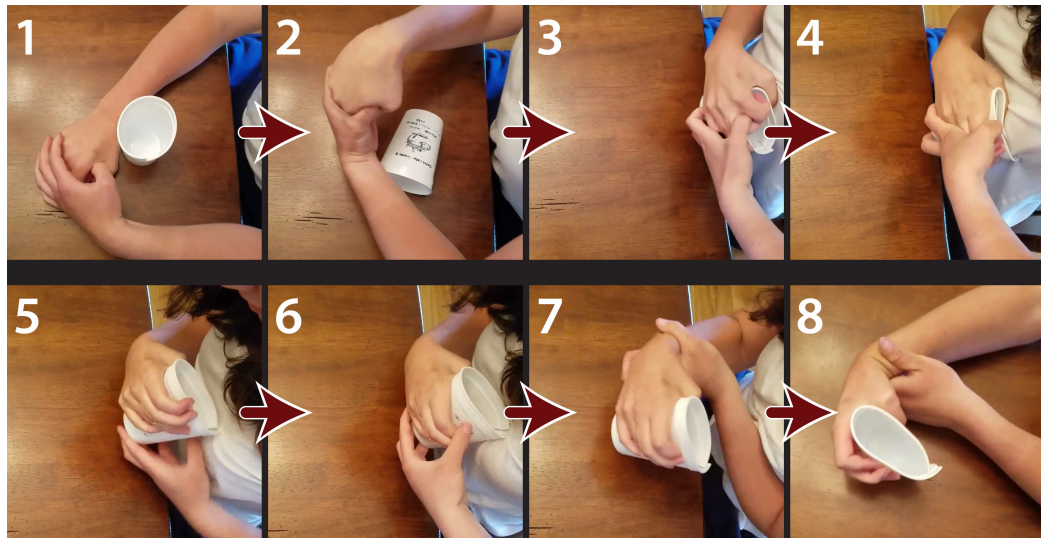
(b) Grasping a cup

Figure 2.3: An individual with increased flexor tone in their right hand due to TBI (a) removing a jar lid and (b) grasping a cup without assistance. The process of getting the impaired hand around each object requires the individual to user their able bodied hand to position and pry the impaired hand open. Once the object is enveloped, the impaired hand provides support while the able-bodied hand can perform more dextrous tasks. In removing the jar lid, the individual took several attempts and over half a minute to go from pane 1 to 6.

2.1.2 Peripheral Nerve Damage

The disorders that arise following damage to the brachial plexus are markedly different from those arising from damage to the upper motor neurons. Impairments from peripheral neuropathy are mostly restricted to deficits in motor function and sensation without disruption to other neurological processes such as cognition. The "positive" features associated with UMN are absent with weakness, loss of sensation, and chronic pain the primary disorders associated with the trauma [73]. Treatment of brachial plexus trauma is heavily focused on acute care. The potential for recovery is assessed and surgical intervention pursued if spontaneous recovery is not expected. Surgical options include nerve grafting, nerve transfers, free functioning muscle transfers, and tendon transfers. The surgeries typically focus on restoring elbow function with procedures for restoring hand function currently more limited in their application and effectiveness [74]. Following acute care and recovery, additional improvements through rehabilitation are unlikely as the neural plasticity leveraged in rehabilitation of upper motor neuron disorders is not present in peripheral nerve disorders [73]. The rehabilitation focus is on building strength and coordination in the unaffected motor units. As time since injury progresses, further atrophy of denervated muscle is expected [75].

While the acute care of brachial plexus trauma can vary substantially between patients, the resulting motor impairment is fairly consistent when compared with upper

motor neuron disorders. Assisting these deficits would focus primarily on restoring strength and dexterity. Counteracting flexor tone and hyper-excitable reflexes would not be necessary in an assistive device focused on this population. These characteristics have led some devices to market themselves heavily towards brachial plexus trauma, even though the number of potential users is more limited than those affected by UMN.

2.1.3 Assessment Scales

Assessing impairment and disability arising from the motor deficits of UMN and peripheral nerve damage can prove challenging due to the often qualitative definitions of the various disorders. Reliably tracking impairment is critical, however, when assessing the efficacy of rehabilitation platforms. In clinical trials of devices, a handful of "standard" assessments are typically performed along with a battery of other assessments which researches employ to evaluate features of specific interest to their study.

The most used tool for grading motor function in patients with UMN is the Fugl-Meyer assessment (**FMA**). Good inter and intra-rater reliably comes from the coarseness of the measurement, with subjects given a 0, 1, or 2 for a series of testable motions. These values correspond to assessments of cannot perform, can partially perform, and performs fully, respectively [76]. The scale consists of 226 total points, with the upper extremity motor function portion consisting of 66 points for 33 as-

sessed motions. For a rehabilitation approach to be considered beneficial, it must not just show a measurable increase in FMA score, but one that is considered meaningful for the patient. Lin et al. found 5.2 points to be the minimal detectable change for the FMA [77]. Similarly, Page et al. found an increase of 4.25-7.25 points on the upper extremity portion was the threshold for being considered a clinically important difference [78]. In addition to the FMA, the Wolf Motor Function Test is also commonly used for grading motor function. The test incorporates elements of strength and ability to complete functional motions. Subjects are graded from 0 to 5 on their functional ability as well as on the time to complete the tasks [79]. Clinically important differences for the test were measured to be a 19s reduction in the time measurement and a 1.0 point improvement on the functional ability measurement [80].

Spasticity is commonly assessed using the Modified Ashworth Scale (**MAS**). The MAS assesses the resistance of 8 joints to rapidly imposed movements by the assessor. Each joint is rated from 0 (no increase in muscle tone) to 4 (rigid in flexion or extension) with good inter-rater reliability of 86% [81]. The MAS, however, can suffer from the manner in which the subject is tested, which is typically to have the subject relaxed and lying in a supine position. With muscle tone in people with UMN dependent on factors such as stress, posture, and activity, the value determined during the assessment has the potential to be unrepresentative of the subject's tone during activities of daily living. While imperfect, the test serves the purpose of providing a consistent comparison between subjects and studies.

To assess an individual's independence and ability to perform activities of daily living, the Barthel Index, a 100 point scale assessing 10 activities [82], and the Functional Independence Measure (**FIM**), a 126 point scale of 18 activities [83], are regularly used. These scales are sometimes considered to have more relevance to the subjects as the outcomes correspond more directly to clinically relevant function. The Stroke Impact Scale (**SIS**) represents a mix of motor function, cognitive, and independence measures with a self assessment covering 8 domains of strength, memory, emotions, communication, independence in ADLs, mobility, hand use, and social participation [84].

These are a handful of assessments commonly encountered in work assessing the rehabilitation or assistance of individuals with impaired motor function. Numerous other tests have been employed in assessing therapeutic and assistive technologies. What's important to consider when evaluating a device's performance is the reason for choosing each assessment and how each of the employed tests corresponds to patient outcomes. For example, improvements in motor function measured on the FMA or reduction in spasticity measured by the MAS without a corresponding improvement on the FIM would indicate a therapy delivers measurable improvements, but those improvements on their own are not clinically important. In the reverse case, improvements on the FIM and not on the FMA, the conclusion may be that subjects had developed new methods of compensating for their impairments without having much change in their physical impairment. These tests, though their effectiveness is often

debated, provide a valuable tool for assessing the performance of various therapies
and devices.

2.2 Robotic Approaches for the Treatment of Motor Deficits

Two fairly distinct approaches of using robotics for improving hand function follow-
ing disease or trauma exist in previous work. The first of these is using robots as
rehabilitation devices intended to perform the function of a physical therapist by lead-
ing patients through specially designed exercise routines. The goal of rehabilitation
robotics is to reduce the individual's impairment and improve function over time by
delivering longer duration or higher intensity of therapy than would be possible with
a physical therapist alone. The form that these devices take can vary substantially,
with some being large, stationary exercise machines and others being wearable ex-
oskeletons. The second robotics approach for improving hand function is to directly
assist a patient's movements in a manner which improves their ability to complete
daily activities. With assistive devices, long term reduction in impairment is not the
primary concern, rather, an instant reduction in disability after donning the device is
pursued. Moderate success has been demonstrated with both approaches, but neither
has established itself as a standard of care. Understanding the approaches tested in
past work, their successes, and their limitations is valuable in guiding the direction

of future work.

2.2.1 Rehabilitation Robotics for Treatment of the Upper Limb

The use of robotics for recovery from stroke started with the MIT Manus arm in the early 1990s [85] which can be seen in Fig. 2.4. The Manus, in its original form, consisted of a planar arm with an impedance controlled end effector. Later, additional degrees of freedom (DOF) were added for wrist and vertical movement [86, 86]. Since then, a commercialized version of the MIT Manus, the InMotion ARM^{TM} (Bionik Laboratories Corp, Toronto, Canada), has added a module for hand training, the InMotion Hand^{TM}. The Manus is designed to lead patients through an exercise routine which requires the user to position the end effector following a pattern displayed on a graphical user interface. The impedance controlled arm will provide assistance in completing the motion by applying force to the user if they deviate from the desired path. The amount of force applied to the user can be adjusted to vary the amount of assistance depending on the user's level of impairment. Clinical trials using the Manus, administering 1 hour long sessions, three times a week, for 6 to 12 weeks, indicate improvements on the Fugl-Meyer assessment of 2-4 points over control groups who receive no additional therapy to their standard care [87–89]. Reductions in time to complete the Wolf Motor Function test of about $8s$ were also observed [89].

Results were not statistically different, however, from control groups who recieved an equal intensity and duration of therapy from a physical therapist [89].

The Manus, without added on modules, predominantly focuses on rehabilitation of the proximal joints (the elbow and shoulder). Several other studies have also employed robots for rehabilitation of the proximal joints. The MIME robot required subjects to grasp a handle affixed to a Puma 560 industrial robotic arm. The robot could provide force to the user either in a manner similar to how a therapist would assist during a standard rehabilitation session, or using a mirror therapy approach. Mirror therapy was applied by having the subject's unimpaired hand move a controller, with that motion replicated on the impaired hand using the robot [90]. Testing of the MIME robot found improvements on the Fugl-Meyer Assessment greater than those expected from spontaneous recovery, though the study used a general model for expected recovery and not a statistically similar control group. The mirror therapy did not compare favorably to robot replicated standard rehabilitation therapy. As was seen with the Manus, improvements with the robot were statistically similar to those in a control group receiving a matched duration and intensity of therapy from a physical therapist [90]. Another robot focused on rehabilitation of the arm's proximal joints is the NeReBot, a suspended sling for the forearm which is moved by 3 motorized cables [91]. Clinical trials with NeReBot carried out during inpatient care, starting 8-10 days after stroke, found partial substitution of standard therapy with robotic therapy resulted in statistically similar outcomes [92]. Use of the NeReBot

during acute care is a departure from the majority of rehabilitation studies where therapy is typically administered during chronic stroke.

Distinct from robots focused on proximal improvements, several end-effector type rehabilitation robots have been designed specifically for treating hand and wrist impairments. The HandCare system uses cable-actuated cuffs to linearly move the hand's finger tips [93] while the HapticKnob is a rigid device for training hand opening and closing as well as wrist pronation and supination [94]. The designs of HandCare and HapticKnob are shown in Fig. 2.4. Pilot studies with the Haptic Knob indicated an average increase of 3 points on the Fugl-Meyer assessment [94], while no clinical studies of HandCare could be found.

Several groups have also developed exoskeleton type rehabilitation robots which are designed to align with and directly move the user's joints. The ARMin robot was designed for assisting the shoulder, elbow, and wrist using a combination of impedance and admittance control [95]. Patients using the ARMin complete games which require positioning their arm to navigate a maze on a graphical user interface, with the intent of training strength and coordination in the affected limb [7]. The Harvard Biodesign Lab developed a hydraulic hand exoskeleton for task-specific training [6, 17] shown in Fig. 2.5(c), though clinical trials of the device have yet to be performed. Fischer et al. developed an exoskeleton for stretching the hand, one of few wearable devices aimed specifically at counter-acting increased flexor tone in the hands [5]. The device was tested on 13 patients with 15 treatment sessions over 5 weeks. No significant

change in spasticity was found, but significant improvements in Action Research
Arm Test, Fugl-Meyer, Wolf Motor Function, and box and block tests were observed
[5, 96]. A recent study by Brokaw et al. looked at the effectiveness of combining
the ARMin III and HandSOME devices, exoskeletons for rehabilitating the arm and
hand respectively. The HandSOME device is technically not robotic, but rather
has a lever which the operator can use their contralateral hand to operate, opening
and closing the impaired hand [97]. The group found significant improvements in
function, with Fugl-Meyer scores improving by an average of 5 points over the course of
rehabilitation. All subjects received 1 month long periods of conventional and robotic
therapy with a 1 month washout period between the two. Fugl-meyer improvements
were similar between robotic and conventional therapy but Action Research Arm Test
results, a metric that assess an individuals ability to grasp and manipulate various
objects, were significantly better with robotic therapy [8]. The converse was seen,
however, with the box and block test which also assess an individual's ability to
grasp and manipulate objects.

Due to limited sample sizes and the variation among patients, it's difficult to de-
termine specifics about the efficacy of rehabilitation robots from analysis of any single
study. Even reasonably large studies, such as the randomized controlled trial of the
MIT Manus conducted by Lo et al. which recruited 127 subjects, can have consider-
able uncertainty regarding measured changes on functional assessment scales. Lo et
al. found a statistically significant improvement in FMA scores over standard care
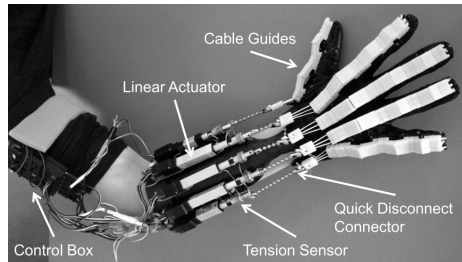
(a) Fischer et al. [5]
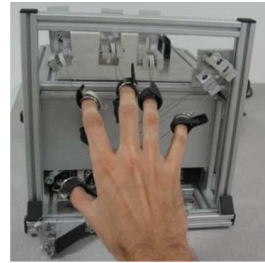
(b) Handcare [93]
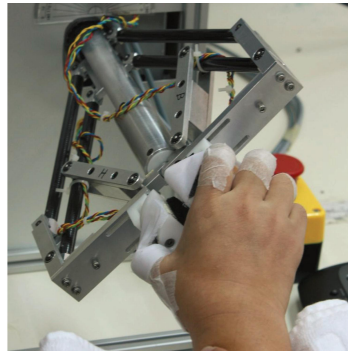
(c) HapticKnob [94]

(d) MIME [90]
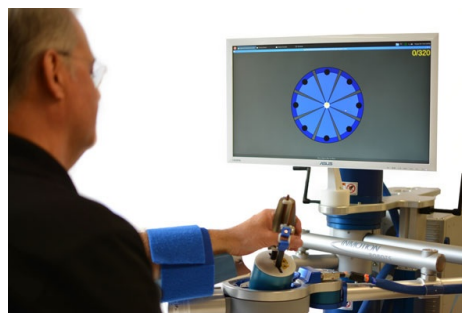
(e) InMotion Arm™

(f) MIT Manus, [86]

Figure 2.4: Examples of rehabilitation robots for the upper limbs and hand. The
InMotion Arm™ is a commercialized version of the pioneering MIT Manus arm.

using the robot, but the 95% confidence interval of this improvement was -0.23 to 4.58 FMA points [89]. This range extends from a slight decrease in motor function, to a potentially clinically important improvement [78]. Because of this uncertainty, aggregation of studies can give better insight into the general effectiveness of robotic rehabilitation. A meta-analysis conducted in 2012 looked at 12 controlled clinical trials using 6 distinct robots. The meta-analysis found that when robotic therapy was compared to a control group receiving the same duration of conventional therapy, no statistically significant difference existed between the results. Significant differences were seen when robotic therapy was administered in addition to conventional therapy, with an average improvement on the Fugl-Meyer upper extremity assessment of 2.85 points [1]. A more recent, 2017, analysis of 44 controlled clinical trials had a similar finding with measurable, but small, improvements on functional assessment scales with 2.23 point (95% CI 0.87 to 3.59) improvements on the Fugl-Meyer upper extremity assessment [2]. The studies used in the meta-analysis included a total of 884 subjects. The meta-analysis also separated end-effector type and exoskeleton type rehab robotics. They found average improvements in both (1.76 FMA improvement for exoskeleton and 2.59 for end-effector) but they were not statistically significant for the exoskeleton type robots while they were significant for end-effector type [2].

Review of past studies using rehabilitation robots has shown some support for the therapy. The benefits found, however, have been mostly the result of increasing the duration and intensity of therapy that would otherwise be administered to a patient.

There is not much support to suggest that current rehabilitation robots provide therapy which is inherently more effective than what is provided by physical therapists. Considering the cost savings potential of automating the rehabilitation process, it's not unreasonable to suggest that rehabilitation robots will ultimately allow patients to access these improved outcomes. A greater intensity of therapy delivered by a human may ultimately prove cost prohibitive. Replacing human-lead rehabilitation completely, however, is probably not in the patient's best interest. Rehabilitation therapists provide encouragement and motivation which may be difficult to replicate using robotic approaches. Furthermore, for individuals with cognitive and communication deficits such as aphasia, the therapist and their rehabilitation clinic may provide beneficial social interaction where they're surrounded by people sympathetic to their disorder. Finally, while improvements with robotic approaches have been measurable, they've typically been small and its not clear how much relevance they have for patients. Most researchers consider robotic therapy, along with assistive robotics, as currently an augmentation to traditional therapy, not a replacement.

2.2.2 Hand Orthoses for Assistance with Activities of Daily Living

As opposed to rehabilitation robotics, assistive devices are not primarily designed to treat an underlying impairment. Instead, these devices are intended to reduce a user's

disability directly by mechanically assisting their joint motion. The devices need to be lightweight, portable, and have sufficient battery power to last throughout most of the day. Secondary rehabilitative benefits are often explored, but they are not the primary metric on which the devices are evaluated.

A handful of commercially available powered hand orthoses have been made available, the most advanced of which is likely the MyoPro (Myomo, Inc., Cambridge, MA), a powered elbow-hand orthosis with electromyography (**EMG**) sensors to detect muscle activity as a means of user input. In addition to assisting elbow flexion, the device moves the index and middle fingers with a single motor while bracing the thumb in opposition to assist a three-jaw-chuck grasp. The full orthosis is shown in Fig. 2.5(b). A study of 18 subjects by Peters et al. found that performance on the Fugl-Meyer upper extremity assessment improved by 8.5 points on average while wearing the device when compared to assessment of the same subjects while not wearing the device [3]. Secondary to this assistive benefit, a potential rehabilitative effect was also found in a separate study by Page et al. where 16 subjects using the MyoPro for repetitive task specific training over an 8 week period saw improvements of 2 points on the Fugl-Meyer scale [4]. It should be noted that studies using the MyoPro had high exclusion rates with one study excluding 60% of subjects evaluated [3]. Subjects were excluded due to increased muscle tone (greater than 1 on the modified Ashworth scale), inability to volitionally elicit biceps brachii EMG signals greater than $5\mu V$, inability to independently flex the shoulder greater than 30°, inability to

(a) Gasser et al. [10]

(b) Myomo, Inc.

(c) Polygerinos et al., [6]
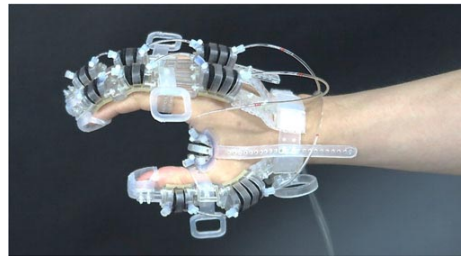
(d) Yun et al., [18]
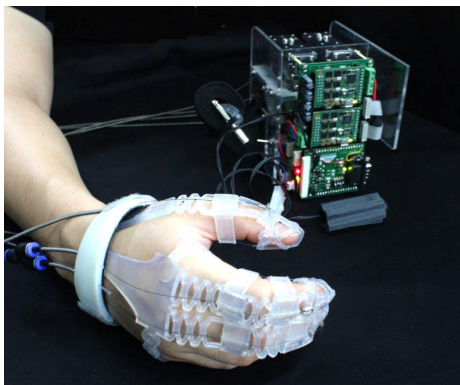
(e) Kang et al., [98]

(f) Saharan et al., [21]

Figure 2.5: Examples of exoskeletons developed previously by research groups and companies.

independently abduct the shoulder greater than 20°, and Fugl-Meyer upper extremity scores outside the range of $10 - 25$ [3, 4]. These exclusion criteria preclude subjects who are not good candidates for the device, not just those whose participation poses a risk to their health. In particular, individuals who are severely impaired, mildly impaired, with spasticity, or irregular muscle tone are deemed not good candidates for the MyoPro. These exclusion criteria are also used when clinically prescribing the MyoPro [99].

2.2.2.1 Rigid-Linkage Hand Orthoses

The hand orthosis offered by Myomo is mechanically simple, with a single DC motor rotating a single joint which moves two splinted fingers. Numerous research works have explored various other designs, with a wide range of complexity. A selection of previously presented hand orthoses, along with the MyoPro are shown in Fig. 2.5. Some of these previously developed devices are also rigid and DC motor driven but with different linkage designs to the MyoPro [9,10,16,33,100–102]. A major challenge faced in the design of a device with rigid joints is needing to properly align those joints with the joints of the user. Over-constraining the finger's motion could easily lead to discomfort for the user and poor function of the device. A simple device developed by Gasser et al., shown in Fig. 2.5, uses a rigid gate-like mechanism to provide coupled motion of the index, middle, ring, and pinky fingers [10]. They solve the alignment problem by roughly placing the exoskeleton's axes directly in-line with the axes of

the finger joints. Strapping the hand to the device in a manner which allows for some
sliding between the skin and linkages prevents over-constraining the movement if some
alignment error is present. In-line placement of the joints is a simple approach to the
alignment problem but is limited. If a designer wants the fingers to be decoupled, for
example, it is not possible to place the exoskeleton directly in-line with the individual
metacarpophalangeal (**MCP**) joints as their axes are contained within the palm of
the hand. Chiri et al. resolved this problem by adding a passive prismatic joint at the
MCP, as can be seen in Fig. 2.6(c) [101]. A linear slide in the exoskeleton's MCP joint
prevents over-constraining the motion, which is necessary with the actuated rotation
for the MCP placed above the anatomical joint. Another design for circumventing
the problems associated with in-line joint placement is to use a four-bar linkage over
the dorsal surface of the hand [9], seen in Fig. 2.6(a). Two mechanical joints and
two anatomical joints make up each four-bar with the mechanical links sized so as to
maintain alignment between device and user throughout the finger's range of motion.
A benefit of the four-bar linkage is that no hardware needs to be placed between
the fingers, which is required with in-line joint placement and can restrict the user's
motion when the fingers are moved independently. Zhang et al. took yet another
approach to the joint alignment problem with what they called a "circuitous joint"
[102], shown in Fig. 2.6(b). A coupled pair of gears move along two pinions affixed to
the joint's proximal and distal segments. The joint creates a remote center of rotation
which can be aligned with the user.
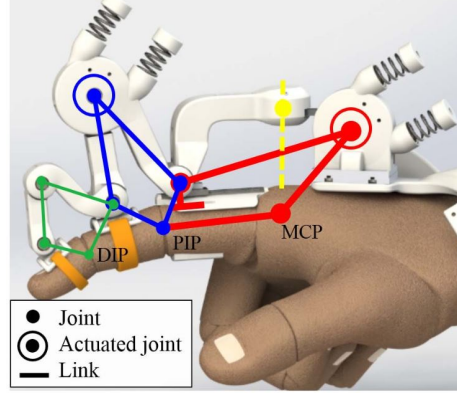
(a) Four-bar linkage [9]
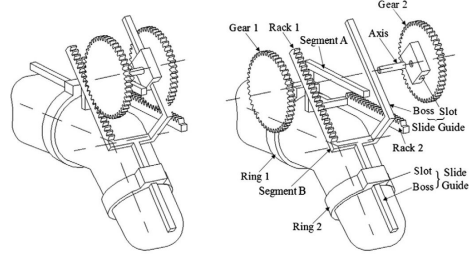
(b) "Circuitous joint" [102]
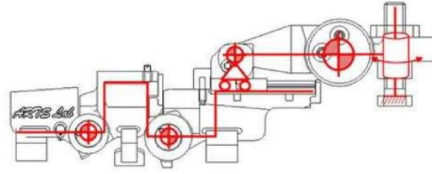
(c) In-line placement of IP joints with combined actuated rotation and slid-
ing passive DoF at the MCP [101]
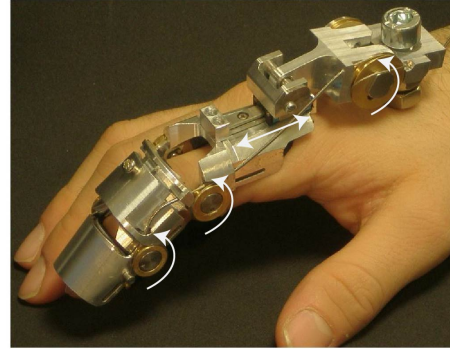
Figure 2.6: Joint kinematic designs for rigid linkage exoskeletons. Various implemen-
tations and methods of aligning the joints of a rigid exoskeleton with the joints of the
user.

2.2.2.2   Mechanically Compliant Hand Orthoses

Even with proper design, rigid exoskeletons still face difficulty with alignment, a need

for customization, and comfort. Soft hydraulic and pneumatic actuators have been

pursued by some due to their compliance, force potential, perceived safety, and sim-

plicity of coupling multiple DOF to a single actuation (i.e. pressure) source [103,104].
While early applications of pneumatics merely employed Mckibben muscles as com-
pliant actuators for rigid mechanisms [32], recently several groups have employed soft
robotics to make flexible finger-like actuated structures. The hydraulic actuators used
by Polygerinos et al. [6] in their rehabilitation exoskeleton follow similar principles to
the pneumatic acutators used by Yun [18], Nuritsugu [20], and several other research
groups [12, 105]. These actuators work on the principle of creating an anisotropic
strain profile across the actuator's thickness. An inextensible layer bonded to the
side of the actuator in contact with the hand's dorsal surface prevents strain while
the unconstrained outer surface is allowed to extend. This imbalance in strain causes
the actuator to curl towards the fingers, pushing them into flexion. Good analytic
models of these actuators are lacking due to the complexity of the deformations and
non-linearity of the materials used. Typically the motion is designed and character-
ized using finite element models (**FEM**) [15, 17, 19, 103, 104]. While hydraulic and
pneumatic actuators of this type are most common, Arata et al. achieved a similar
effect through the forced displacement of a flat blade of spring steel [15]. Illustra-
tions demonstrating the motion of Arata's actuator as well as the concept behind
pneumatic and hydraulic actuators are shown in Fig. 2.7. One negative of pneu-
matic and hydraulic systems is the size and weight of their control and actuation
units. The need for pumps, reservoirs, and valves makes packaging in a portable
manner difficult [106]. Polygerinos et al. did expanded on their rehabilitation ex-

(a) Reproduced from Arata [15]   (b) Reproduced from Ilievski [103]
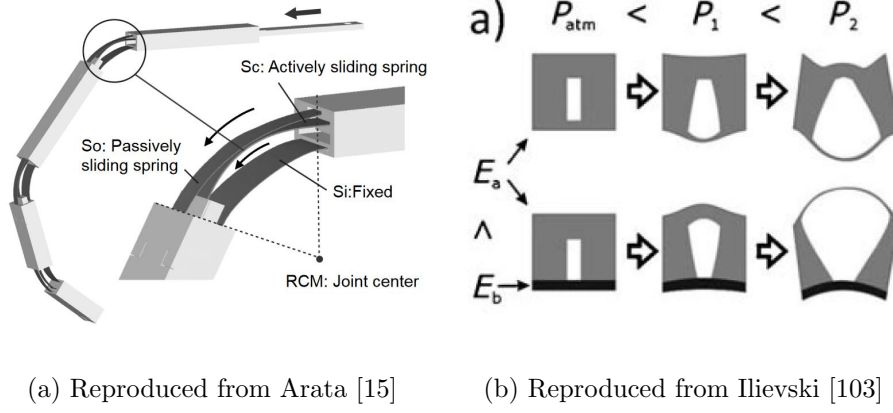
Figure 2.7: Examples of actuators designed to bend by creating anisotropic strain between multiple layers of material. (a) Arata achieved this by mechanically pushing an outer flat spring blade while (b) Ilievski demonstrates a similar principle using pneumatics. The pneumatic approach shows two methods, one creates a stiffness imbalance by having walls of differing thickness and one by bonding an inextensible layer to one surface.

oskeleton [19] with a portable version for assistance. A utility-belt like apparatus for containing the fluid reservoir, pump, valves, battery, and electronics weighing $3.3 lbs$ was used in place of a bench-top control box [17]. A similar setup was developed by Yap et al. [12]. The research group associated with Polygerino's work seemed to abandon the portable device, however, reverting to a dedicated benchtop design in future work [6, 107]. Many of the presented hydraulic and pneumatic devices are early stage prototypes, tethered to bench-top actuation. In Chapter 3 we explore the packaging and portability of a control system for Arata's exoskeleton in more depth with comparatively promising results [23].

2.2.2.3 Cable-Actuated Hand Orthoses

Another approach to assistive orthoses is to use soft cable or "tendon" actuated devices [11, 13, 14, 21, 98, 108–110]. These devices do not apply rigid kinematic constraints, rather, they apply forces to the segments of the fingers through tensioned cables. The manner in which these cables apply forces to the fingers is broadly similar among past designs, with an example being the glove of Kang et al. shown in Fig. 2.5(e) [98]. Cables are routed along the palmar surface of the finger to aid in flexion while a cable routed along the dorsal surface of the finger aids in extension, illustrated in Fig. 2.8. As a function of the cable having tension and not passing through the joint axes, torque is generated at each of the joints. These designs will be explored in more depth in Chapter 3. Randazzo et al. used a slightly different approach with a semi-rigid cable for pushing and pulling on the fingers, aiding in flexion and extension [108]. It's unclear from their work how effective this simple method is, but a commercial rehab glove, the Gloreha (Idrogenet srl., Lumezzane (Brescia), Italy), uses a similar approach. Tendon based devices have some downsides over rigid mechanisms, primarily they apply unsupported translational loads to the joints as a consequence of using a single cable to generate an applied torque. Depending on the torques required and the cable's moment arm, these loads may pose a risk to the users.
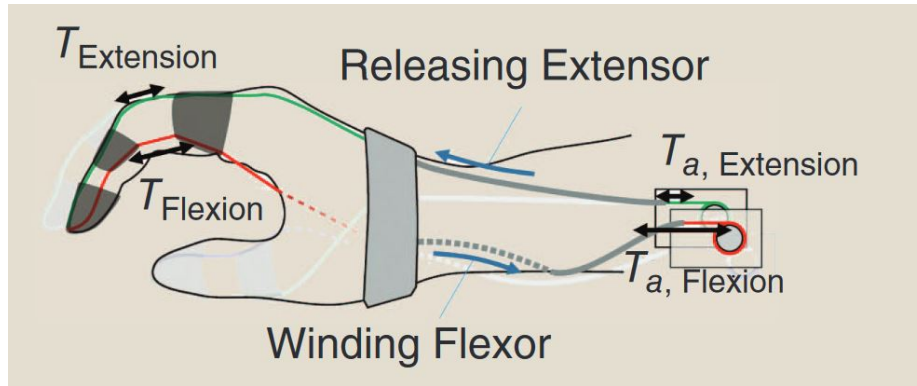
Figure 2.8: Depiction of the tendon-actuated glove developed by In et al. [13]. Palmarly routed cables provide flexion assistance while dorsally located cables assist extension. Pulleys are used to provide tension to the cables.

2.2.2.4 Clinical Testing of Hand Orthoses

Testing by research labs of powered hand orthoses on disabled populations has been somewhat limited. More commonly, an assessment of the constructed device's kinematics and measurement of the force they are capable of applying to the dorsal surface of the finger tip are often used to evaluate performance [12, 16, 102, 105]. In a few more mature designs, pilot studies with one or two disabled persons have been conducted. One such trial with the kinematically simple device of Gasser et al. on a single stroke patient showed that the time taken to remove the lid from a jar was significantly reduced wearing the device from $40s$ down to $10s$ [100]. The pilot study also showed that the improvements mostly came during grasping, as the subject had increased flexor tone in their hand and struggled to shape their hand around the jar when unaided. Once the subject grasped the jar, they were able to support it well

enough to remove the lid with and without the device. This is similar to the obser-
vations we made of the TBI patient in Fig. 2.3. Another pilot study, by Polygerinos
et al. using a soft hydraulic glove on a patient with muscular dystrophy, showed an
improvement from 10 to 14 blocks moved over a period of $60s$ in a Box-and-Block
test after the device had been put on [6]. The subject in this trial was described in a
separate publication as weak with no presence of spasticity or contractures [107].

2.2.2.5   Summary of Hand Orthoses as Assistive Devices

Review of past works in assistive devices demonstrates vastly different concepts of
how to assist finger motion using exoskeletons and orthoses. While there has been
some success with devices such as the MyoPro, use of powered hand orthoses has not
been widely adopted by disabled individuals. There are many factors contributing
to this such as device weight, cost, complexity, and function. Notably, many devices
are designed and evaluated on their ability to aid weakness in flexion, not to coun-
teract the flexed postures associated with UMN. Cross comparison of the relative
effectiveness of devices is also difficult as there are no standards for how devices are
evaluated. Many assessment metrics, such as the typical singular "force" value given
by research groups along with a workspace analysis, does little to quantify device
function. While the fundamental concept of assisstive hand orthoses seems valid, as
Myomo has demonstrated when matching the functionality of the device to the im-
pairments of the user, expanding upon the function offered by orthoses is necessary

45

to reach a larger portion of individuals needing hand assistance.

2.3 Bio-mimetic Hand Robotics

In deriving inspiration for hand orthosis designs, there are tangentially related works which are beneficial to explore. One such body of work is that of bio-mimetic robotic hands. These hands have life-like bones and joints and are actuated by life-like tendon networks. The designs are a study of how to robotically replicate the full natural motion of the hand. Limitations imposed by an orthosis, such as the inability to rigidly attach cables to the users bones or to route them through the palm of the hand, limit the degree to which these designs can be directly applied to orthoses. The function of the various structures, methods for regulating force between joints, methods for stabilizing joints, and the mechanics of constructing complicated tendon networks are interesting topics which are elucidated by the designs.

Examples of highly biomimetic hands are shown in Fig. 2.9. Work conducted under the guidance of Yoky Matsuoka over the course of a decade focused on replicating all components of the hand's anatomy in a functional physical model called the Anatomically Correct Testbed (***ACT***) hand [111–115]. More recently, Emanuel Todorov has continued on the work of the group with even more detailed robotic hand models [116, 117]. These works are periodically referenced in later chapters.
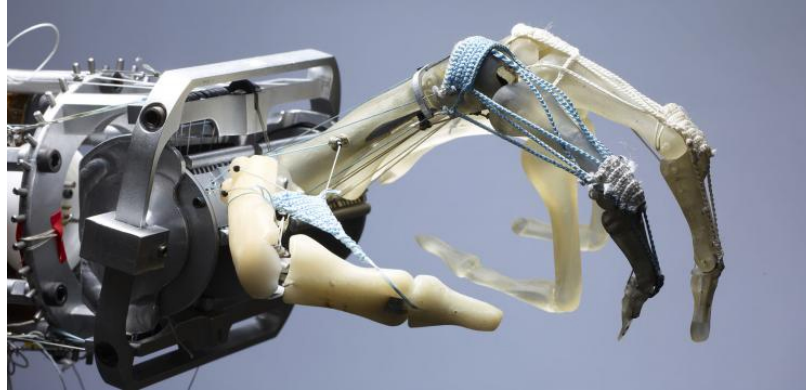
(a) The ACT Hand [115]

(b) Biomimetic Anthropomorphic Hand [117]

Figure 2.9: Examples of anatomically accurate robotic hands. Bone structures, joint kinematics, and tendon networks are replicated robotically in great detail. These designs may provide a source of inspiration for robotics engineers developing hand orthoses.

47

2.4 Summary

The prevalence of hand impairment due to neurological injury or disease establishes a strong need for new technologies to treat or assist the various manifestations of those impairments. What is evident from these manifestations is that counteracting increases in muscle tone as well as assisting with muscle weakness are both important mechanical functions. A lot has already been learned regarding the effectiveness of using robotics as a method to treat these impairments. The large body of work in the field of rehabilitation robotics has shown that increasing the amount of therapy an individual receives, through the use of robotics, can improve measured outcomes on assessment scales. Likewise, the field of powered assistive orthoses has developed several devices which have demonstrated significant benefits for users with specific subsets of impairments. Our research group has focused mostly on wearable assistive orthoses. We feel that there are merits in both fields, but enthusiasm of occupational and physical therapists for at-home robotic solutions has been shown, in our experience, more heavily towards assistive devices which would rectify the shortcomings of current offerings. An ultimate desire for assistive devices which provide a rehabilitative benefit has been the primary need identified by clinicians. We feel that such devices would see more regular use by patients than purely rehabilitative platforms as it would not be chore to do their therapy, but rather something that provides both immediate and long-term benefits.

2.5 Dissertation Contributions

- **Contribution 1**

  A presentation of two distinct methods for bi-directional cable actuation. Cable transmissions are popular in orthosis design due to the allowance for relocating the bulk and weight attributed to the motors away from the hand. In Section 3.1.3 and 3.1.4 we model and expand upon the antagonistically actuated pulley implemented by Delph et al. [11] while in Section 3.2.2 we design a push-pull Bowden cable and pair it with a sliding spring actuator developed by Arata et al. [15] for aiding finger flexion. Our experience with these two designs indicate that a push-pull design has benefits regarding packaging and precision in position control.

- **Contribution 2**

  A system architecture of a portable actuation unit for a hand exoskeleton. We present the necessary elements in a portable system needed to successfully actuate the hand and modify a device originally designed with hand-mounted motors to use remote actuation. This process allows for direct comparison of the benefits and drawbacks of both remote actuation and hand-mounted actuation.

- **Contribution 3**

An assessment of two distinct approaches for designing a hand orthosis. Here we look at a popular method of using cables or "tendons" routed through a soft glove to provide force to flex and extend the fingers. We document how deformations of the glove brought on by the application of tension to the tendons can lead to irregular finger postures or cause failures within the device. The other design evaluated, a more unique sliding spring design, is assessed on it's ability to conform to irregularities in an individual's hand. Further questions are raised regarding the forces each applies to the fingers, questions which are addressed in Chapter 4.

- **Contribution 4**

A protocol for tracking the fingers and load cells using motion capture cameras allowing for measurement of finger pose and force vectors during various activities. This protocol includes a method for fitting a kinematic model to a captured data-set, allowing for accurate tracking of different subjects. We also provide an assessment of the quality of this fitting technique through comparison with CT scans of 5 subjects.

- **Contribution 5**

The measurement of fingertip forces and joint torques during activities of daily living in a manner which can directly be applied to the design of hand orthoses. Activities were chosen based off consultation with occupational therapists to

ensure an orthosis would benefit an individual's ability to complete them. These
measurements will allow for better assessment and design of orthoses for aiding
finger flexion.

- **Contribution 6**

  The measurement of externally applied joint torques required to assist the ex-
  tension of fingers of individuals following a traumatic brain injury. Three sub-
  jects with increased flexor tone (hypertonia) had their thumb and index finger
  extended while tracking the finger motion and applied force vectors. Subjects
  were tested while relaxed and while attempting to volitionally extend. These
  measurements will allow for better assessment and design of orthoses for aiding
  finger extension.

- **Contribution 7**

  Demonstration of how the measurements made in Chapter 4 can be applied to
  better design an orthosis. Actuators are sized by calculating the power needed
  to assist the extensions performed in Section 4.4. The tendon path, motor
  gearing, and ball-screw selection are also designed around the requisite forces.

- **Contribution 8**

  Construction of an orthosis, it's actuation unit, and software interfaces for aiding
  finger extension. We sought to develop a capable research platform that is not
  far removed from a practical assistive orthosis. The device is designed to be

well-packaged, portable, and reasonably lightweight.

2.6   Dissertation Overview

This chapter presented the need and population characteristics for advanced hand orthoses. Descriptions of the resulting motor deficits were included along with a review of prior robotic devices developed for treating these deficits. The information presented is a necessary background to understanding the motivation and thought process behind work presented in later chapters.

Chapter 3 presents work conducted towards better understanding the robotic system design of hand orthoses. Applied work with previously developed prototypes outlines the components need for an orthosis, as well as some of the outstanding questions regarding their optimization.

Chapter 4 presents modeling and studies of able-bodied and impaired grasping as it pertains to orthosis design. We better quantify and describe some of the critical design criteria of an orthosis such as the joint torques needed to complete activities of daily living and the assistance needed to extend the fingers of individuals with increased flexor tone in the hand.

Chapter 5 presents the design of a cable-actuated orthosis for extending the fingers against increased flexor tone. Methods for improving efficiency, packaging, and function over previous prototypes are detailed.

Chapter 6 summarizes this work, it's impact, and the questions raised during it's completion leading to suggestions for future work.

CHAPTER 3

Evaluation of Orthotic Technologies:

Assessment and Refinement of Previous Work

Understanding the limitations of a technology, or unanswered questions in a field of research, is often difficult without prior application experience. Design constraints related to packaging, ergonomics, and maufacturability become unavoidably apparent when building physical hardware. Gaps in published data needed for accurate modeling and assessment are similarly evident after going through the design process. To begin our work in the field of hand orthotics, we gained application experience with two very distinct prototypes; one a tendon actuated design developed by Delph et al. at WPI [11] and one a sliding-spring design developed by collaborators at Kyushu University and ETH Zurich [15]. In this chapter, we present work we conducted on refining and updating these devices. Evaluation of their performance is presented and the necessary system architectures are determined. While making claims that

one engineering design concept is objectively better or worse than another is often dubious, gaining experiences with multiple approaches allows for reasoning about inherent strengths and weaknesses of each. We try to objectively present our design process, point out remaining limitations of specific design choices, while suggesting ways in which those limitations could be addressed. Finally, we outline outstanding questions regarding function of an orthosis which need to be answered in order to improve upon the design process. The contributions of this chapter can be summarized as:

- **Contribution 1**

  A presentation of two distinct methods for bi-directional cable actuation. Cable transmissions are popular in orthosis design due to the allowance for relocating the bulk and weight attributed to the motors away from the hand. In Section 3.1.3 and 3.1.4 we model and expand upon the antagonistically actuated pulley implemented by Delph et al. [11] while in Section 3.2.2 we design a push-pull Bowden cable and pair it with a sliding spring actuator developed by Arata et al. [15] for aiding finger flexion. Our experience with these two designs indicate that a push-pull design has benefits regarding packaging and precision in position control, at the trade-off of a thicker cable and housing.

- **Contribution 2**

  A system architecture for a portable actuation unit for a hand orthosis. We

present the necessary elements in a portable system needed to successfully actuate the hand and modify a device originally designed with hand-mounted motors to use remote actuation. This process allows for direct comparison of the benefits and drawbacks of both remote actuation and hand-mounted actuation. In particular, we were able to reduce by half the amount of weight placed directly on the hand at the cost of a greater system weight and reduced efficiency.

- **Contribution 3**

  An assessment of two distinct approaches for designing a hand orthosis. Here we look at a popular method of using cables or "tendons" routed through a soft glove to provide force to flex and extend the fingers. We document how deformations of the glove brought on by the application of tension to the tendons can lead to irregular finger postures or cause failures within the device. The other design evaluated, a more unique sliding spring design, is assessed on it's ability to conform to irregularities in an individual's hand. Further questions are raised regarding the forces each applies to the fingers, questions which are addressed in Chapter 4.

The impact of this chapter is in providing context and motivation for work conducted in Chapters 4 and 5 which address the identified gaps in knowledge and further progress the performance of these two orthoses. The lessons learned in this chapter

regarding good design practice and the limitations of certain designs has broader impact to those working in the field as many others have explored similar design elements including cable-actuated soft gloves [13, 14, 21, 98, 108–110] and cable-based remote actuation [9, 16, 98, 102, 108, 109].

3.1 Evaluation of a Tendon-Actuated Glove

Work originally conducted in the WPI AIM Lab by Delph et al. [11] explored the use of soft, tendon-actuated orthoses for the hand which resulted in the prototype shown in Fig 3.1. The concept, in part, mimics the function of the hand's extrinsic muscles with motor units placed extraneously and tension transmitted to the phalanges via inextensible cables similar to the long tendons of the *flexor digitorum profundus* (**FDP**) shown in Fig 3.2. The routing of the palmar cables closely mimics the tendons of the FDP by crossing superficially to the carpal tunnel, running medially down the palmar surface of each finger, and inserting at the distal phalanx. The point-like cable guides, however, detract from the anatomical accuracy wherein cruciform and annular ligaments known as "pulleys" constrain the tendon along the lengths of the phalanges preventing palmar excursions. Injury to these pulleys in humans can result in a deformity referred to as "bowstringing" which is similar to the cable motion seen on the prototype. This deformity results in an increased flexion moment arm, as the cable or tendon moves away from the joint center. For the orthosis this increased

Figure 3.1: The soft tendon-actuated hand exoskeleton originally developed by Delph et al. [11]. 3D printed plastic cable guides (orange pieces) are attached to the palmar and dorsal surfaces of a neoprene glove. Kevlar cables are used as "tendons" to apply flexion and extension forces to the fingers.

moment arm is somewhat beneficial as smaller tension forces can be used to provide sufficient flexion torques, in humans it can lead to extension deficits due to an imbalance in antagonist forces [118]. Bowstringing does hamper the orthosis' ability to assist in daily tasks as holding objects with enveloping grasps interferes with the tendon path.

The extensor design of Delph et al.'s original prototype was not as biologically inspired as that of the flexors. In the design, a single cable is guided medially down the dorsal surface of each finger, inserting into the distal phalanx. This design is simple
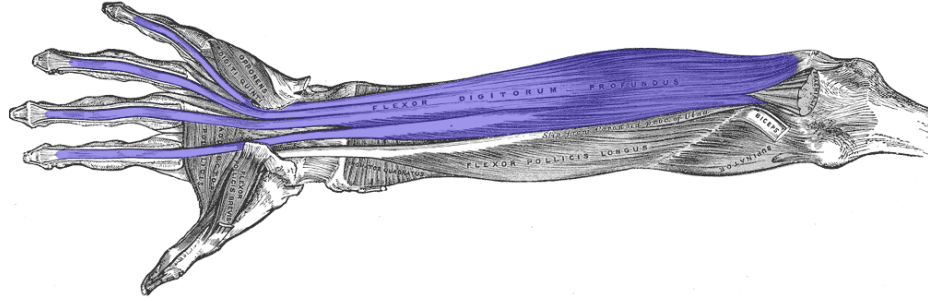
Figure 3.2: Anatomy of the flexor digitorum profundus. Reproduced from https://commons.wikimedia.org/wiki/File:Flexor-digitorum-profundus-horizontal.png

in comparison to the extensor hood of the human hand which plays a critical role in distributing the tension supplied by the *extensor digitorum communis* (**EDC**), the lumbricals, and the interossei between the DIP, PIP, and MCP joints. The simplified design implemented by Delph et al. suffers from a small moment arm at each of the joints, sharp pressures applied to the user where the tendon crosses each joint, and instability of the tendon path causing the tendon to slip to either side of the joints rendering it ineffective.

The original concept by Delph et al. provided an interesting take on the orthosis concept. The softness and compliance of the device make it comfortable to wear with a very natural feeling when used to assist with finger flexion. The non-rigid kinematics meant precise alignment and customization for a user is not needed for the device to function effectively. The materials used are also durable while keeping weight on the hand to a minimum. Since this work, several other groups have explored similar concepts of using tendons routed through fabric or flexible polymer gloves [13, 14, 21, 98, 108–110]. These devices were covered briefly in the Chapter 2.2.2. The

work of Kang et al., which can be seen in Fig. 2.5(e), is a refined example of the concept with improved ergonomics and packaging [98] to the original design of Delph et al.

Following on from the initial work of Delph, the contributions presented here are an expanded modeling and evaluation of Delph et al's device mechanics [22]. Limitations of the device are quantitatively, as well as qualitatively, assessed and documented. Minor changes are also made to the device to improve the accuracy of the model. Finally, we present a list of outstanding issues indicated by observation of the device function and feedback from clinicians.

3.1.1 Description and Observation of the Tendon Actuated Orthosis of Delph et al.

The orthosis presented by Delph et al. consists of a soft tendon-actuated glove, an actuation unit to provide tendon tension located inside a portable backpack, and a network of Bowden cables to connect the two. The soft nature of the glove means that the the user's movements are not rigidly constrained and thus the glove does not require precise alignment with the user's joints. The Bowden cables allow for placing the actuation unit, which is large and bulky weighing 13.2 lbs, away from the hand. The choice of remotely locating the source of actuation is common in hand orthoses as space on the hand is severely limited, but, there are trade-offs in efficiency, complexity,

total system weight, control precision, and reliability. Managing these trade-offs is crucial for obtaining an effective design.

The construction of the glove uses point-like plastic cable guides glued directly to the fabric. This construction method has both positive and negative features. On the positive side, the construction is simple, light weight, and non-restrictive to the user. Negatively, the soft nature of the glove allows for motion of the cable guides relative to the hand when tension is applied to the tendons. This motion can result in several distinct deformations of the glove which lead to poor performance. Since the glove is under-actuated, in that one tendon is responsible for flexing or extending the three separate joints, active compensation of these deformations is not possible and thus result in irregular and undesired finger postures. Pictures of these deformations are shown in Fig. 3.3. In flexion, the primary deformation is pulling of the cable guides radially away away from the finger surface. This deformation changes the moment arms to the joints and changes the tendon path. Movement of the cables in this manner makes accurate modeling of the joint torques or the expected tendon excursions difficult as well as interferes with the ability to grasp objects due to further intrusion of the tendon into the grasping envelope.

In addition to the flexion deformity, extension deformities exist which are severely detrimental to performance. Since the extension cable passes over the joints, which are typically convex in shape, the tendon path becomes inherently unstable when under tension. The cable has a tendency to slip to the side of the joint, moving the

(a) Index Flexor Tensioned

(b) Index Extensor Tensioned

(c) Index Extensor Tensioned

(d) Index Extensor Tensioned
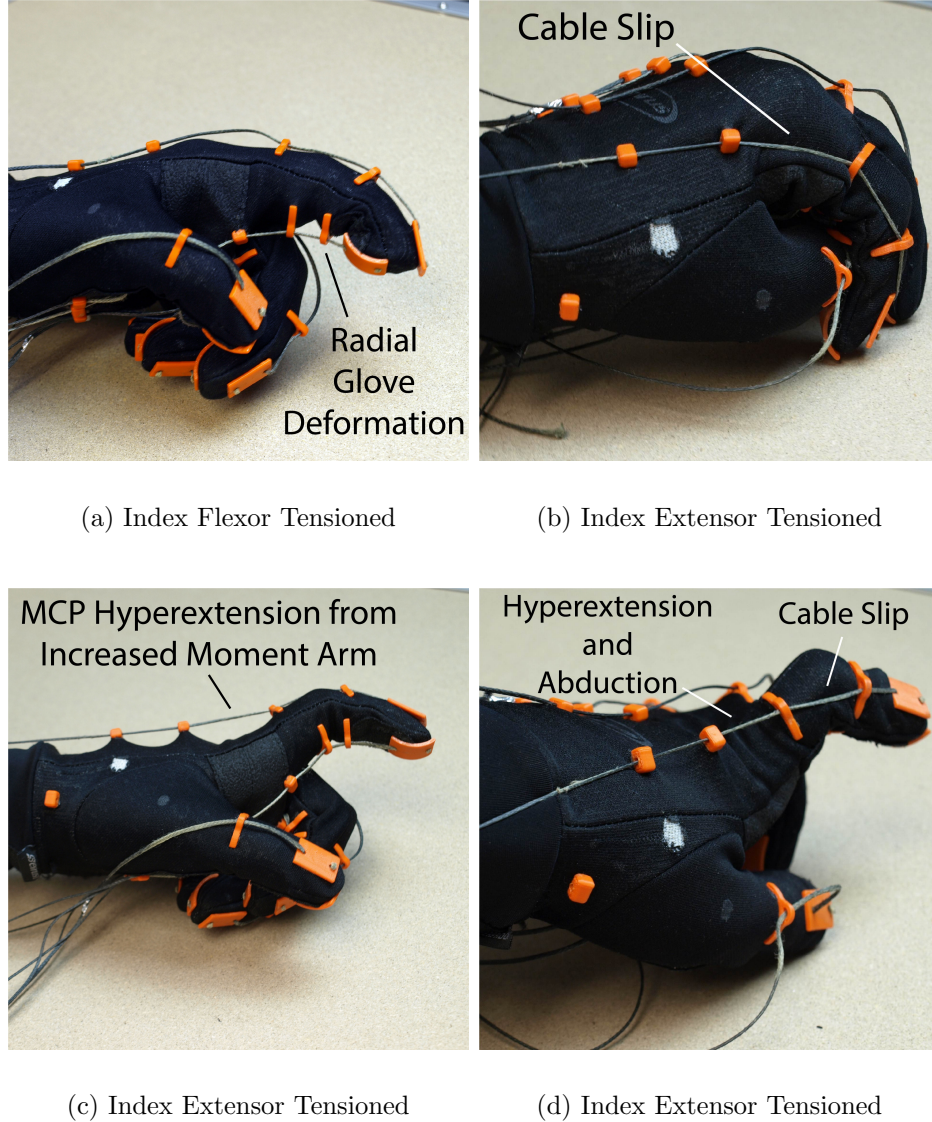
Figure 3.3: Various deformations of a soft tendon actuated glove caused by the application of tension its tendons. (a) Tension in the flexor tendon pulls palmar cable guides away from the finger surface interfering with grasp and complicating accurate modeling. (b) Tension in the extensor tendon causes it to slip off the joints, the tendon now passes near the joint axes reducing the applied torque. (c) Extension of the MCP causes the extensor tendon to pull away from the joint, increasing the moment arm forcing the MCP into hyperextension. (d) A combination of cable slip at the PIP joint and hyperextension of the MCP causes an irregular finger posture.
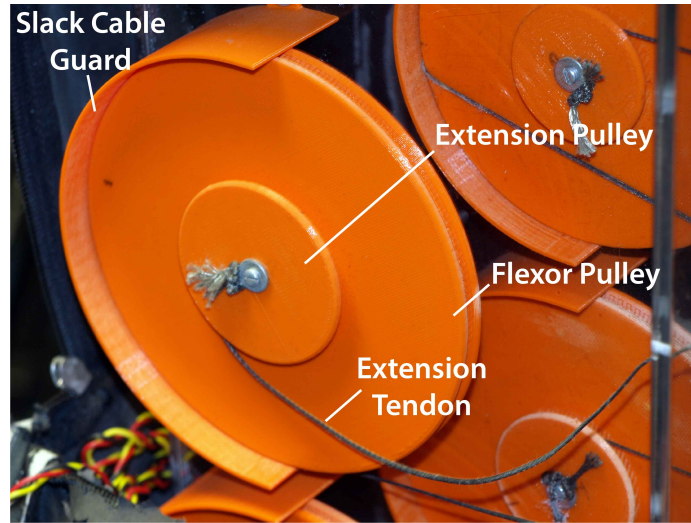
Figure 3.4: The antagonistically wound pulleys used in the orthosis developed by Delph et al. Two pulleys of different radius are joined and used to regulate the excursions of the flexor and extensor tendons.

tendon closer the joint axis and thus reducing its moment arm and applied torque.

In some cases, the cable will pass below the joint axis and force the joint into flexion instead of extension, as can be seen with the PIP joint in Fig. 3.3(d). Even if the cable remains balanced along the center-line of the finger, extension of the MCP typically occurs first. Once the MCP is fully extended, the tendon begins to pull away from the surface of the MCP, increasing its moment arm and forcing the MCP into hyper-extension. Extension of the inerphalangeal (*IP*) joints is not typically possible without hyperextension of the MCP. Fig. 3.3(c) is representative of a best-case extended finger posture obtained with the device.

Tension for the tendons is provided via pulleys attached to five small servo motors, shown in Fig. 3.4. Each motor actuates both the extensor and flexor tendons for a given finger. This is accomplished by separating the pulleys into two sections which

are antagonistically wound, so that as one tendon is being shortened the other is being lengthened. The sections for flexion and extension are made with different radii, as it was found empirically that a given change in length of the flexor did not result in an identical change in the extensor. These radii were made constant, however, based on the total change in tendon lengths between full flexion and full extension. This assumption is imperfect, as will be shown in Section 3.1.4, which contributes to the untensioned tendon becoming slack at various points in the range of motion. Furthermore, the previously described deformations of the cable guides on the glove also cause imbalances in tendon length leading to additional slack in untensioned tendons as force is applied to their tensioned pairs. This slack can lead to failure as a result of the tendon becoming entangled within the actuation unit. Delph et al. added a guard to contain the slack within the pulley. While this partially alleviates the entanglement issue, slack also causes control issues as it leads to a large amount of backlash between flexion and extension. This inability to regulate tendon length and minimize slack was a major shortcoming of Delph et al.'s design. In Section 3.1.4 we expound upon these issues and explore possible solutions. In Section 3.2.2 we present an alternative to the antagonistically wound pulley with a push-pull Bowden cable design. This design is shown to be effective at flexing the fingers under compression and while being able to regulate its position to within $\pm 0.3mm$ at its output against perturbations.

The final portion of the system, the Bowden cable transmission, is something that

has been used by many other orthosis designs [16, 98, 102, 119]. The orthosis designed by Delph et al. uses a flexible Kevlar cable running through a semi-rigid plastic tube functioning as the cable housing. Some deficiencies in this design, such as losses in the transmission, housing stretch, housing buckling, and backlash, were noticed. In Section 3.2.2 we explore the causes for these deficiencies and explore best practices to optimize transmission performance.

3.1.2 Design Modifications to the Tendon Actuated Orthosis of Delph et al.

After observing the function of the orthosis as it was originally designed by Delph et al., we made a few minor changes to improve the consistency of the orthosis' function so that we could more predictably model its movements. The first change implemented was the addition of rubber rings passing through each of the palmar cable guides. These rings wrap around the fingers and increase the radial stiffness of the glove in the regions where force is applied. The motion of the cable guides seen in Fig. 3.3(a) was reduced with this modification. The second modification was the addition of sectioned tubes running medially down the dorsal surface of each finger to guide the extensor cables more accurately and prevent some of the instability seen in Fig. 3.3(b) and 3.3(d). To completely rectify the extension deficits observed in Section 3.1.1, however, a more extensive redesign was clearly needed. This is later

addressed in Chapter 5 where we design and construct an orthosis for extending the fingers.

(a) Palmar View   (b) Dorsal View

Figure 3.5: An updated version of the glove developed by Delph et al. [11]. Rubber rings are added to stiffen the glove at the attachments of the palmar cable guides, preventing excessive motion under load. Guides for the extension tendons are placed on the dorsal surface to reduce instability of the cable path.

3.1.3 Modeling of Tendon Excursions and Forces in a Tendon-Actuated Orthosis
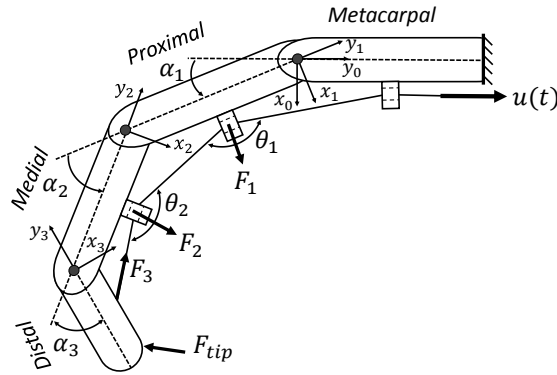
(a) Flexor tendon routing and joint reference frames
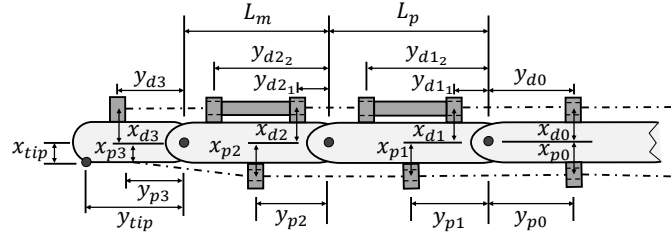
(b) Physical parameters for the modeling of tendon motion

Figure 3.6: Simplified model of flexor tendon motion in a soft tendon-actuated glove. The fingers are modeled with three fixed center revolute joints connecting 4 rigid segments. Cable guides are assumed rigidly fixed relative to their respective finger segments.

In order to better understand the function of the orthosis as observed in Section 3.1.1, an analytical model of the tendons needed to be created. The work conducted

by Delph et al. was mostly empirically based from iterative prototyping and testing. Issues such as the formation of slack in untensioned cables, however, can better be understood and remedied through modeling. The manner in which cable tensions apply forces to the orthosis and contribute to joint torques can also be better understood. Here, we construct such a model as an expansion of the previously presented design.

To construct our model, we made several simplifying assumptions regarding the finger kinematics and orthosis behavior. These assumptions are as follows:

- The metacarpal bone is fixed and cable guide forces do not cause any rotation of the segment

- Each joint is a pure revolute joint with a fixed axis center

- The tendon passes through the cable guides with negligible friction

- No movement of the cable guides occurs under application of force

Under these assumptions, and using the parameters of Fig. 3.6, the finger is modeled as a planar three link kinematic chain. The transformation matrix from reference *frame i* to *frame i+1* is given by Eq. 3.1

$$T_{i+1}^i = \begin{bmatrix} cos(\alpha_{i+1}) & -sin(\alpha_{i+1}) & 0 \\ sin(\alpha_{i+1}) & cos(\alpha_{i+1}) & -L_{i \to i+1} \\ 0 & 0 & 1 \end{bmatrix} \quad (3.1)$$

To model the movement of the tendons and the forces at a given pose, all cable guide positions were written in *frame 0* using Eq. 3.2, where $P_{cg_i}^i$ is the position vector of cable guide i in *frame i*. The vector, $v_{cg_j}^{cg_i}$, pointing from guide i to guide j, in the home reference frame, is calculated using Eq. 3.3, it's unit vector is calculated with Eq. 3.4.

$$P_{cg_i}^0 = T_i^0 P_{cg_i}^i \tag{3.2}$$

$$v_{cg_j}^{cg_i} = P_{cg_j}^0 - P_{cg_i}^0 \tag{3.3}$$

$$\hat{v}_{cg_j}^{cg_i} = \frac{v_{cg_j}^{cg_i}}{|v_{cg_j}^{cg_i}|} \tag{3.4}$$

Using the vectors $v_{cg_j}^{cg_i}$ we can define the change in length of the flexor tendon from a fully extended position using Eq. 3.5. Here, A, is used to represent the set of joint angles α_{MCP}, α_{PIP}, and α_{DIP}. $A = 0$ is used to represent a fully extended finger with $\alpha_{MCP} = 0$, $\alpha_{PIP} = 0$, and $\alpha_{DIP} = 0$.

$$\Delta l_{flexor}(A) = (|v_{cg_1}^{cg_0}(A)| + |v_{cg_2}^{cg_1}(A)| + |v_{cg_3}^{cg_2}(A)|) - (|v_{cg_1}^{cg_0}(0)| + |v_{cg_2}^{cg_1}(0)| + |v_{cg_3}^{cg_2}(0)|) \tag{3.5}$$

The bend angle, θ, at each cable guide is calculated in Eq. 3.6 using the dot product of unit vectors pointing from cable guide i to the guides on the adjacent

links.

$$\theta_i = cos^{-1}(\hat{v}^{cg_i}_{cg_{i+1}} \cdot \hat{v}^{cg_i}_{cg_{i-1}}) \tag{3.6}$$

Under the frictionless cable guide assumption, force vectors F_1 and F_2 bisect the bend angles θ_1 and θ_2 respectively. The magnitudes of the cable guide forces F_1 and F_2 are given by Eq.3.7. The distal force vector F_3 has magnitude $u(t)$. The force vectors at the proximal and medial cable guides are given by Eq.3.8. The force vector at the distal guide is given by Eq.3.9

$$|F_i| = 2u(t)cos(\frac{\theta_i}{2}) \tag{3.7}$$

$$F_i = |F_i|\frac{\hat{v}^{cg_i}_{cg_{i+1}} + \hat{v}^{cg_i}_{cg_{i-1}}}{2} \tag{3.8}$$

$$F_3 = u(t)\hat{v}^{cg_2}_{cg_3} \tag{3.9}$$

Modeling of the extension tendon path differs from the point-to-point modeling of the flexor tendon because the extensor tendon follows the dorsal surface of the finger. The tendon paths for the extensors are modeled using an assumption that the dorsal surface of the joints act like constant radii pulleys with fixed rotation centers. In Chapter 4 we conduct motion capture studies which verify the assumption of a fixed

axis center is reasonable to make. A depiction of the extensor model is shown in Fig. 3.7 where r_{MCP}, r_{PIP}, and r_{DIP} are the fixed radii of the MCP, PIP, and DIP joints respectively. The flexion angle of each joint, α_{MCP}, α_{PIP}, and α_{DIP}, are defined as $0°$ at full extension with flexion a positive rotation about the z-axis.
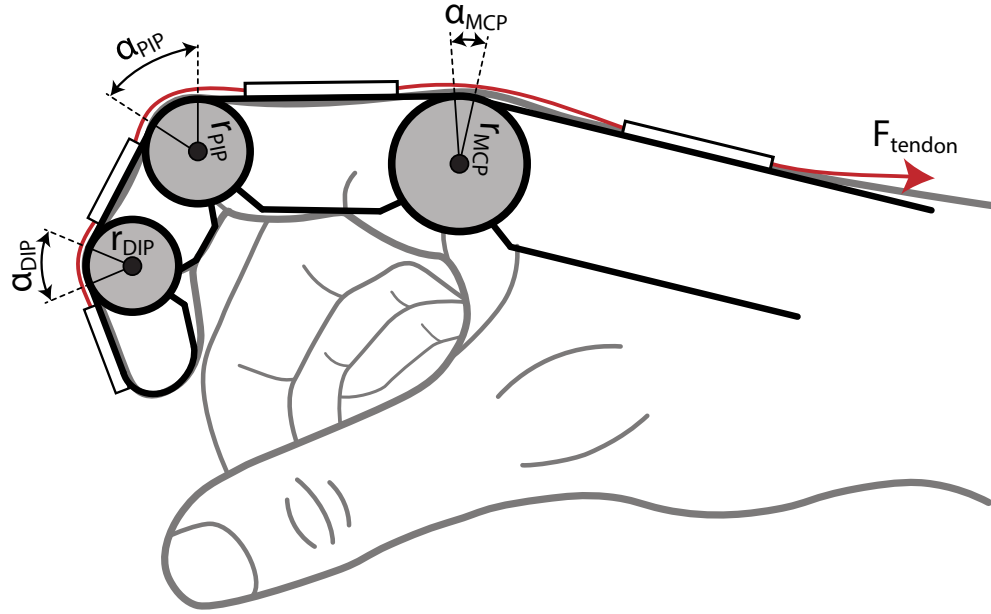
Figure 3.7: Simplified model of extensor tendon motion in a soft tendon actuated orthosis. It is assumed that the dorsal surface of each joint acts as a constant radius pulley.

The extensor tendon excursion can be approximated by summing the changes in arc length of the tendon across the three joints from the fully extended position. This excursion is given by Eq. 3.10 where $\Delta l_{extensor}$ is the change in tendon length from the fully extended position.

$$\Delta l_{extensor} = r_{MCP}\alpha_{MCP} + r_{PIP}\alpha_{PIP} + r_{DIP}\alpha_{DIP} \qquad (3.10)$$

3.1.4 Evaluation of Antagonistically Actuated Cables in a Tendon Actuated Orthosis
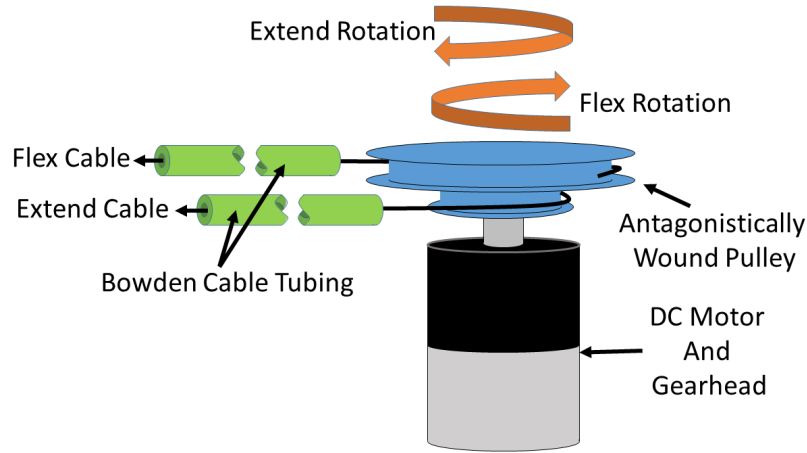
Figure 3.8: Diagram of an antagonisitcally wound pulley and motor assembly. Clockwise rotation of the motor shaft provides tension to the extensor tendon while counterclockwise rotation provides tension to the flexor.

The model of tendon excursions presented in Section 3.1.3 allows us to now understand a component of the cable slack problems experienced with the original orthosis as were described in Section 3.1.1, and reason about possible solutions. We accomplish this by first selecting the parameters listed in Figs. 3.6 and 3.7 so as they are representative of an average user, specifically the parameters are based on the able-bodied adult male that the prototype was built for. Based on Table 5.1, as well as measurements made on the adult male, Table 3.1 specifies the parameters used in the model. Though these values are somewhat arbitrarily chosen, the purpose here is to

Table 3.1: Parameters related to finger size and orthosis construction used for modeling tendon excursions in a tendon actuated glove.

Parameter	Value (mm)
L_p	47
L_m	26
y_{tip}	25
r_{MCP}	11
r_{PIP}	7
r_{DIP}	5
x_{p0}	18
x_{p1}	17
x_{p2}	17
x_{p3}	9
y_{p0}	20
y_{p1}	-23.5
y_{p2}	-13
y_{p3}	-12.5

demonstrate a representative behavior of the glove which would not be fundamentally different with slightly different sized hands.

A key issue thought to be associated with the antagonistically wound pulley presented by Delph et al. [11] was the potential for a non constant ratio of flexion and extension tendon excursions. To investigate this, we simulated three different flexion motions of the index finger and calculated the instantaneous change in tendon length throughout these motions. We used these changes in cable length to calculate representative plots of the instantaneous ratio between flexor and extensor tendon movements. For these motions, it was assumed the PIP and DIP joint motions were coupled and equal to each other. The flexion motions tested were as follows:

- MCP flexion followed by flexion of the IP joints

- IP flexion followed by flexion of the MCP joint

- MCP flexion and IP flexion in unison with each other

These motions are representative of what is observed while using the orthosis, in particular flexion of the IP joints followed by flexion of the MCP is commonly how the glove is observed to flex a relaxed finger. Since the glove is under-actuated and does not rigidly constrain the fingers, coordination of the joint motions is not possible and the resulting motion is dependent on the sum of the forces acting on the finger. In particular, the muscle contractions and passive joint stiffness of the user dictate the finger motion when the finger is not in contact with any external objects. Plots of these motion profiles are shown in Fig. 3.9(a).

The instantaneous change in tendon length was calculated by discretizing the joint motion of Fig. 3.9(a) into N steps. The tendon excursions described by Eqs. 3.5 and 3.10 were calculated at each step, n. The ratio of flexor excursion to extensor excursion, $R_{excursion}$ was then calculated using Eq. 3.11.

$$R_{excursion}(n) = \frac{\Delta l_{flexor}(n) - \Delta l_{flexor}(n-1)}{\Delta l_{extensor}(n) - \Delta l_{extensor}(n-1)} \qquad (3.11)$$

Plots of the ratio between flexor and extensor excursions for the three motion profiles are shown in Fig. 3.9(b). As expected, the ratio is not constant meaning the fixed radius pulleys used by Delph were contributing to the issues associated with
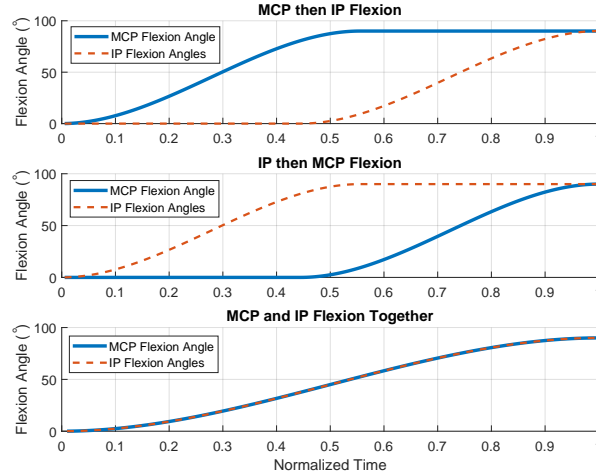
(a)
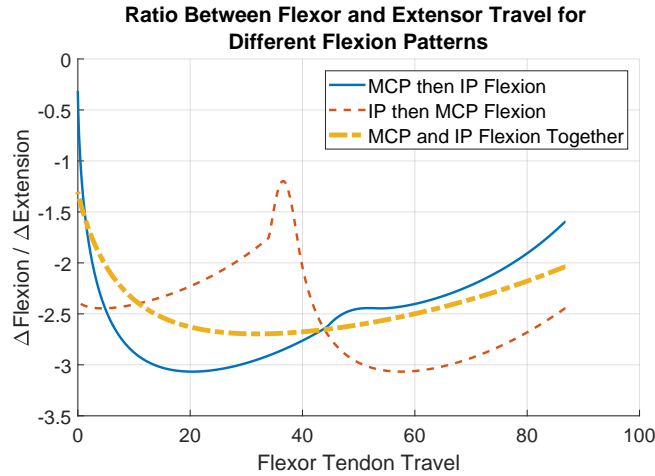
(b)

Figure 3.9: Simulated ratios between flexion and extension tendon excursions for the index finger of an adult male. (a) 3 flexion profiles were simulated, one in which the MCP flexes fully followed by IP joint flexion, one in which the IP joints flex followed by MCP flexion, and finally one in which MCP and IP joints flex in unison. (b) The results show that the ratio between flexion and extension excursions are not constant and also depend upon the pattern of joint motion.
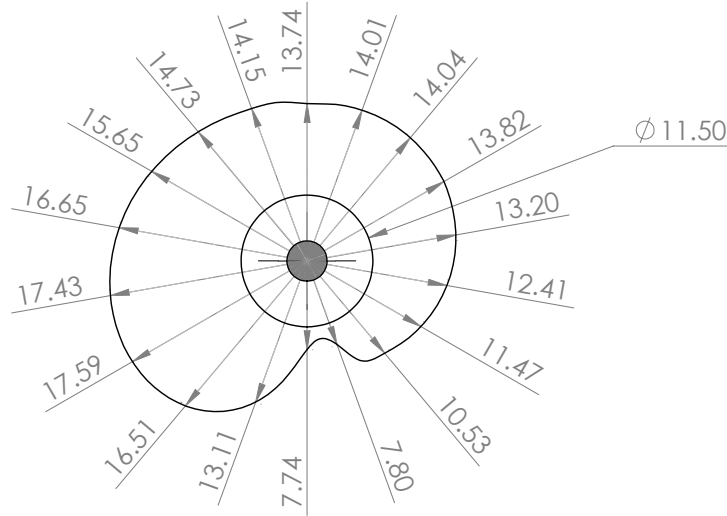
Figure 3.10: An eccentric profile antagonistic pulley design for non-constant ratios of flexion and extension tendon excursions. This pulley is designed from the profile of IP then MCP flexion of Fig. 3.9. The concave portions of the pulley would make it ineffective at regulating the motion between the two cables.

slack in untensioned tendons. An option for improving upon Delph's design would be to design an antagonistic pulley with non-constant radii based off the calculated ratios of Fig. 3.9(b). To illustrate this, we designed a pulley with non-constant radius shown in Fig. 3.10. A fixed radius extension pulley was used with a circumference equating one complete pulley rotation to the full range of motion of the finger. The shape of the flexor pulley was defined from the calculated excursion ratio using the motion of IP flexion followed by MCP flexion, as this is the commonly observed motion when using the glove.

The design of the variable radius pulley in Fig. 3.10 would not completely solve the problems associated with the actuation unit developed by Delph et al. An obvious issue is the presence of concave regions within the shape, which would prevent the

tendon from following the surface of the pulley. This could be resolved by making both the extensor and flexor pulleys variable in radius. To constrain the design in this case a cost metric, such as one which minimizes the maximum radius of the pulley and places a large penalty on concavity, would need to be added. Another issue with this pulley is the physical size of it. A render of what a constructed pulley would look like is shown in Fig. 3.11. The overall diameter of the pulley would be about *42mm*. This limits packaging options for the actuation unit. Ideally the actuation unit should be thin, small, and lightweight. We later present in Section 3.2.3 an actuation unit that is only *25mm* tall by using linear actuators as opposed to motor-driven pulleys. To compete with this design using a pulley such as the one in Fig. 3.11 would require pairing the pulley with an unusually flat motor, limiting design options. The actuation unit presented by Delph et al. was impractically large, in part because of the need to contain such large pulleys within it. A possible solution for this packaging problem would be to make a multi-turn variable radius pulley which would wind the tendons along a helical profile. This would allow for a reduction in the overall pulley diameter while still maintaining the specified ratios throughout the tendon pull. However, we ultimately decided not to pursue these design paths as they would not alleviate the primary issue revealed by Fig. 3.9, that is the relationship between flexion and extension is dependent upon the trajectory that the finger takes. As was mentioned earlier, the under-actuated nature of the design prohibits coordination of joint motions and thus the trajectory will not be
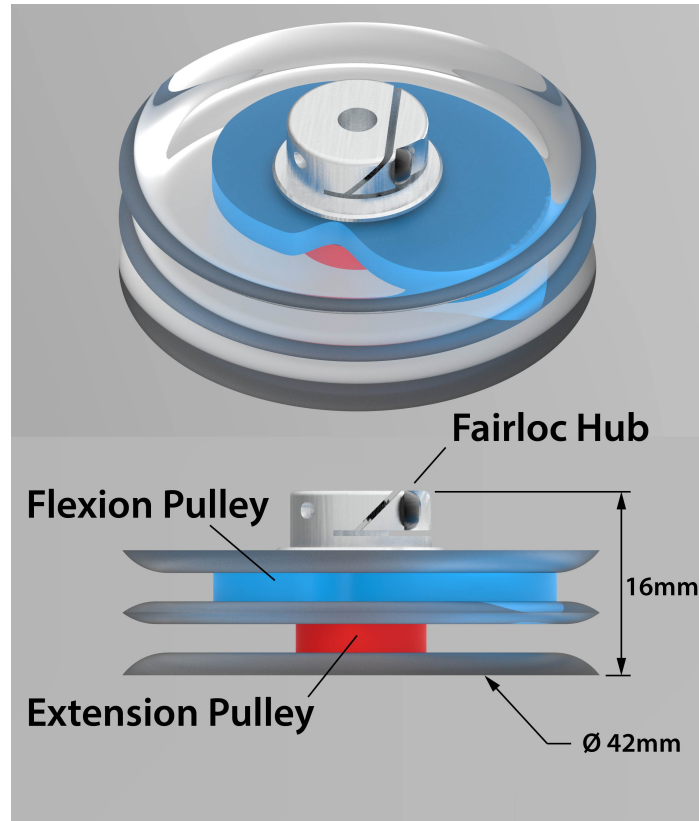
Figure 3.11: Conceptual implementation of a variable radius antagonistic pulley design.

consistent. Hard coding one of the profiles from Fig. 3.9 into the pulley design would only be beneficial in the rare occurrence that the finger follows the trajectory that the design is based on.

The issue of cable slackness from antagonistically wound pulleys has been approached by other research groups using self adjusting or "slack-enabling" mechanisms [13, 109, 119]. One such device is shown in Fig. 3.12 which allows for slack but manages it so as to prevent derailing of the tendon and failure of the actuation unit. It does not eliminate the precision issues associated with backlash caused by slackness. One could also argue that the added weight, bulk, and complexity of such
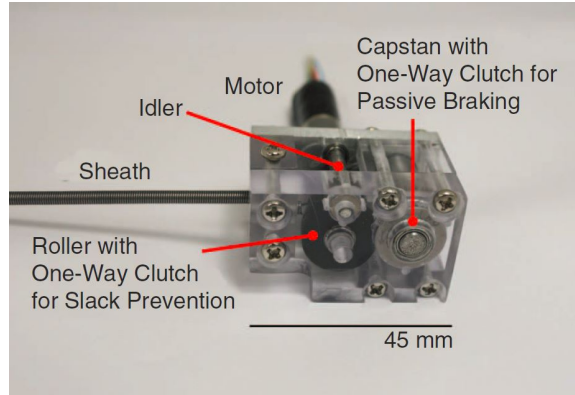
Figure 3.12: Reproduced from In et al [13]. Above is a slack-enabling actuator which compensates for cable stretch, glove deformation, and the non-constant relationship between flexion and extension cables.

mechanisms offsets the benefits of the antagonistic approach and a second motor would provide more control without much drawback.

3.1.5 Ergonomics of a Tendon Actuated Glove
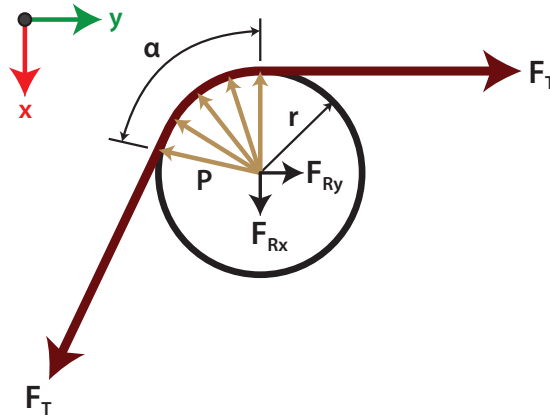
Figure 3.13: Model of pressure exerted by extensor tendon onto the joints by a soft tendon actuated glove.

One issue observed with using the glove of Delph et al. for extension was the

discomfort associated with tension in the extensor cable. As was described in Section 2.1.1, individuals with the upper motor neuron syndrome can commonly exhibit resting flexed postures associated with spasticity and increases in resting muscle tone. Counteracting these forces can require substantial tension in the glove's extensor tendon. Due to the thinness of the cable and it's use of the user's skin as a load-bearing surface, high pressure along the dorsal surface of the joints can be experienced as a result of the cable tension. This was realized qualitatively upon initial evaluation of the device, with a quantitative assessment difficult to determine as published data regarding torques need to assist finger extension of individuals with UMN found to be sparse. We address this gap in published data in Chapter 4 where we measure the amount of torque needed to assist finger extension of three individuals who have suffered a traumatic brain injury. We found maximum torques applied to the index finger's MCP joint on the order of *0.5 - 1.5Nm* were needed to force the joint into extension. This measurement has allowed us to retroactively estimate the tension required to assist MCP extension using the presented tendon-actuated glove and the resulting force applied to the user. With an MCP moment arm of *12mm*, as is representative according to Table 5.1, a tension of 83N would be needed to counteract 1Nm of flexion torque. Using Eqs.3.12 and 3.13 we can describe the reaction force F_{Ry} in terms of the pressure along the pulley surface P and the tension in the tendon F_T. Combining these two equivalent equations and solving for P yields Eq. 3.14 describing the pressure applied by a cable of diameter, d, on a pulley of radius, r. The diameter

of the kevlar cable used by Delph et al. was approximately *1.5mm*. This would result in *4.6MPa* of pressure applied to the user. The thresholds for pain on the surfaces of the hand are on the order of *0.5 - 1.5MPa* [120, 121], which is surpassed at about 1/4 the potentially needed cable tension. In Chapter 5 we address this shortcoming of cable-based extension with a new orthosis design containing segmented rigid structures to distribute the load without constraining the joint motion.

$$\sum F_y = F_T - F_T cos(\alpha) + F_{Ry} = 0 \tag{3.12}$$

$$\sum F_y = \int_0^\alpha Prdsin(\alpha)d\alpha + F_{Ry} = 0 \tag{3.13}$$

$$P = \frac{F_T}{rd} \tag{3.14}$$

3.1.6 Lessons Learned from Tendon-Actuated Soft Orthoses

This initial work with tendon-actuated soft gloves provided some insight for our research group into the design of hand orthoses. The work also provided prototypes which we could demonstrate to occupational and physical therapists to receive feedback regarding their function. Some conclusions we came to based off this work and these conversations with clinicians were as follows:

- The placement of tendons or rigid hardware on the palmar surfaces of the hand

interferes with the ability to use the glove as an assistive device. These components obscure the grasping surfaces making holding and manipulating objects difficult.

- Donning a full glove for individuals with the upper motor neuron syndrome (**UMN**) is prohibitive as these individuals can commonly exhibit increased flexor tone resulting in a resting closed fist posture. Fitting a glove around a hand in such a posture poses obvious difficulties.

- Using purely soft structures for a tendon actuated orthosis is challenging as these structures tend to deform under load. A combination of soft and rigid sections would likely better constrain the tendon motion and distribute the forces through the soft tissues of the hand.

- Supporting the wrist so as to keep it in a more functional position would likely be necessary for the device to have an assistive benefit. As can be seen in Fig. 2.3 the wrist of an individual suffering from UMN will tend to flex as the arm is moved.

In Section 3.2 and Chapter 5 we explore different designs which address some of these issues.
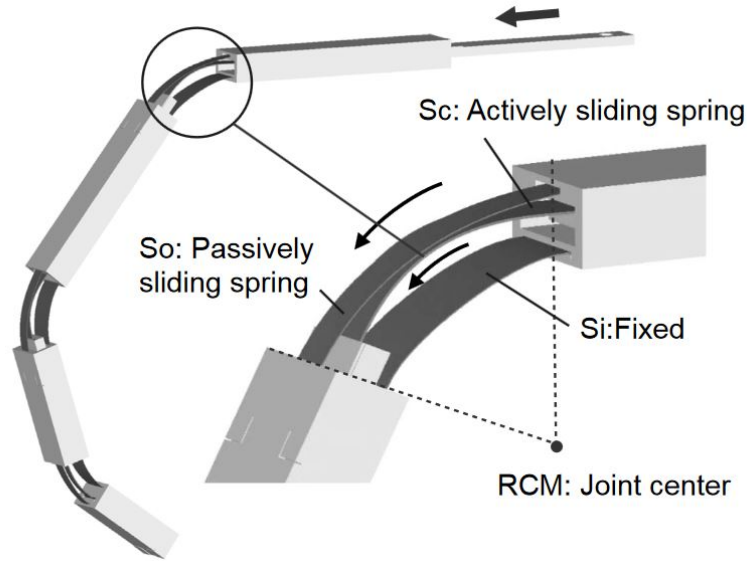
Figure 3.14: Sliding spring finger mechanism developed by Arata et al. [15]. A mechanically imposed strain on the actively sliding spring causes bending towards a fixed spring.

3.2 Sliding Spring Orthosis

As a means of exploring possible solutions to some of the issues found with the fully soft, tendon-actuated glove of Section 3.1, we worked with collaborators at ETH Zurich and Kyushu University on advancing an orthosis developed by Arata et al. [15]. The orthosis uses a novel mechanism consisting of three layers of flat sliding springs shown in Fig. 3.14. The design alleviates some of the flexion deficits associated with the soft tendon actuated glove, in particular, Arata's design places all hardware on the dorsal surface of the hand making donning the device more practical for someone with UMN and causing less obtrusion to the grasping surfaces.

We expanded on Arata's work through a collaboration with the Rehabilitation
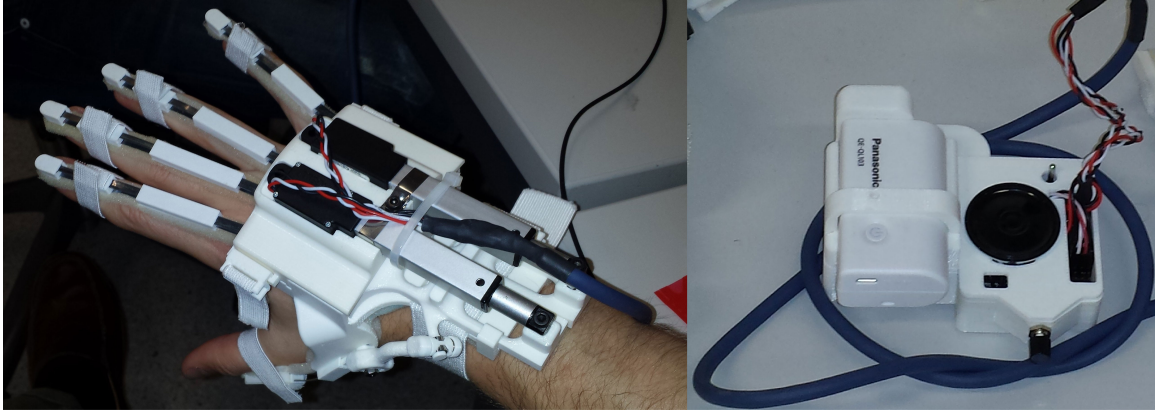
Figure 3.15: Original sliding spring exoskeleton produced by Arata with motors located on the hand [15].

Engineering Lab at ETH Zurich [23]. Our starting point was the constructed device shown in Fig. 3.15 which contained two hand-mounted motors connected to an off-board box containing the battery and control electronics. The placement of the motors on the hand meant that further development incorporating more degrees of freedom or more powerful actuators was limited due to the additional weight such changes would incur. During pilot trials on several stroke patients with the device in Fig. 3.15, Arata recieved feedback from all participants that the *250g* weight of the device was a concern. Since a remotely located electronics unit was already employed by Arata's device, placing the actuators with the electronics in a single actuation unit was considered as a possible evolution of the orthosis. Our contribution to this work was to design and implement such an actuation unit with new electronics and a push-pull Bowden cable for remote bi-directional actuation. Our intent was to make the actuation unit non-specific to any one orthosis while using Arata's device as a test-case for its implementation. In Chapter 5 we use a refined version of this

actuation unit for a cable-actuated orthosis focused on finger extension.

3.2.1 Remote Actuation Unit System Design

To implement a remote actuation unit, we proposed the system architecture shown in Fig. 3.16. A central microcontroller regulates the position of 4 linear actuators through pulse width modulation ($\boldsymbol{PWM}$) of h-bridge motor drivers. The motor setpoints are received via wireless communication from a touch screen tablet. Analog position sensors located in the orthosis are converted to 10bit values using a small peripheral microcontroller and sent via a single serial cable to the central microcontroller for use in regulating the desired setpoint. The use of a simple low-power central microcontroller was chosen over more powerful options due to the under-actuated nature of most orthoses and the critical need to minimize weight. The optimization of weight results in the selection of small motors which must be over-driven to achieve relevant forces at a sufficient speed for useful finger motion. Because of this mechanical implementation, the motor control ultimately allows for motion in one of two directions while applying near-maximum control input with little un-tapped performance left to implement more advanced controls. A more powerful processor is not needed as computationally intensive control implementations are not achievable due to the hardware limitations. Selection of a low power option improves battery life and reduces cost with no performance trade-off.

The physical implementation of the system architecture, attached to an updated
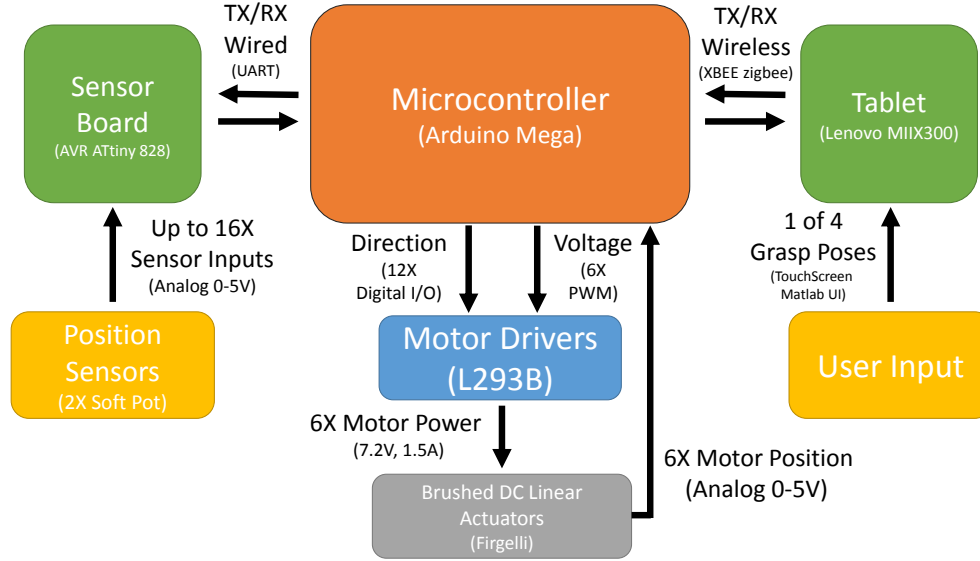
Figure 3.16: System architecture of a remote actuation unit for a hand orthosis.

version of Arata's orthosis, is shown in Fig. 3.17. A tablet interface with pictures of 4 possible hand poses is used to control the device. Compared to the original implementation of Arata, this design has allowed for 2 additional motors with their additional weight born by the user's shoulders. The following sections describe the construction of the device and the implementation of the push-pull cable transmission.

3.2.2 Evaluation of Push-Pull Bowden Cable Transmissions

As stated previously, cable-type transmissions are popular in exoskeletons as remotely locating the motors can be beneficial for packaging. Bi-directional actuation of a joint with cable-based designs can be approached in a couple different ways. The anatag-
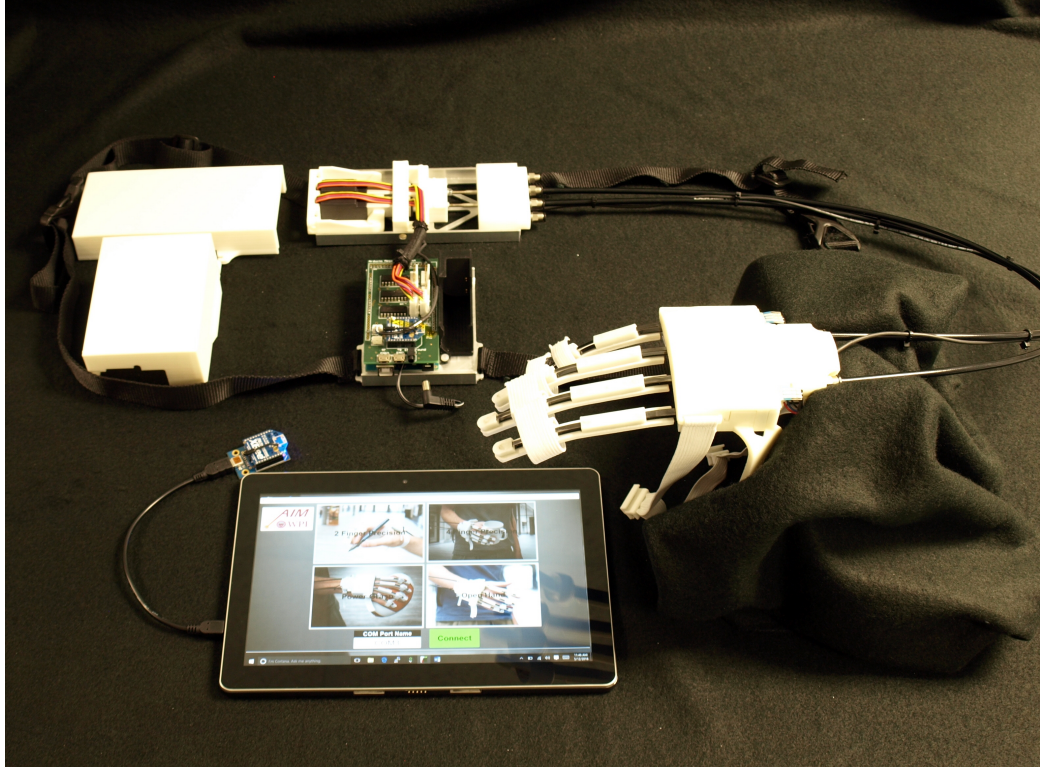
Figure 3.17: Sliding spring exoskeleton developed with ETH Zurich. Exoskeleton, actuation unit with cover removed, and tablet for user interface are shown.

onistically actuated design described in Section 3.1.4 relies on having two cables, one for each direction of motion with each only operating under tension. For remotely actuating the sliding spring exoskeleton we explored an alternative method of a push-pull Bowden cable transmission. The implemented design can deliver tensile and compressive forces from a single cable allowing for finger flexion and extension, dependent upon the exoskeleton design it is paired with. Prior to implementing the design, we sought to model the expected efficiency in order to rectify some of the issues associated with the Bowden cable of Delph et al.'s design in Section 3.1.1.

Bowden cable efficiency has previously been modeled using the capstan equation
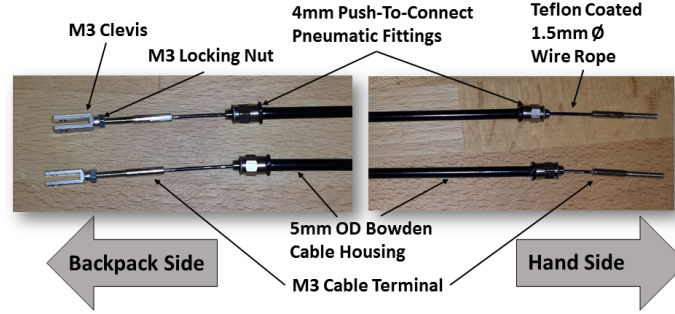
Figure 3.18: Constructed push-pull Bowden cables for the sliding spring exoskeleton [122, 123] which describes how bends in the cable housing contribute to frictional losses. The model, however, neglects losses other than those due to cable bend. We assumed that there would also be some constant amount of resistance due to factors such as pressure between the cable ends and their guiding structure. As such, a modified version of the capstan equation was used and is shown in Eq. 3.15 with F_{out} equal to the Bowden cable output force, F_{in} the Bowden cable input force, μ_s the static friction coefficient of the Bowden cable, θ the sum of all bending angles in the cable, and F_{static} equal to the amount of force needed to induce motion on a straight cable.

$$\frac{F_{out}}{F_{in}} = e^{-\mu_s \theta} - \frac{F_{static}}{F_{in}} \qquad (3.15)$$

Eq. 3.15 was evaluated for a Teflon-coated cable inside a housing with a greased nylon liner. This combination was expected to result in a friction coefficient of *0.052* [123]. It was assumed that a value of F_{static} would be around *5%* of the max input force, or about *2N*. This value is shown through later measurements as

a reasonable estimation of efficiency. A resistance of up to *5%* of the actuator force could be expected, however resistance greater than this would seem indicative of poor tolerances. The operational range of the Bowden cable bend angle was determined to be 0° to 180°, allowing for 90° bends at the shoulder and elbow from a back mounted device. The typical operational range of the actuators was expected to be *10* to *40N* as Arata's orthosis, among several others, use actuators with forces in this range [5, 15, 33]. From these parameters a range of expected efficiency was modeled and is shown in Fig. 3.19. For all operational conditions, the efficiency was expected to be greater than *65%*, with most operation being *70%* to *80%* efficient.
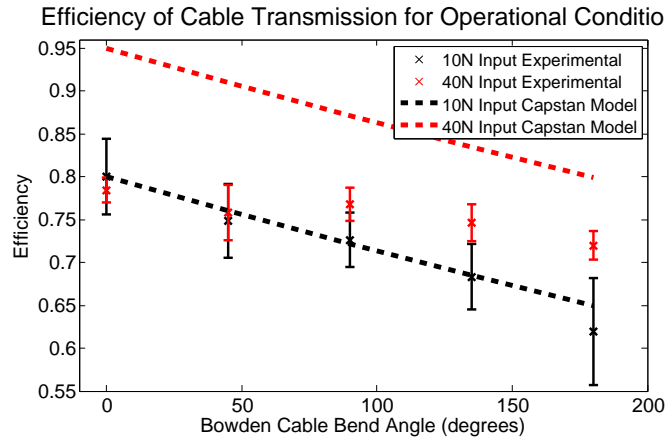
Figure 3.19: Realized Bowden cable efficiency.

To implement this design, a *5mm OD* Bowden cable housing (Basics Brake Housing, Jagwire USA, Bloomington, MN) with a *2mm ID* greased nylon liner is used to guide the motion of a *1.5mm* Teflon-coated braided steel cable (Teflon Slick Stainless, Jagwire). The greased liner is expected to reduce by about half the friction associated with Delph's design [123]. *M3* threaded terminals are soldered onto the cable ends

with clevises threaded onto the input side to allow for pinning to linear actuators. Cable terminals have *15mm* long, *3.5mm* diameter shanks which are inserted into ultra-high-molecular-weight polyethylene (UHMWPE) guide blocks mounted in the backpack and exoskeleton. The shanks slide inside these guide blocks, providing linear motion and preventing buckling of the cable end under compression. A pneumatic quick connect placed on either end of the Bowden cable assembly allows for threading the housing into Helicoil® inserts on the guide blocks. The constructed cables are shown in Fig. 3.18.

The constructed cables were tested by measuring input and output forces for a range of bend angles and forces. The output-side of the Bowden cable was held in place with the cable terminal allowed to push freely against a *100N* force sensor (AFG 100N, Mecmesin Limited, Slinfold, West Sussex, UK). The input-side of the Bowden cable was moved to various positions, wrapping around a *100mm* radius block, to test efficiency at bend angles from 0° to 180° at 45° intervals. Force was applied to the input side of the Bowden cable by pushing on a *50N* force sensor (Type 9205, Kistler Holding AG, Winterthur, Switzerland). Tests were conducted under a low load input condition of *10N* and a maximum load input condition of *40N*. Force was applied slowly to avoid any dynamic effects until the desired measurement force was reached. Applied forces were kept to within *+2N* of the desired setpoint. The test setup is shown in Fig. 3.20.

Also measured with this test setup was the value of F_{static} from Eq. 3.15. This was
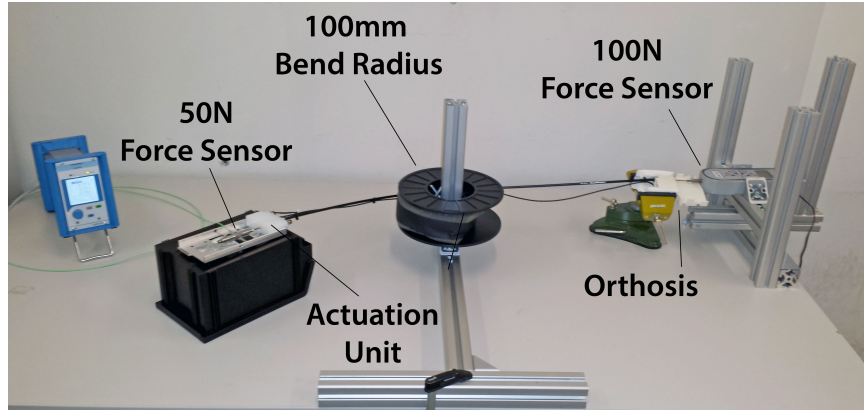
Figure 3.20: Test setup used for measuring the efficiency of a push-pull Bowden Cable. The actuation unit was positioned during the test with Bowden cable bends from 0° to 180° at 45° intervals.

done by straightening the Bowden cable and removing the force sensor from in front of the output. Force was slowly applied until motion was induced, the value of this force was then recorded. The average value of F_{static} from *15* trials was determined to be *1.7N*.

The results of the efficiency tests are shown in Fig. 3.19 alongside the capstan model of Eq. 3.15. For the *10N* trial, the model can be seen as a reasonable predictor of transmission loss. The model, however, was no longer accurate at the *40N* input case. During testing, housing stretch was observed under larger compressive loads leading to a breakdown of the model. Regardless of this effect, reliable operation was observed and efficiency for all inputs was above 60% with most tested conditions above 70% efficient.

Finally, we tested the positioning accuracy of the cable. Two forms of positional error occur in push-pull Bowden cables. One is backlash, brought on during the
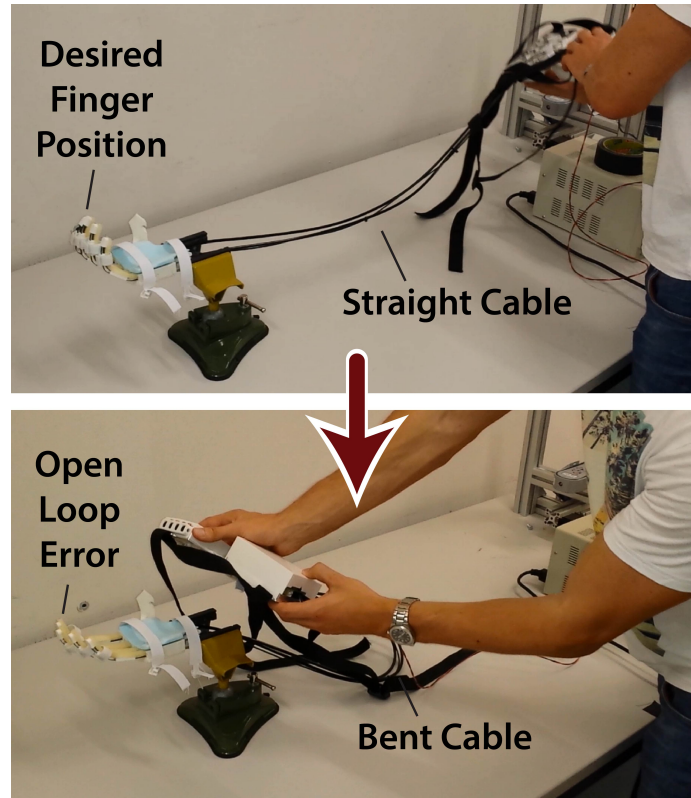
Figure 3.21: Effect of Bowden cable position error caused by flexing the cable housing. As the cable is flexed from 0° to 180°, the path length of the cable changes causing motion of the orthosis.

transition from compression to tension, as the cable moves from the outer radius to

the inner radius of bends in the Bowden cable. For our constructed cable, we found

this backlash to be on the order of $5mm$. The other form of positioning error occurs

due to a slight change in the path length through the cable housing as the housing is

bent. This causes movement of the cable output as a result of movement of the cable

housing. The impact of this on the sliding spring exoskeleton is shown in Fig. 3.21

where the finger pose changes substantially when the cable is flexed. To regulate this,

we incorporated position sensors in a modified version of Arata's orthosis and used

these to regulate the Bowden cable position. A bang-bang controller with a small deadband running on the actuation unit's central microcontroller is used to regulate this position. Initially we implemented a PID controller but found that the requisite gains for reasonable operational speed saturated the control input with a position error of just $0.5mm$. The results of the bang-bang control are shown in Fig. 3.22 alongside the open loop performance of setting motor position alone. The controlled cable achieves an accuracy of $\pm 0.3mm$ while a maximum error of over $1.5mm$ was seen with the open loop control.
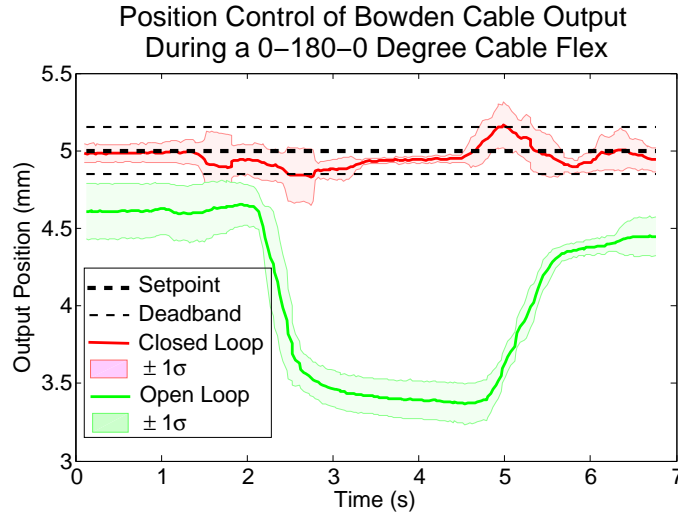
Figure 3.22: Position control performance a push-pull bowden cable against perturbation of the cable housing. Bending the cable housing from 0° to 180° to 180° causes an open loop error of over $1.5mm$. A bang-bang controller regulates the position to with in $0.3mm$.

The presented design process for the Bowden cable implemented on our remote actuation unit resulted in a reliable, precise, and reasonably efficient transmission. As general rules, we found the design should:

- Allow for a cable path with minimal bending, as increasing the total number of bends negatively effects the efficiency.

- Use low friction housing liners and cables to minimize losses.

- Consider the positional errors associated with Bowden cables and provide methods of compensation if necessary.

- Properly dimension the cable diameter and housing inside diameter. A clearance is needed to prevent binding of the cable, but additional clearance results in an increase in backlash.

3.2.3 Remote Actuation Unit Mechanical Design

The remote actuation unit is split into two sections, an actuation module and an electronics module, which allowed for simpler construction and modularity in the prototype. The actuation module mounts four DC linear actuators (L12-30-100-6-P, Firgelli Technologies Inc., Victoria BC, Canada) and an ultra high molecular weight polyethelyne (**UHMWPE**) Bowden cable guide block on a *2mm* thick aluminum frame. The motors were chosen for their light *35g* weight, compact *74 X 15 X 18 mm* size, *40N* output force, and *6 mm/s* speed at peak power. In general, we've found DC motors to be desirable due to their benefits in size, cost, energy storage, and control. These motors allow for an exoskeleton like Arata's to fully open or close, against *60%* of it's maximum force, in less than *1.5s*. This linear actuator is popular
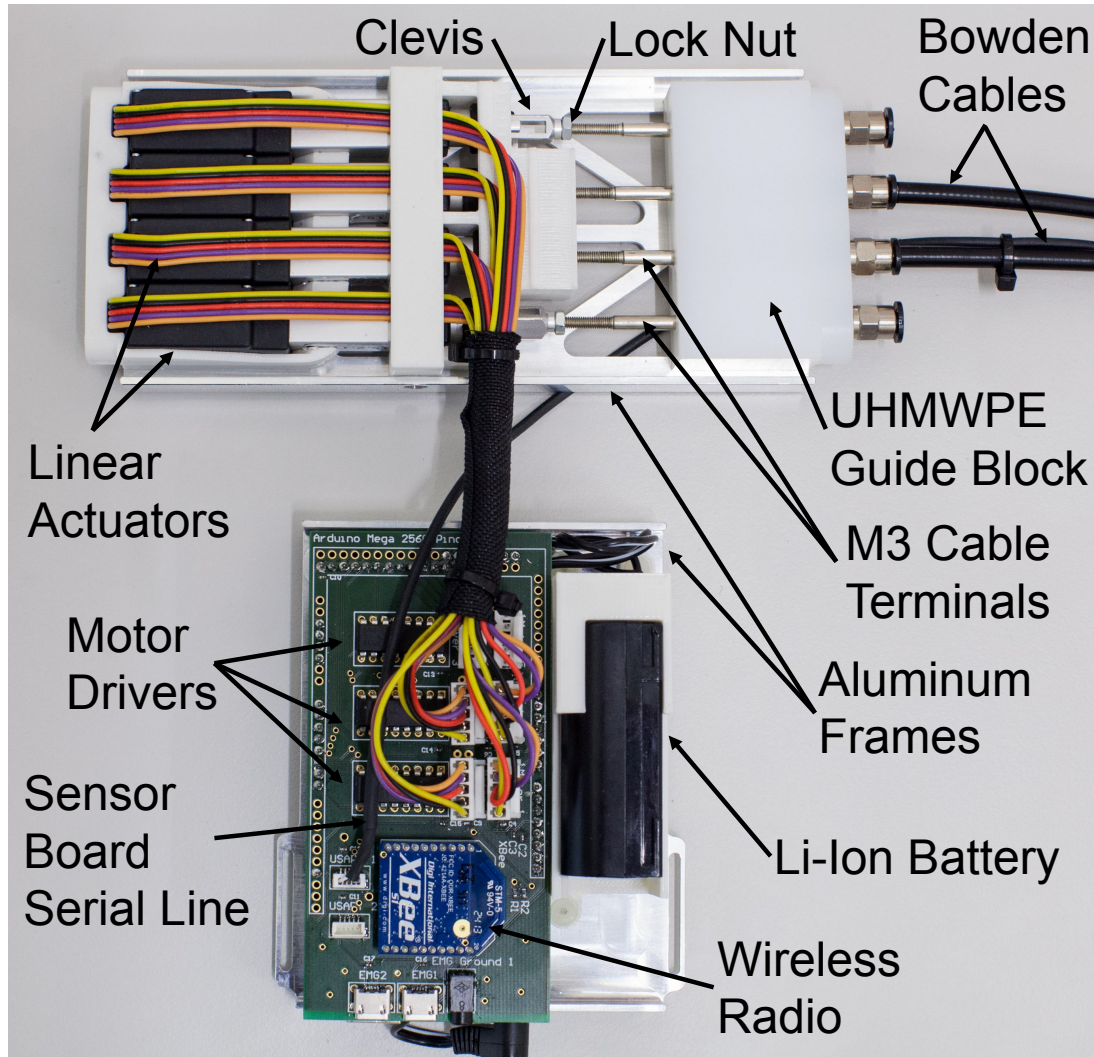
Figure 3.23: Construction of the a remote actuation unit based on a push-pull bowden cable.

among hand exoskeleton prototypes with several research groups using it in vastly different design concepts [5,33]. In our device, printed polylactic acid (**PLA**) plastic mountings hold the motors in place with a PLA cover protecting internal mechanics. The actuation module, with cover removed, is shown in Fig. 3.23. The electronics module follows a similar construction, with *2mm* thick aluminum frame and printed

Figure 3.24: An individual wearing a remotely actuated version of Arata's exoskeleton PLA cover, and is shown in the bottom half of Fig. 3.23.

An image of the complete system, with hand exoskeleton attached, is shown in Fig. 3.17. The actuation module and electronics module are joined with fabric allowing for the pack to bend and form better to the user's back. Fig. 3.24 shows an individual wearing the final device. The actuator module is centered on the back, mounted above the scapula (roughly between vertebrae T2-T4) while the electronics module is mounted between the scapula (roughly vertebrae T4-T7). This design orients the Bowden cables for efficient operation and minimally interferes with sitting and arm movement.

3.2.4 Remote Actuation Unit Electronics Design

The electronic design consists of a central control board, a peripheral sensor board, and an interface device. A commercially available microcontroller board (Mega2560 R3, Arduino LLC) is used for the central control board. This board handles wireless communication with the interface device as well as UART communication with the peripheral sensor board. The central control board also handles running motor control loops and setting inputs on up to three dual H-bridge L293B motor drivers. Control electronics and motors are powered from a *7.2V, 1700mAh* Li-ion battery (PS-BLM1, Olympus Corporation, Shinjuku, Tokyo, Japan). Under heavy use (maximum motor force with a *50%* duty cycle), the average current draw of our final device was *500mAh*, conservatively allowing for a battery life of about *2.5hrs*.

The custom peripheral sensor board uses an 8-bit microprocessor (ATTINY828R, ATMEL Corporation, San Jose, California) to read 18 analog input channels, serialize the data, and send it via UART to the main control board with a bit rate of 250kbps. The abundance of analog channels was included to allow for the addition of sensors to meet application need. The board footprint was *22 X 22mm* making it possible to embed in the exoskeleton without increasing the overall size.

For testing, a PC is used for interfacing between user and device. Sensor values from the peripheral board, EMG inputs, and actuator positions are relayed to the computer for storage or viewing. The PC can also directly issue motion commands

to the device, this control was used for all testing. Communication between the PC and main board is handled with a wireless radio transmitter (XBEE S1, Digi International, Minnetonka, MN, USA) operating at a bit rate of 57.6 kbps.

3.2.5 Ergonomics of a Sliding Spring Orthosis

(a) Torsional compliance about y   (b) Torsional compliance about x
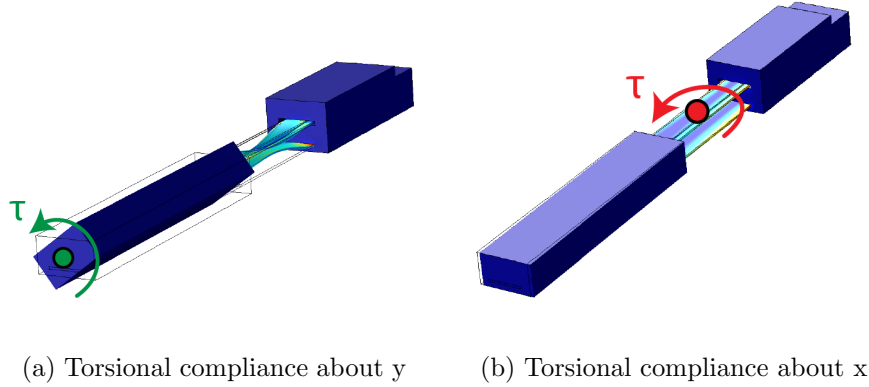
Figure 3.25: A 0.12Nm torque applied about y and x directions of a representative sliding spring joint.

One of the benefits of the sliding-spring design is its compliance, allowing for imperfect fits and imperfect assumptions of the underlying skeletal structure. Small deformations of the device to conform to the user's skeletal kinematics are permitted by the device without applying large amounts of force to the user. One issue noticed, however, was that the amount of torsional compliance is not uniform about all axes. To demonstrated this, we constructed a simplified FEM model consisting of a single joint from Arata's device using COMSOL Multiphysics (COMSOL Inc., Stockholm, Sweden). The simulation confirmed this observation with the compliance about y

being initially 117.0°/Nm prior to a steep increase as the mechanism buckles with around 0.08Nm of applied torque. The compliance about x is constant in this loading range at 4.42°/Nm, two orders of magnitude less than that of the y compliance. This becomes problematic if the user's finger's are not straight, which we've found to be not uncommon.
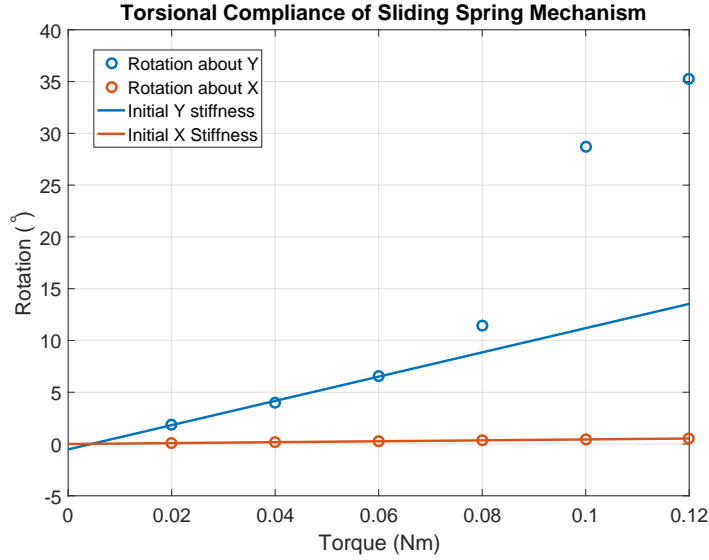
Figure 3.26: Torsional compliance of the sliding spring mechanism

3.2.6 Comparison Between Integrated and Remote Actuation

Modifying the design of Arata et al. allowed for us to make direct comparisons between an orthosis using a remote actuation unit and one using actuators which are integrated into the orthosis. The actuation unit we developed included an additional

2 motors to allow for added function in future iterations. Integrating these two motors in the orthosis would likely have made the device impractical due to the added weight and bulk. The need to wear a back pack and manage the cables connecting between it and the hand can also be cumbersome, but results in a lighter weight placed on the hand with a lower-profile orthosis. A detailed comparison of the two devices is given in Table 3.2. The correct design direction will ultimately be dependent on the specific orthosis and its desired performance. In Chapter 5 we explore a design to assist finger extension for people with moderate to severe increases in flexor tone, requiring higher power actuators than used in this device. The incorporation of these actuators directly into the orthosis would have proved impractical but a remote actuation unit was seen to be a reasonable alternative.

3.3   Discussion and Conclusions

The work conducted on the orthoses of Delph and Arata provided some insight into the design of hand orthoses in general. The compliance of each device was beneficial as specific sizing and adjustment was not needed for each user. Remote actuation was applied to different design philosophies and found to allow for extra flexibility in packaging, especially during the prototype phase. Cable transmissions can prove effective if certain design elements, such as using low-friction materials and routing the cables in as straight a path as possible, are taken into consideration.

Table 3.2: Comparison of Arata et al.'s original orthosis and our Remotely Actuated (RA) Designs.

	Arata et al. [15]	RA
Orthosis Weight (g)	256	113
Remote Weight (g)	201	754
Actuator Pack Weight (g)	N/A	346
Electronics Pack Weight (g)	201	286
Transmission Weight (g)	N/A	61 /each
_____	_____	_____
Actuated DOF	2	4
_____	_____	_____
Exoskeleton Size (mm)	130 X 84 X 32	98 X 84 X 18
Actuation Pack Size (mm)	N/A	175 X 79 X 26
Electronics Pack Size (mm)	88 X 103 X 49	83 X 114 X 46
Transmission Size (mm)	N/A	5⌀X 750
_____	_____	_____
Battery Capacity (Wh)	10.4	12.2

Informal testing of these two orthoses left us with questions regarding future development. The glove developed by Delph et al. showed poor extension performance characterized by irregular finger movement and postures. We wanted to improve upon this performance, but since the glove is under-actuated its movement is dependent upon the torques acting at the finger's joints. Analytically designing an improved device we found difficult as we could not find detailed characterization of what these torques may be. As was covered in Section 2.1.1, these torques are expected to be non-trivial among a portion of individuals with UMN. We needed a better understanding of these forces to improve upon the glove of Delph et al., this motivated a study on extension assistance for individuals with traumatic brain injury which we

present in Chapter 4.

We were also left wondering how best to assess and optimize the flexion forces provided by both devices. The sliding spring mechanism developed by Arata provided about *4N* of force to the dorsal surface of the fingertips [15]. Qualitatively this seemed sufficient to position the fingers in free space, but insufficient for successfully holding and manipulating objects. Quoted tip forces ranging from *4-15N* are fairly common among orthoses presented by various research groups [17,102,108]. The studies used to justify these forces, however, were found difficult to apply directly to the evaluation of orthosis performance. The work of Mathesus et al. [124], used as a reference for the work of Polgerinos et al. [17], measured the coefficient of friction between objects of daily living and household surfaces. If we wished to improve upon the flexion performance of Arata's design, we felt we were lacking a meaningful reference of grasping data to inform these improvement design. We address this as well in Chapter 4 by measuring forces and joint torques during 10 activities of daily living.

CHAPTER 4

Study of Able-Bodied and Impaired Grasping:

Finger Torques for Orthosis-Aided Motion

The preliminary work presented in Chapter 3 exposed questions regarding orthosis function needed for design and optimization. Out of this, there were two measurements we sought to make in order to better understand the needed function from an orthosis. The first was measurements of joint torques need to complete activities of daily living while using an orthosis. The second was measurements of torques needed to assist finger extension of individuals with the upper motor neuron syndrome (**UMN**). In this chapter we present a motion capture protocol for tracking the position, orientation, and movement of the joints in the thumb, index, and middle fingers. Combining this protocol with the tracking of load cell positions and vectors, we were able to calculate torques at the individual joints. We applied this protocol to track 10 able-bodied subjects as they completed 9 activities of daily living with

specially instrumented house-hold objects. We then applied the same protocol to track 3 subjects suffering from UMN due to a traumatic brain injury (***TBI***) as a physical therapist applied forces to extend their fingers against an increase in muscle tone. The specific contributions of this chapter can be summarized as follows:

- **Contribution 1**

  A protocol for tracking the fingers and load cells using motion capture cameras allowing for measurement of finger pose and force vectors during various activities. This protocol includes a method for fitting a kinematic model to a captured data-set, allowing for accurate tracking of different subjects. The data processing for model generation and hand tracking are implemented in simple graphical user interfaces, streamlining their use in future work. We also provide an assessment of the quality of the fitting technique through comparison with CT scans of 5 subjects.

- **Contribution 2**

  The measurement of fingertip forces and joint torques during activities of daily living in a manner which can directly be applied to the design of hand orthoses. Activities were chosen based off consultation with occupational therapists to ensure an orthosis would benefit an individual's ability to complete them. These measurements will allow for better assessment and design of orthoses for aiding finger flexion.

- **Contribution 3**

  The measurement of externally applied joint torques required to assist the extension of fingers of individuals following a traumatic brain injury. Three subjects with increased flexor tone (hypertonia) had their thumb and index finger extended while tracking the finger motion and applied force vectors. Subjects were tested while relaxed and while attempting to volitionally extend. These measurements will allow for better assessment and design of orthoses for aiding finger extension.

4.1 A Unified Thumb-Finger Motion Capture Protocol

Studying the motions and torques of the hand requires a method for deriving subject-specific skeletal kinematics along with continuous measurement of joint angles in a manner which is both accurate and inconspicuous to the study subject. For our work, we employed optical tracking of reflective surface markers to accomplish this. This method has the benefits of not obstructing the palmar surface of the hand and not restricting the hand's natural motions. Motion capture also allows for 3D localization of the joints relative to objects in the environment, not just measurement of the joint angles such as would be provided by the use of an electrogoniometer. Downsides to

this method include the potential for lost data due to occlusion of markers and errors due to motion of the skin relative to the skeleton being tracked. With a proper study protocol, however, these negatives can be mitigated and quality data recorded.

There are some existing software packages for performing inverse kinematics on marker data. One such package for this is the open source software OpenSim [125]. These packages, however, are tailored towards tracking of larger body segments for applications such as gait analysis. Detailed models of the hand are limited in these packages with currently published OpenSim models accurately representing only IP and MCP joints of the thumb and index finger [126]. OpenSim and other commercial packages are also setup around the method of placing markers on anatomical land-marks, assuming they are placed accurately, and scaling the model to fit an individual subject [127]. While this is an effective approach when tracking large body segments, the several mm of marker placement error is substantial given the finger sizes. With these software packages poorly tailored to finger tracking, we decided to implement our own motion capture protocol and data processing interfaces using Matlab 2016a (The MathWorks, Inc., Natick, Ma). Our approach uses optimization methods to accurately locate the joints relative to surface markers for each subject. The fitting techniques and protocol implemented are based on review of past works evaluating the efficacy of hand tracking using surface markers [128–135]. The implemented protocol integrates aspects of these past works and expands on them to form a complete hand tracking protocol including CMC, MCP, and IP joint models.

The contributions of this section are an easy to use application for generating a subject-specific kinematic model of the hand from motion capture data. This interface, and the joint angle calculations also described in this section, are utilized in the remainder of this chapter for studying the forces and torques which are required by a hand orthosis for individuals with the upper motor neuron syndrome **UMN**.

4.1.1 Marker Placement Protocol

To ensure consistent and accurate data collection, a marker set needed to be defined which allowed for tracking the 6DOF pose of each presumed rigid segment of the thumb, index, and middle fingers. For our study, we implemented the marker frames and naming convention shown in Fig. 4.1. This marker set is similar to the reference marker sets used by Nataraj et al. [128], Hulst et al. [135], and the thumb set used by Chang et al. [129]. The markers used are reflective 3mm hemispheres (Optitrack Reflective Markers: Facial 3mm, NaturalPoint, Inc., Corvallis, Or.) attached with a temporary cosmetic adhesive (Ardell® LashGrip®, American International Industries, Los Angeles, Ca.). The convention held in numbering the markers of each frame is as follows:

- Marker 1 is distally placed on the ulnar side of the reference frame.

- Marker 2 is proximally placed on the ulnar side of the reference frame.

- Marker 3 is placed on the radial side of the reference frame (either proximally

or distally).

Consistent numbering of the markers allows us to know generally how the joints should be oriented relative to the tracking frames. This allows us to be consistent with how we define the positive and negative directions of the joint vector, in particular we define the flexion/extension axis so that flexion is positive.
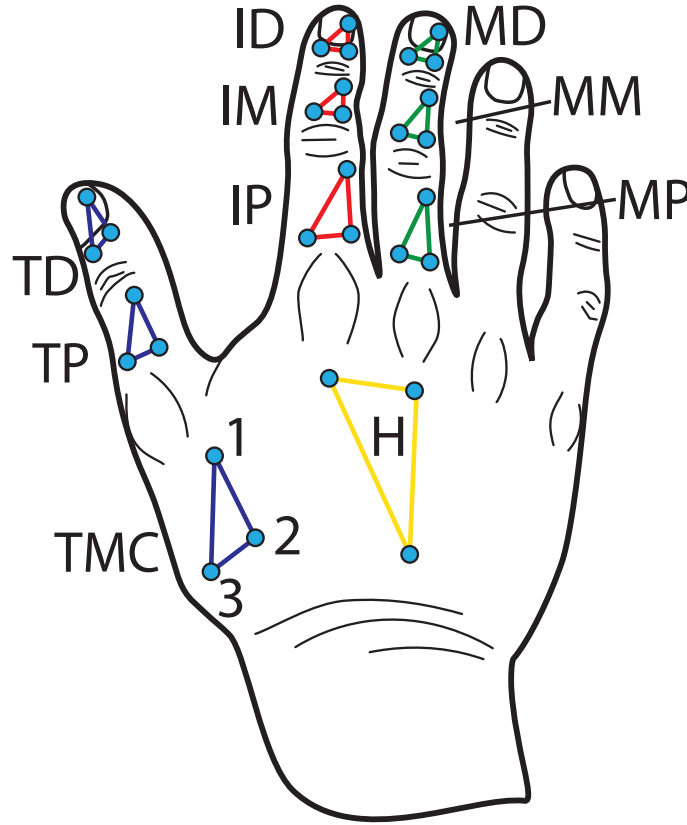
Figure 4.1: Marker set used for all experiments involving motion capture of the hand. Each marker is named in post-processing following this convention and referred to consistently throughout all data processing interfaces.

4.1.2   Camera Placement and Setup

Data is collected using eight 1.3 megapixel optical tracking cameras (Optitrack Flex13, Natural Point, Inc.) placed around a capture volume of approximately $1m^3$ with the center of the volume approximately $1m$ from each camera. The system is calibrated to a mean error of $< 0.3mm$ each time the camera's are re-positioned or at the beginning of each experiment.

Note: For proper data collection with the marker protocol of Fig. 4.1, following camera calibration the reconstruction error must be set to 1.25mm. For the tracking software Motive^{TM} this is under the reconstruction properties tab. If this setting is not changed, the software may incorrectly merge adjacent markers. The default using this setup in Motive is typically set at approximately 2.5mm.

4.1.3   Kinematic Model and Reference Frame Definitions

It is common practice in human body tracking to approximate the subject's skeleton as a series of rigid-body segments connected by simplified joint models [127]. Our goal was to locate the position and orientation of each of these simplified joint models relative to a reference frame for the joint formed by the measured motion

capture markers. Reference frames for each finger segment are calculated using the raw x,y,z coordinates of the individual markers output as a csv file by the motion capture software (Optitrack Motive 1.8.0, Natural Point, Inc.). All marker data from the software is referenced to an arbitrarily defined global reference frame. The marker frames for each skeletal segment are defined as follows; given a marker frame, $F \in \{TD, TP, TMC, ID, IM, IP, MD, MM, MP, H\}$, the transformation matrix from the global reference frame, 0, to frame F is defined by Eqs. 4.1 - 4.7. Here, P_{Fm}^0 represents the x,y,z position vector of marker m of frame F in the global coordinate frame 0, R_F^0 is the rotation matrix describing the orientation of frame F in frame 0, P_F^0 is the position of frame F in frame 0, and T_F^0 is the transformation matrix describing the position and orientation of frame F in frame 0.

Using the markers of a given tracking frame, F, a unit vector, $\hat{x}$, is defined as the normal to the plane formed by markers 1,2, and 3. The direction is chosen to point in the palmar direction in order to roughly match the International Society of Biomechanics (**ISB**) standard for frame definitions [136]. Mathematically, this is represented by Eq. 4.1.

$$\hat{x} = \frac{(P_{F2}^0 - P_{F1}^0) \times (P_{F3}^0 - P_{F1}^0)}{|(P_{F2}^0 - P_{F1}^0) \times (P_{F3}^0 - P_{F1}^0)|} \tag{4.1}$$

The unit vector, $\hat{y}$, is defined as pointing from marker M_1 to marker M_2 and is calculated using eq. 4.2. Again, the direction was chosen to roughly match the ISB

standard [136] while maintaining orthogonality to $\hat{x}$.

$$\hat{y} = \frac{(P^0_{F2} - P^0_{F1})}{|(P^0_{F2} - P^0_{F1})|} \tag{4.2}$$

The final unit vector, $\hat{z}$, is mutually orthogonal to $\hat{x}$ and $\hat{y}$. This vector is calculated following the right hand rule with Eq. 4.3.

$$\hat{z} = \hat{x} \times \hat{y} \tag{4.3}$$

These three unit vectors form the 3×3 rotation matrix, R^0_F, from the global motion capture frame to frame F using Eq. 4.4.

$$R^0_F = \begin{bmatrix} \hat{x} & \hat{y} & \hat{z} \end{bmatrix} \tag{4.4}$$

The frame position, P^0_F, was calculated by first rotating markers M_1-M_3 into frame F using Eq. 4.5.

$$P^F_{Fm} = R^{0^{-1}}_F P^0_{Fm} = \begin{bmatrix} x^F_{Fm} \\ y^F_{Fm} \\ z^F_{Fm} \end{bmatrix} \tag{4.5}$$

Finally, P^0_F is calculated using Eq. 4.6. A simple average could also be used, however this method was chosen in an attempt to reduce weighting the effects of tissue motion.

$$P_F^0 = R_F^0 \begin{bmatrix} x_{F1}^F \\ \frac{1}{2}(y_{F1}^F + y_{F2}^F) \\ \frac{1}{2}(z_{F2}^F + z_{F3}^F) \end{bmatrix} \tag{4.6}$$

Finally, the transformation matrix, T_F^0, is formed by Eq. 4.7.

$$T_F^0 = \left[\begin{array}{ccc|c} & R_F^0 & & P_F^0 \\ \hline 0 & 0 & 0 & 1 \end{array} \right] \tag{4.7}$$

Measuring this 6DOF reference frame for each bone of the fingers forms the basis for fitting parameters of a kinematic hand model for each subject. These parameters allow for tracking the position and orientation of the joints during the study, even even when data is partially occluded. To fit these parameters, an underlying model of joint motion must be assumed. The following assumptions were made:

- IP joints have a single rotational DOF of flexion/extension [137, 138].

- MCP joints have 2 rotational DOF of flexion/extension and abduction/adduction with intersecting and orthogonal axes [137, 138].

- The basal joint of the thumb, the CMC joint, has two primary DOF of flexion/extension and abduction/adduction which are non-intersecting and non-orthogonal [139].

The kinematic model is represented in Fig. 4.2 and Detailed diagrams of the joints

in Fig. 4.3. The orientation of the axes used in this model, and throughout this work, are based on the standards set by the ISB [136] where positive rotation about the z-axis represents flexion, rotation about the x-axis represents abduction\adduction, and rotation about the y axis represents pronation\supination [136]. The notation specified by the ISB is as follows:

- α: Flexion\Extension Angle (rotation about z)

- β: Abduction\Adduction Angle (rotation about x)

- γ: Pronation\Supination Angle (rotation about z)

- $q3$: Proximal or Distal Translation

Further keeping with the ISB definitions, the flexion\extension axis is assumed fixed relative to the bone proximal to the joint and the abduction\adduction axis is assumed fixed relative to the bone distal to the joint. The forward kinematics of the joint using the ISB notation is described by Eqn. 4.8. The order of motions is assumed as: first rotation α about z, followed by translation $q3$ along y, rotation $gamma$ about y, and finally rotation β about x. Eqn. 4.8 is general to the three types of aforementioned joints. The assumptions made for the MCP and IP joints lead to simplifications of this general model. The previously stated assumptions are interpreted mathematically as:

- The MCP assumption of intersecting FE and AA axes necessitates $q3 = 0$
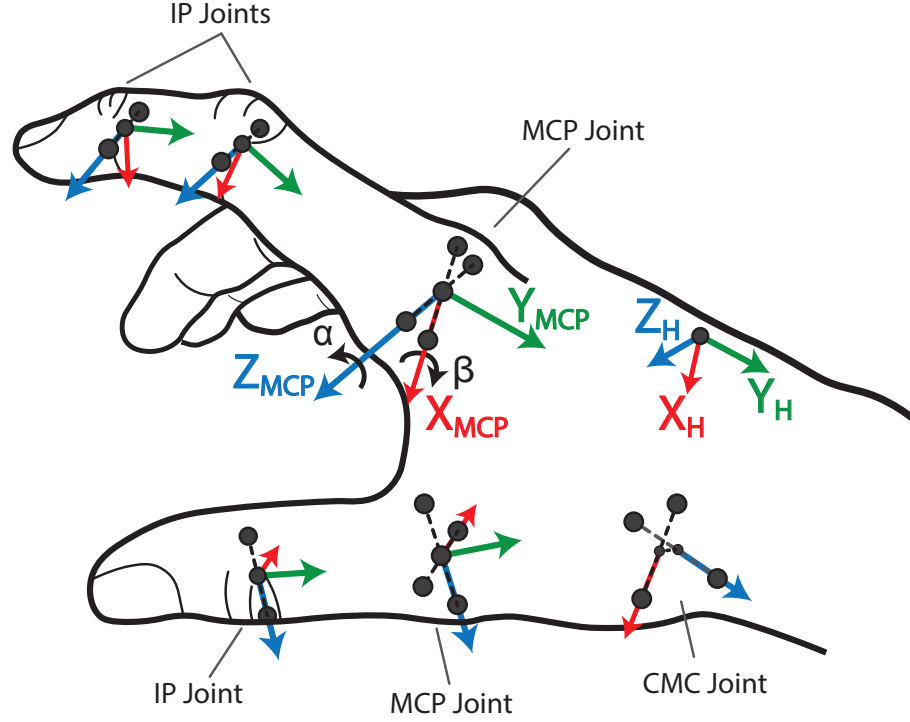
Figure 4.2: Kinematic models of the joints used for tracking hand motion. The IP joints are assumed to be perfect hinge joints, the MCP joints assumed as universal joints, and the CMC joint assumed as having 2 rotational DOF with non-intersecting and non-orthogonal axes.

- The MCP assumption of orthogonal FE and AA axes necessitates $\gamma = 0$

- The IP assumption of a single rotational DOF necessitates $\beta = 0$, $\gamma = 0$, and

  $q_3 = 0$

- The CMC assumption of fixed spacing and fixed skew angle necessitates that

  q_3 and γ are both constants.
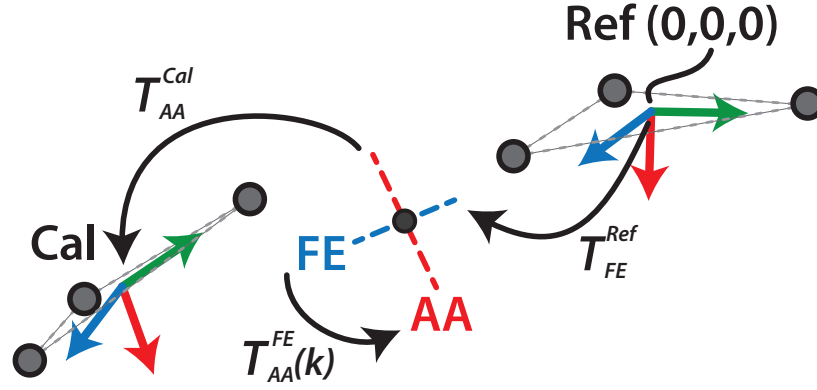
(a) IP and MCP Joints
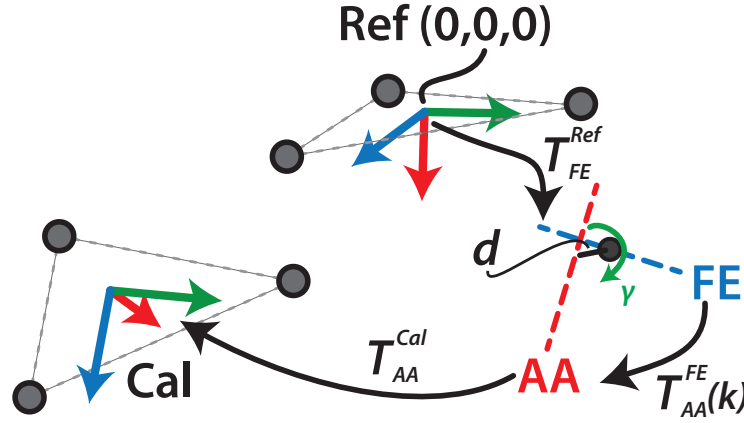
(b) CMC Joint

Figure 4.3: Kinematic models of the finger joints. The IP joints are a simplified version of the MCP joint where β is assumed to be 0. Each joint is tracked relative to the bone immediately proximal using frame *Ref*. The joint model is fit using the motion of the immediately distal frame *Cal*

$$T_{AA}^{FE}(k) = \begin{bmatrix} c_\alpha c_\gamma & -s_\alpha c_\beta + c_\alpha s_\gamma s_\beta & s_\alpha s_\beta + c_\alpha s_\gamma c_\beta & -q_3 s_\alpha \\ s_\alpha c_\gamma & c_\alpha c_\beta + s_\alpha s_\gamma s_\beta & -c_\alpha s_\beta + s_\alpha s_\gamma c_\beta & q_3 c_\alpha \\ -s_\gamma & c_\gamma s_\beta & c_\gamma c_\beta & 0 \\ 0 & 0 & 0 & 1 \end{bmatrix} \tag{4.8}$$

While a unified kinematic representation of the joints is possible, their unique motions necessitate variations in the methods used to fit their kinematic parameters. For our work, 4 different methods were implemented to fit the 9 joints of the thumb, index, and middle fingers. Three of these methods are for the IP, MCP, and CMC joints, the fourth method was required for the special case of the thumb's MCP joint. The MCP joint of the thumb has limited range of motion compared to the same joint on the fingers and subjects had difficulty isolating the FE motion from the AA motion. These characteristics necessitated a modified method to a standard MCP joint, which was less computationally efficient but more robust to small range of motions. The methods implemented valued anatomical relevance over outright minimization of reconstruction error.

4.1.4 Data Collection for Kinematic Model Fitting

In order to accurately fit our kinematic model, a dataset is collected on subjects as they are instructed to perform various movements of their joints, repeatedly exercising each through its range of motion. The motions, shown in Fig. 4.4 and 4.5, are:
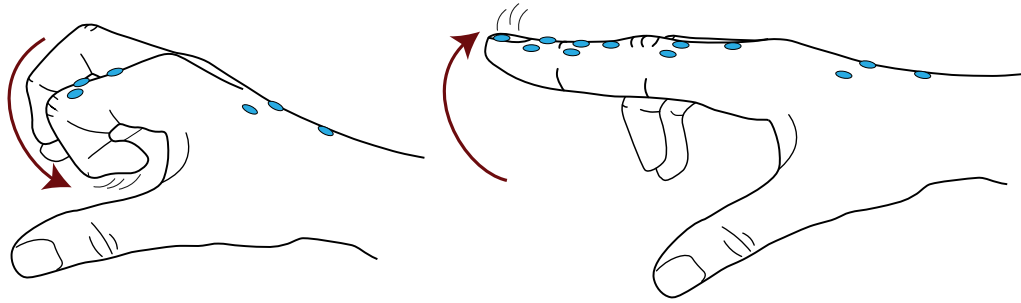
(a) Repeated flexion and extension of the IP joints
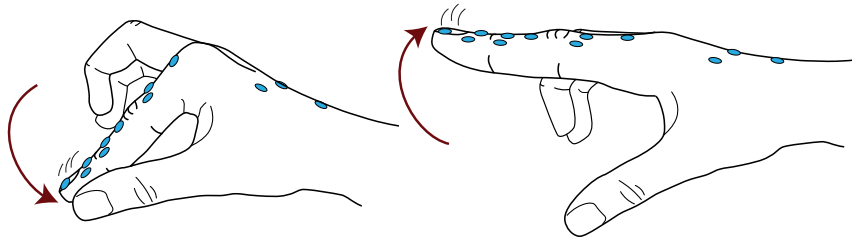
(b) Repeated flexion and extension of the MCP joints
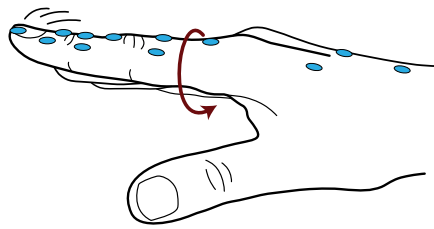
(c) Repeated circumduction of the MCP joints

Figure 4.4: Illustration of finger motions during data collection for fitting a kinematic model to motion capture markers placed on a subject's hand. Each subject independently performed these motions several times each to generate a data-set that fully describes the kinematics of the joints.
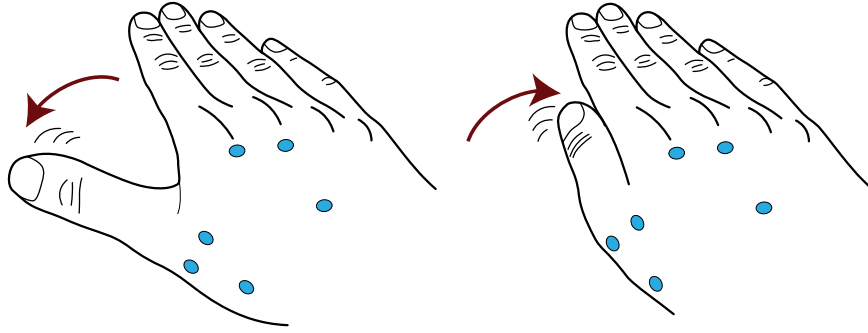
(a) Repeated abduction and adduction of the CMC joint
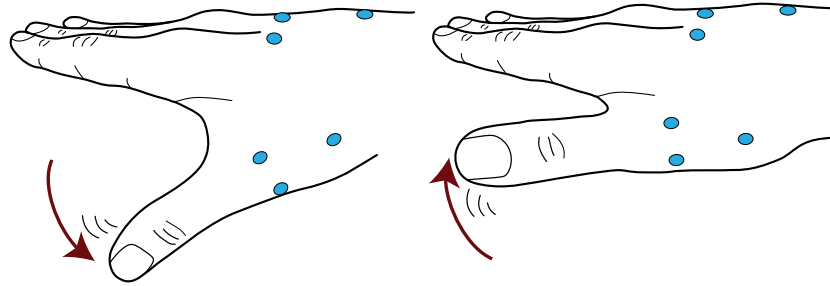
(b) Repeated flexion and extension of the CMC joint
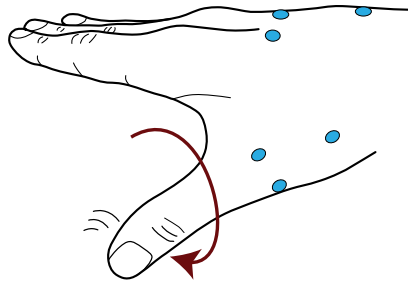
(c) Repeated circumduction of the CMC joint

Figure 4.5: Illustration of thumb motions during data collection for fitting a kinematic model to motion capture markers placed on a subject's hand. Each subject independently performed these motions several times each to generate a data-set that fully describes the kinematics of the joints.

- Flexion/Extension of the IP joints

- Isolated flexion/extension of the MCP joints with neutral abduction

- Circumduction of the MCP joints

- Flexion/Extension of the Thumb's CMC joint

- Abduction/Adduction of the Thumb's CMC joint

- Circumduction of the Thumb's CMC joint

After collection this data is segmented by specifying a window of data used to fit each joint, has outliers removed, and redundant data rejected prior to fitting the joint models. A high quality data set is desired which avoids artificially weighting certain joint poses. We found during our work that there are certain points of the motion where people naturally stop, this occasionally results in over-fitting to these points and illogically oriented joints.

Outlier removal consists of two parts. First, for each joint the presence of all markers in its the Ref and Cal frames is checked. If a marker is missing from either frame, that sample is excluded from the data used for fitting that joint. Next, the distance between the markers on each frame is calculated on all remaining samples. Since the markers of any given tracking frame are assumed rigidly fixed relative to each other, their distances would be expected to remain relatively constant allowing only for a small amount of skin motion and measurement error. A large change in
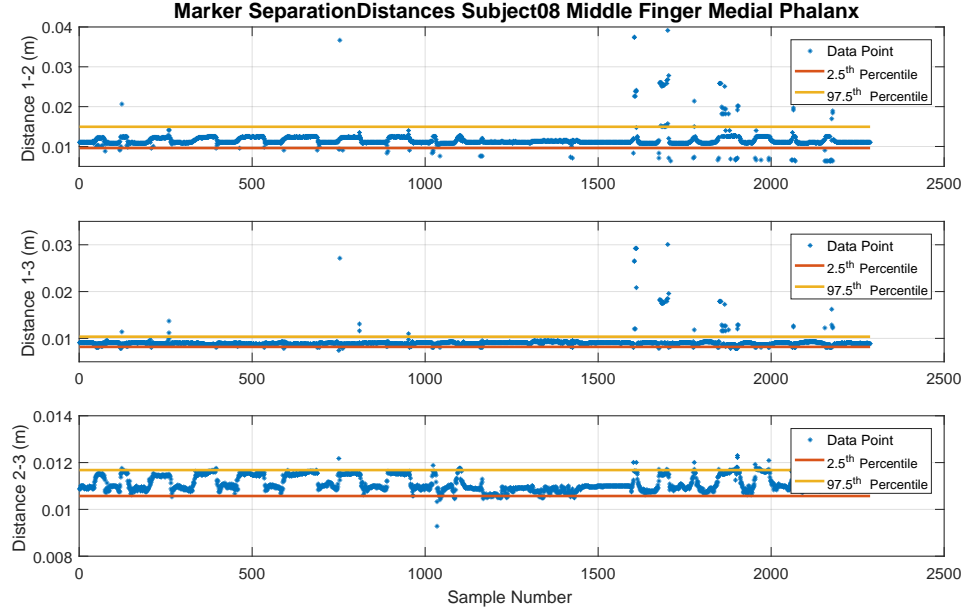
Figure 4.6: Noise detection thresholds based on marker separation distances on the middle finger's medial phalanx for Subject08. Noisy data points are readily apparent when examining this metric. Exclusion of data corresponding to the bottom and top 2.5% of marker separation distances removes the majority of noisy data with minimal exclusion of accurately acquired data.

this distance is a reliable predictor of corrupted or improperly labeled data. To be clear, reflections, occlusions, and the close proximity of multiple markers can cause the motion capture system to improperly label one marker as another, it is this type of error that we sought to remove. For a given joint, samples in which the distance between any two markers of its Ref or Cal frame were outside the middle 95th percentile were rejected. These thresholds are shown in Fig. 4.6. The results of this outlier detection, for a particularly noisy dataset, are shown in Fig. 4.7.
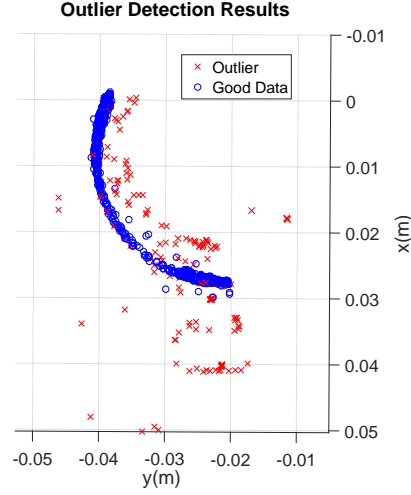
Figure 4.7: The performance of an algorithm for detecting outliers in motion capture data. Reflections, occlusions, or the close proximity of multiple markers can cause improper labeling by the motion capture system. It is expected that the marker for a hinge joint as shown should follow a circular arc. The detection algorithm correctly identifies most false readings.

Following outlier rejection, the data for each joint has densely populated regions thinned. Examples of these densely populated regions are shown in Fig. 4.8. As the individual repeatedly flexes and extends their joints, they pause briefly at full extension and full flexion causing these regions to be artificially weighted more heavily than the joint poses in the middle of their range of motion. This causes the previously mentioned over-fitting and illogical joint orientations.

To get a more even distribution of data, we calculate the 5th nearest neighbor of each point. Through testing it was seen that this metric was indicative of markers in densely populated regions without including markers in sparse regions that happen

to have a couple points within close proximity. Using this metric, we set a threshold at the 33rd percentile of 5th nearest neighbors. We then randomly remove 10% of the points above this threshold and recalculate nearest neighbors. We repeat the process of randomly removing markers and recalculating nearest neighbors until all data points fall below the originally defined threshold. These threshold values were tuned and selected during testing to achieve the desired results. The thinning process is shown in Fig. 4.8.

After the data has been filtered and weighted more evenly, it is ready to be used for locating the joint axes. In total, between 100 and 1000 samples are typically remaining after this condition process.

4.1.5 Carpometacarpal Joint Model Fitting

The carpometacarpal (**CMC**) joint is fit with a slightly modified implementation of Chang et al.'s work with notation modified to be consistent with our work. This method optimizes FE and AA axis positions and orientations by minimizing a cost metric based on anatomical features of the joint [129]. The implementation of this method involves first assuming two candidate axis reference frame orientations parameterized by 4 rotation values. The rotation from the Ref frame to the FE axis is parameterized by a rotation about x and a rotation about y. The rotation from the AA axis to the Cal frame is parameterized by rotations about y and about z. These candidate values give R_{FE}^{Ref} and R_{Cal}^{AA}, components of the transformation matrices
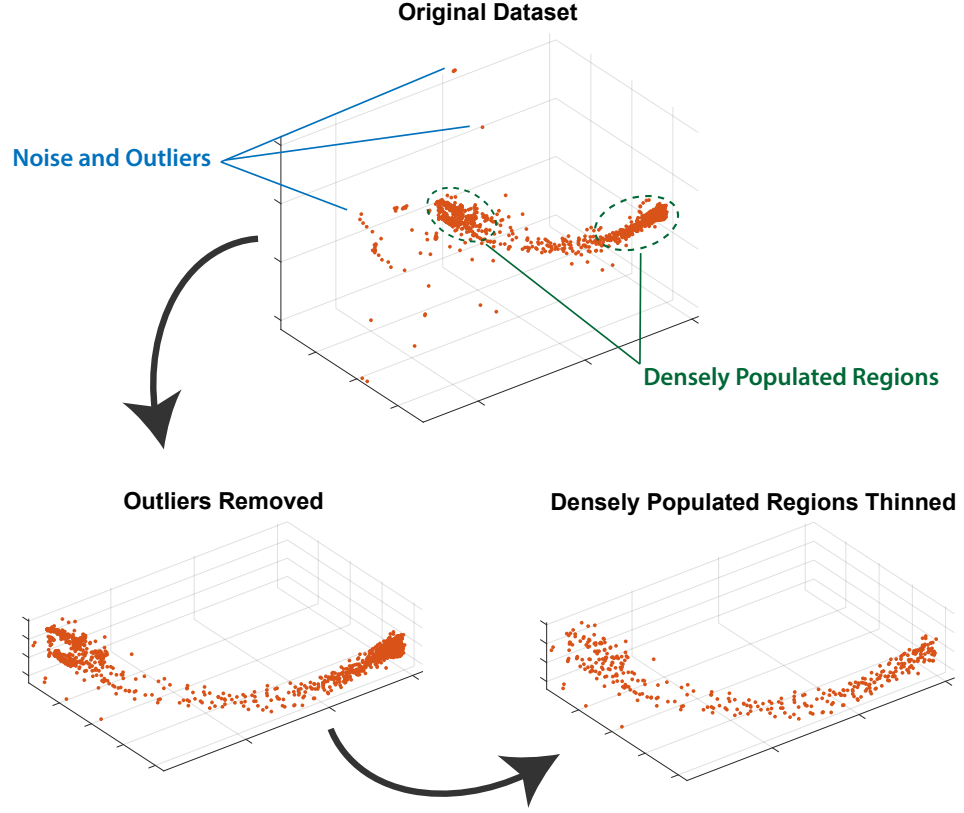
Figure 4.8: Process of preparing motion capture data prior to its use in fitting the joint models. Outliers are removed from the dataset followed by a de-weighting process to filter out dense areas of data. The result is a high quality dataset evenly distributed across the joint's range of motion.

shown in Fig. 4.3(b).

Next, for each sample, k, of the calibration data set, the frame transformation $T_{Cal}^{Ref}(k)$ is found using Eqns. 4.1 - 4.7. The forward kinematics of the joint is then found using Eqn. 4.9 [129].

$$R_{AA}^{FE}(k) = (R_{FE}^{Ref})^T R_{Cal}^{Ref}(k)(R_{Cal}^{AA})^T \qquad (4.9)$$

From this measured rotation matrix, the joint kinematics of Eqn. 4.8 are used to solve for the joint angles at each time step using Eqns. 4.10 - 4.12. Two equivalent solutions exist, we take the solution where $\frac{-\pi}{2} < \gamma < \frac{\pi}{2}$ [129].

$$\gamma(k) = asin(-R^{FE}_{AA_{3,1}}(k)) \tag{4.10}$$

$$\alpha(k) = atan2(\frac{-R^{FE}_{AA_{2,1}}(k)}{cos(\gamma(k))}, \frac{-R^{FE}_{AA_{1,1}}(k)}{cos(\gamma(k))}) \tag{4.11}$$

$$\beta(k) = atan2(\frac{-R^{FE}_{AA_{3,2}}(k)}{cos(\gamma(k))}, \frac{-R^{FE}_{AA_{3,3}}(k)}{cos(\gamma(k))}) \tag{4.12}$$

The frame rotations are then used to generate the matrices of Eqn. 4.13 [129] which is of the form of Eqn. 4.15. The vector y is of length $9K$, where K is the total number of samples, and consists of the measured x,y,z positions of the 3 markers forming the *Cal* frame. The Matrix X is of size $9K \times 13$ and consists of the forward kinematics which relate the vector of fixed joint parameters, b, to the measured marker positions of y. The joint parameters are solved for with Eqn.4.16 using a linear least squares approach of the More-Penrose pseudo-inverse.

$$
\begin{bmatrix}
p_{Cal_1}^{Ref}(0) \\
p_{Cal_2}^{Ref}(0) \\
p_{Cal_3}^{Ref}(0) \\
\vdots \\
p_{Cal_1}^{Ref}(k) \\
p_{Cal_2}^{Ref}(k) \\
p_{Cal_3}^{Ref}(k) \\
\vdots \\
p_{Cal_1}^{Ref}(K) \\
p_{Cal_2}^{Ref}(K) \\
p_{Cal_3}^{Ref}(K)
\end{bmatrix}
=
\begin{bmatrix}
I_3 & R_{FE}^{Ref} u_1(0) & R_{FE}^{Ref} R_{AA}^{FE}(0) & 0_3 & 0_3 \\
I_3 & R_{FE}^{Ref} u_1(0) & 0_3 & R_{FE}^{Ref} R_{AA}^{FE}(0) & 0_3 \\
I_3 & R_{FE}^{Ref} u_1(0) & 0_3 & 0_3 & R_{FE}^{Ref} R_{AA}^{FE}(0) \\
\vdots & \vdots & \vdots & \vdots & \vdots \\
I_3 & R_{FE}^{Ref} u_1(k) & R_{FE}^{Ref} R_{AA}^{FE}(k) & 0_3 & 0_3 \\
I_3 & R_{FE}^{Ref} u_1(k) & 0_3 & R_{FE}^{Ref} R_{AA}^{FE}(k) & 0_3 \\
I_3 & R_{FE}^{Ref} u_1(k) & 0_3 & 0_3 & R_{FE}^{Ref} R_{AA}^{FE}(k) \\
\vdots & \vdots & \vdots & \vdots & \vdots \\
I_3 & R_{FE}^{Ref} u_1(K) & R_{FE}^{Ref} R_{AA}^{FE}(K) & 0_3 & 0_3 \\
I_3 & R_{FE}^{Ref} u_1(K) & 0_3 & R_{FE}^{Ref} R_{AA}^{FE}(K) & 0_3 \\
I_3 & R_{FE}^{Ref} u_1(K) & 0_3 & 0_3 & R_{FE}^{Ref} R_{AA}^{FE}(K)
\end{bmatrix}
\begin{bmatrix}
p_{FE}^{Ref} \\
q_3 \\
p_{Cal_1}^{AA} \\
p_{Cal_2}^{AA} \\
p_{Cal_3}^{AA}
\end{bmatrix}
\tag{4.13}
$$

$$
u1(k) = \begin{bmatrix} -sin(\alpha(k)) & cos(\alpha(k)) & 0 \end{bmatrix}^T
\tag{4.14}
$$

$$
y = Xb
\tag{4.15}
$$

$$
b = X^+ y
\tag{4.16}
$$

The quality of the candidate rotations R_{FE}^{Ref} and R_{Cal}^{AA} are then assessed using the anatomically relevant cost metric presented by Chang et al. [129]. Chang used three components in this cost metric. The first considered that the average amount

of pronation/supination, γ, should be small. Eq. 4.17 is used to put a penalty on PS rotation, weighted by the expected amount of PS rotation, σ_γ, which Chang considers to be $5°$ [129]. The second component was that the range of motion of abduction/adduction, β, should be less than the range of flexion/extesnion, α. This is quantified by Eq. 4.18 [129]. Finally Chang considered the separation between the axes, q_3, using Eq. 4.19. Here Chang considers an expected separation, μ_{q3}, of *5mm* weighted by an expected range, σ_{q3}, of *5mm*. We found that the minimization of AA rotation relative to FE rotation could, in some cases, outweigh the other metrics and result in an AA axis that pointed perpendicular to the expected AA axis. This orientation would see little rotation of the axis, which would be reduce Chang's cost metric, but result in poor reconstruction error and a non-anatomical joint position. To remedy this, we added a penalty on the reconstruction error using Eq. 4.20. We weight this by the expected reconstruction error, σ_e, of *5mm*. The complete cost metric is shown in Eq. 4.21. We use the function *fminsearch* in Matlab to optimize the 4 rotation angles parameterizing R_{FE}^{Ref} and R_{Cal}^{AA} based on this cost metric.

$$f_{PS} = \frac{\sum_0^K (\gamma(k) - mean(\gamma))^2}{K\sigma_\gamma^2} \tag{4.17}$$

$$f_{ROM} = \frac{range(\beta)}{range\alpha} \tag{4.18}$$

$$f_d = \frac{(q_3 - \mu_{q3})^2}{2\sigma_{q3}^2} \tag{4.19}$$

$$e = \frac{1}{\sigma_e^2 K} \sum_{i=1}^{3} \sum_{k=0}^{K} \left(P_{m_i}^{Ref}(k) - T_{AA}^{Ref}(k) P_{Cal_i}^{AA} \right)^2 \tag{4.20}$$

$$C = f_{PS} + f_{ROM} + f_d + e \tag{4.21}$$

4.1.6 MCP and IP Joint Model Fitting

For the IP and MCP joints, the FE axis orientation was determined using the axis fitting technique of Gamage et al. [140], which is similar to that of Halvorsen [141]. First, all data for the joint is transformed into the joint's "Ref" frame so that the motion of markers from the "Cal" frame can be assumed due only to motion of the joint. This transform is done simply with Eqn. 4.22 where p_m^0 is the position of marker m in frame 0, p_m^{Ref} is the position of marker m in frame Ref, and T_{Ref}^0 is found using Eqns. 4.1-4.7.

$$\begin{bmatrix} p_m^{Ref} \\ 1 \end{bmatrix} = (T_{Ref}^0)^{-1} \begin{bmatrix} p_m^0 \\ 1 \end{bmatrix} \tag{4.22}$$

If the assumption of a single DOF rotational joint is correct, following this transformation the markers of the "Cal" frame should move on concentric arcs lying on

127

parallel planes. The observed behavior closely matches this as can be seen in Fig. 4.9.

The normal to these planes should be parallel to the joint axis and the axis should

pass through the center of these arcs.
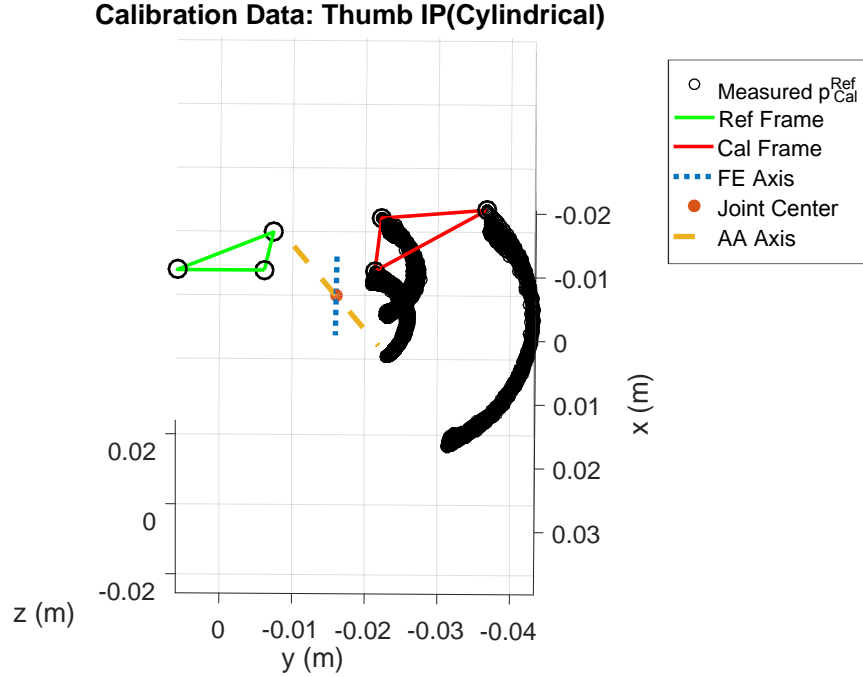
Figure 4.9: Example of measured IP joint data when viewed from the joint reference frame. The data is transformed into the "Ref" frame so that the markers of the "Cal" frame trace out concentric arcs which lie on parallel planes. An arbitrary AA axis is fit.

For the MCP joint, we assumed that subjects could effectively isolate the FE

motion from the AA motion. Post-analysis of subject data using Eqns. 4.9 - 4.12

indicates that this was mostly the case. A plot of one subject's FE and AA angles

during the data collection period of isolated FE motion at the MCP is shown in Fig.

4.10 and confirms minimal AA motion.
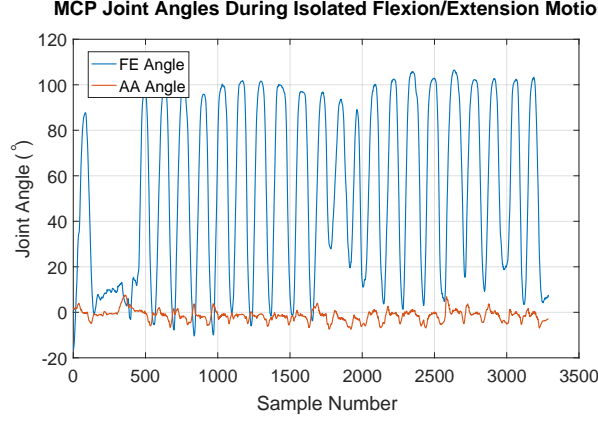
Figure 4.10: FE and AA angles at one subject's Index MCP joint. The subject had been asked to flex their MCP through its ROM with minimal AA motion. The observed behavior verifies minimal AA motion relative to FE motion.

To find the axis orientations, the method of Gamage et al. minimizes a cost function which describes the parallel plane condition [140]. They assume an arbitrary point, $p_{plane_m}^{Ref}$, on the plane containing marker Cal_m. The common normal, n, to each of the m planes should be perpendicular to the vector pointing from $p_{plane_m}^{Ref}$ to a measured position of Cal_m at any time k, $p_{Cal_m}^{Ref}(k)$. The error is quantified as the sum of squares of the projection of $p_{Cal_m}^{Ref}(k) - p_{plane_m}^{Ref}$ onto n. This is described by Eqn. 4.23 reproduced from Gamage et al. [140] with notation changed to be consistent across our work.

$$C = \sum_{m=1}^{3} \sum_{k=1}^{N} \left[(p_{Cal_m}^{Ref}(k) - p_{plane_m}^{Ref}) \cdot n \right]^2 \tag{4.23}$$

Eqn. 4.23 is then differentiated with respect to n and set equal to zero to find the minimum of the cost function. Eqn. 4.23 is also differentiated with respect to $p_{plane_m}^{Ref}$

to find the optimal fixed point on the plane in terms of known parameters. Doing this and re-arranging the parameters results in Eqn. 4.24 [140].

$$\sum_{m=1}^{3} \left[\left\{ \frac{1}{N} \sum_{k=1}^{N} p_{Cal_m}^{Ref}(k)(p_{Cal_m}^{Ref}(k))^T \right\} - \overline{p_{Cal_m}^{Ref}} \left(\overline{p_{Cal_m}^{Ref}} \right)^T \right] n = 0 \qquad (4.24)$$

$$\overline{p_{Cal_m}^{Ref}} = \frac{1}{N} \sum_{k=1}^{N} p_{Cal_m}^{Ref}(k) \qquad (4.25)$$

Eqn. 4.24 is of the form $An = 0$ where the solution for n is the eigenvector corresponding to the eigenvalue of smallest magnitude. For a more complete derivation see the work of Gamage et al. [140] as well as Halvorsen [141]. The values of Eqns. 4.24 and 4.25 are calculated in Matlab and solved by using the function eig(A) to generate the eigenvectors and eigenvalues. The result is a unit vector oriented with the axis of the joint.

$$\hat{z}_{FE}^{Ref} = eigenvector(A) \mid min(eigenvalue(A)) \qquad (4.26)$$

In order to completely describe the IP joints, a point on the axis is also needed. Gamage used a similar method to determine a point on the axis of rotation as they did to determine its orientation, finding a closed form solution using a cost metric. However, for our work we again use the linear least squares method based on the thumb fitting work of Chang et al. [129]. This method has the benefit of finding a fixed "average" position for the markers of the *Cal* frame relative to the joint's AA

axis. For the IP joints, the AA axis orientation is arbitrary as the rotation about it is assumed zero. The important properties of the axis are that it is fixed relative to the distal bone of the joint and that it intersects the FE axis. The axis parameters are determined using the following method.

First, a reference frame orientation is determined for the FE axis. The z-axis of this frame is aligned with the previously determined joint axis. The y axis is arbitrarily set to be orthogonal to the FE axis and the Ref frame's x-axis. The x axis is orthogonal to both. This is given by Eqns. 4.27 - 4.29

$$\hat{y}_{FE}^{Ref} = \hat{z}_{FE}^{Ref} \times \begin{bmatrix} 1 & 0 & 0 \end{bmatrix}^T \tag{4.27}$$

$$\hat{x}_{FE}^{Ref} = \hat{z}_{FE}^{Ref} \times \hat{y}_{FE}^{Ref} \tag{4.28}$$

$$R_{FE}^{Ref} = \begin{bmatrix} z_{FE}^{Ref} & \hat{y}_{FE}^{Ref} & \hat{x}_{FE}^{Ref} \end{bmatrix} \tag{4.29}$$

Following definition of R_{FE}^{Ref}, a candidate value for the rotation R_{Cal}^{AA} was parameterized by two rotations as was done in Section 4.1.5. Solving for the joint parameters of Eq. 4.13 now follows the same process as for the thumb's CMC joint in Section 4.1.5. Using *fminsearch* in Matlab, the rotations parameterizing R_{Cal}^{AA} are then optimized so as to minimize the reconstruction error, e, of Eq. 4.20. For the IP joint, the reconstruction error is calculated with $\beta = 0$ and $q_3 = 0$. For the MCP joints, the reconstruction error is calculated with $q_3 = 0$.

4.1.7 Joint Angle Calculations

Once a kinematic model was fit to the data, joint angles were calculated by "driving" the joint rotations to minimize the distance between measured and modeled markers, as depicted in Fig. 4.11. Doing this allowed for the calculation of joint angles in the presence of occluded data as only a single marker on the joint's distal bone was needed to define the joint rotations. Angles were calculated, for each sample of motion capture data, by minimizing the cost function of Eq. 4.30. Here, M is the total number of un-occluded markers on the distal bone, $P^{Ref}_{Cal_m}(k)$ is the measured position of marker m at time k, PAA_{Cal_m} is derived during the joint fit in Eq. 4.13, T^{Ref}_{AA} is a function of β and α derived using Eq. 4.8 and the parameters determined in Eq. 4.13. The cost function is optimized for α and β using the Matlab function *fminsearch*.

$$C(k) = \sum_{m=1}^{M} \left(P^{Ref}_{Cal_m}(k) - T^{Ref}_{AA}(k) P^{AA}_{Cal_m} \right)^2 \tag{4.30}$$

4.1.8 Defining a "Zero" Posture

The previously described analysis will track joint positions, the orientation of the joint axes, and relative rotations of the joints but does not define an absolute joint angle. A reference value needed to be provided to define 0° for each joint rotation. To
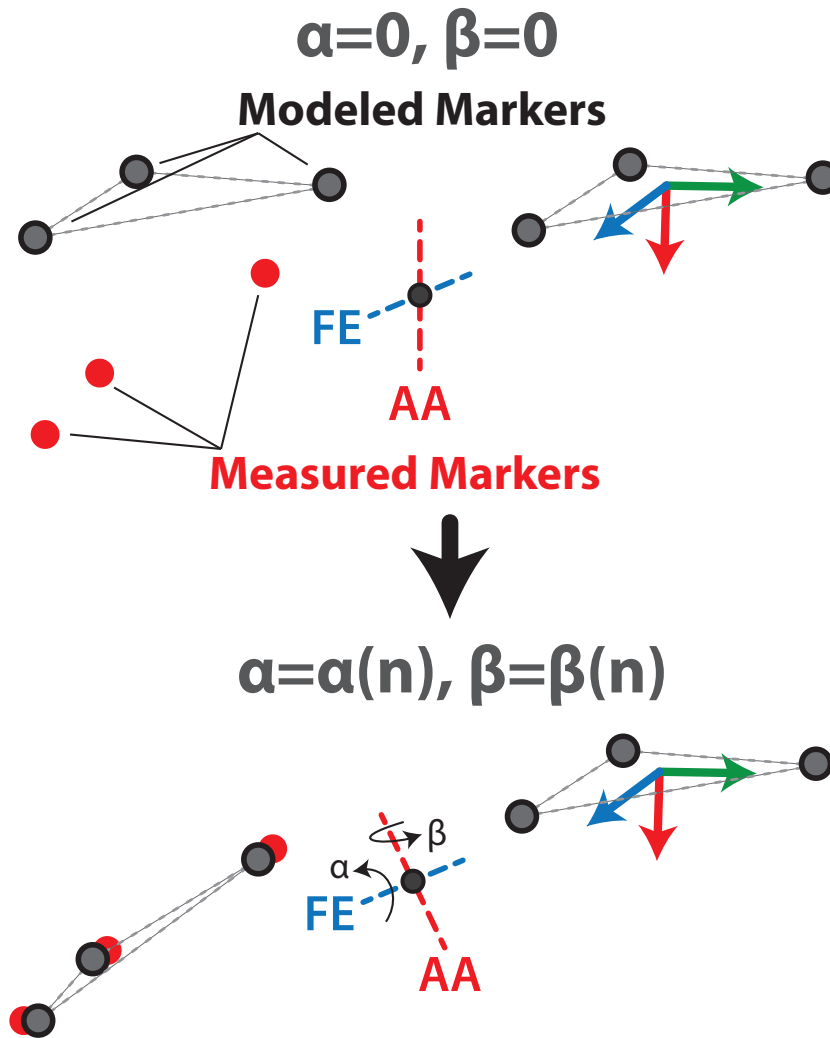
Figure 4.11: Diagram depicting a derived joint model being used to calculate joint rotations from measured marker data. The model is rotated until
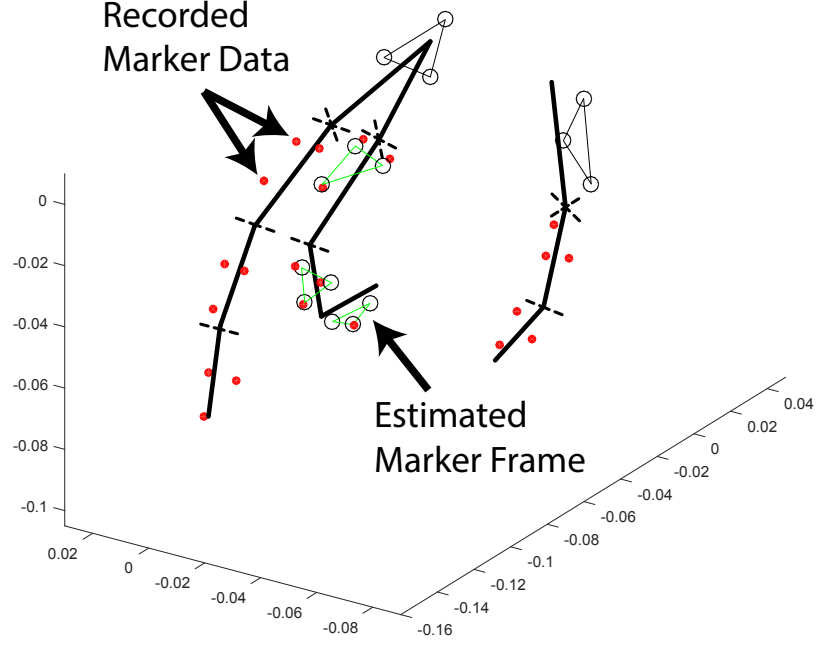
Figure 4.12: Fitting the skeletal model to motion capture data with missing markers. Markers on the distal tip of the index finger have been occluded, the fitting method has filled in an estimated frame with the data available.

do this, we have subjects place their hand flat on a table with their joints neutrally abducted. We find the angles α and β at this pose and use them to apply an offset rotation to the matrices R_{FE}^{Ref} and R_{Cal}^{AA}.

4.1.9 Kinematic Model Fitting Implementation

The previously described process for deriving a kinematic model of the joints from motion capture data was implemented in Matlab 2017a (MathWorks Inc., Natick, MA). A simple to use graphical interface was developed which loaded a ".csv" file of labeled marker positions output from the software Motive. The window of data used
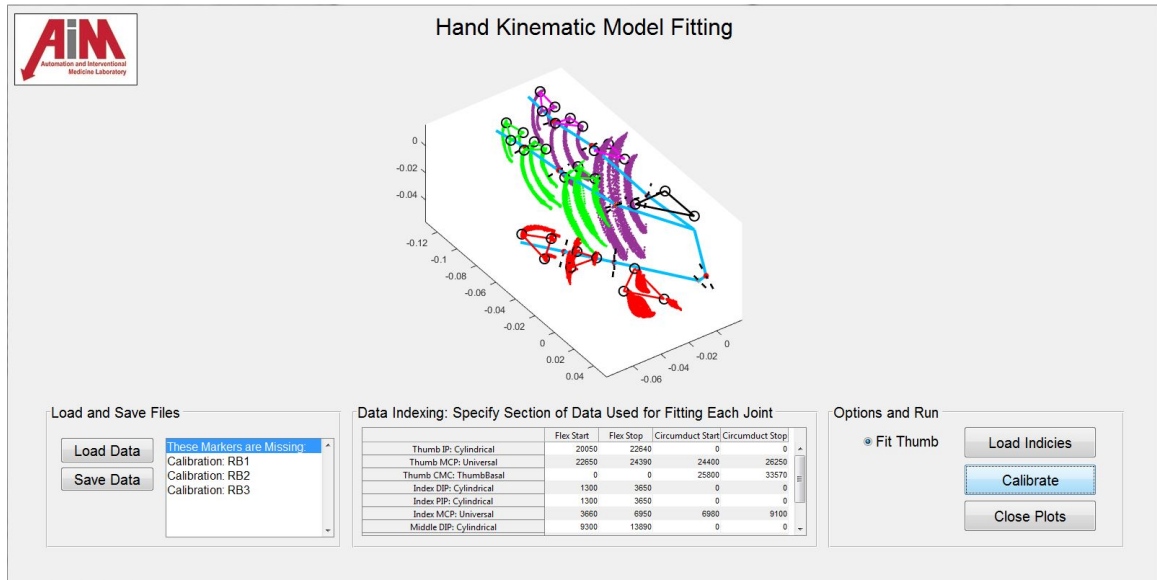
Figure 4.13: User interface developed for generating kinematic models from motion capture data. The user can load a data set, select the indicies used for fitting each joint and save the calculated joint parameters.

for fitting each joint could be specified in a table in the UI or by loading an equivalent table from a ".csv" file. By pressing calibrate, the software would find the parameters of each joint and store them in a struct which could be saved for use in further data processing. The user interface is shown in Fig. 4.13. The implementation of a simple user interface will enable easier implementation of the analysis in future studies by robotics researchers who may have limited biomechanics background.

4.2 Motion Capture Validation

To validate our motion capture protocol, we conducted a study to compare our ability to localize the joints using motion capture with a method using computed tomography

($\boldsymbol{CT}$) scans of subjects' hands. The hard plastic motion capture markers were found to be radiopaque, and as such they could be used as fiducials within both imaging modalities allowing for overlaying and comparison of the two datasets.

Upon approval from the Worcester Polytechnic Institute's IRB, we recruited 5 subjects aged $23\pm2.5years$, 3 males, 2 females, all right hand dominant for the study. After administering the markers as specified by Fig. 4.1, we had subjects gently hold a foam pad which kept their hand in a neutrally flexed posture. Their hand was then wrapped in an ace bandage to limit movement and inserted into a high-resolution peripheral quantitative computed tomography ($\boldsymbol{HR\text{-}pQCT}$) scanner (XtremeCT, Scanco, Switzerland). A single scan was taken with a resolution of $492\mu m$, about equal to the accuracy of the motion capture system. Following this scan, the subjects' hands were removed from the machine and the ace bandages were carefully removed so as not to disturb the motion capture markers.

Immediately following imaging with the HR-pQCT, subjects performed the motions described in Section 4.1.4 while data was collected with the motion capture setup described in Section 4.1.2. After this data was collected, the subject's participation in the study was complete. The marker data was manually labeled according to Fig. 4.1 and processed using the protocol of Section 4.1 to locate the joint axes.

HR-pQCT images were post-processed using 3D Slicer 4.8.1, an open source software for medical image processing and visualization. First, the images were thresholded to produce a 3D rendering containing both the skeleton and the markers. The

centroids of these markers were then manually located by scrolling through the orthogonal slice planes provided by slicer. Once located, the marker centroids in RAS coordinates were marked and recorded. A view of the thresholded 3D render with located markers is shown in Fig. 4.14.
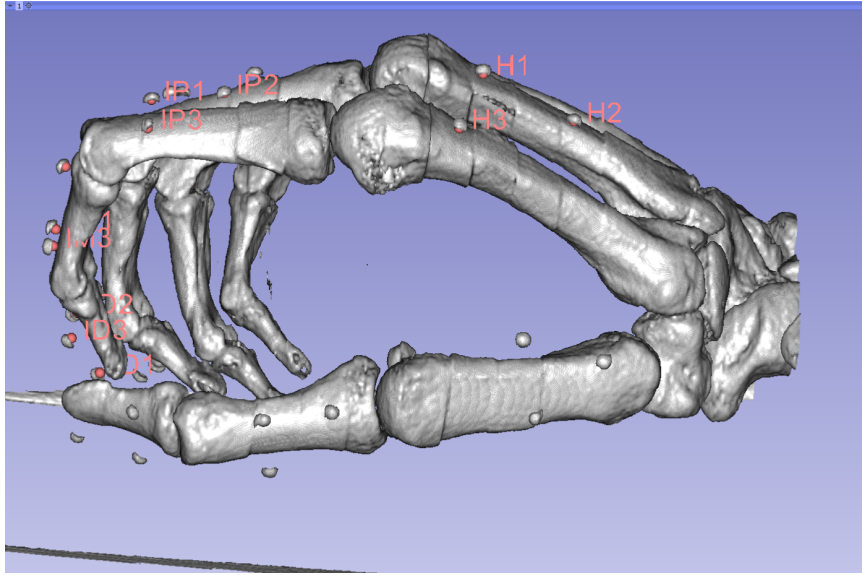
Figure 4.14: CT Scan of a hand instrumented with motion capture markers. The markers are located and marked with fiducials (the pink dots seen in the image) using the open source software 3D slicer.

Once the markers were located in the CT image, they could be used as reference frames to establish the position of the joint axes in the CT image as determined by the motion capture dataset. The analysis of Section 4.1 provides the position and orientation of each axis relative to the reference frame formed by the three markers on the bone proximal to the joint, making the registration of the two datasets now trivial. A render of the overlaid joints is shown in Fig. 4.15.

To get an estimate of the joint location from the CT image set, we made the
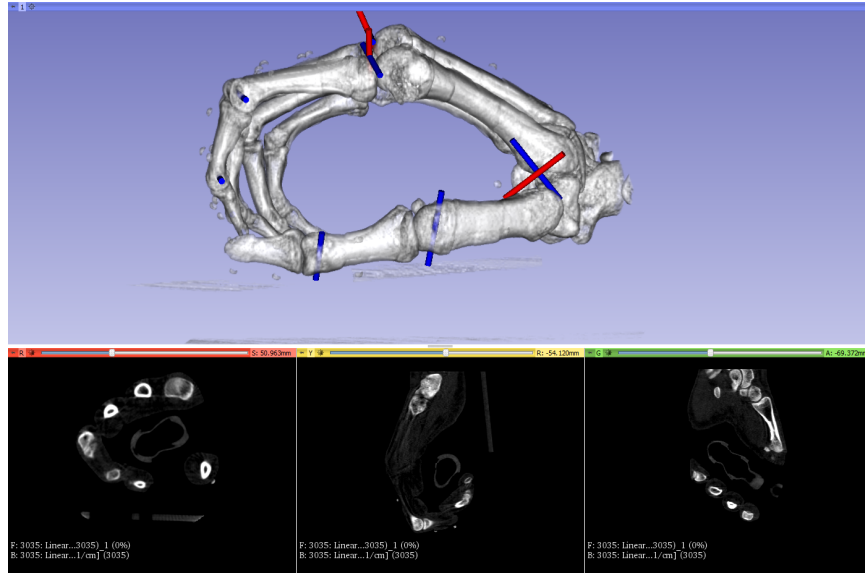
Figure 4.15: Overlay of joint axes determined by a motion capture analysis with a CT scan of the hand. Blue lines indicate flexion/extension axes and red lines indicate abduction/adduction axes.

assumption that the intersection point of the long axes of the bones that make up a joint occurred at the joint axis. We defined the long axis of each bone as coincident with the axis of minimal moment of inertia. We found this axis by segmenting out the bones of the thumb, index, and middle fingers using the Segment Editor module in 3D Slicer. A depiction of this segmentation is shown in Fig. 4.16.

Once the bones were segmented, we opened the stl files generated by 3D slicer in the CAD software Solidworks 2016 (Dassault Systmes, Waltham, MA). Using the mass properties tool, we located the long axes of each bone from its center of mass and its principal axis of inertia corresponding to its smallest principal moment of inertia. A depiction of these long axes overlaid on the CT images is shown in fig. 4.19.
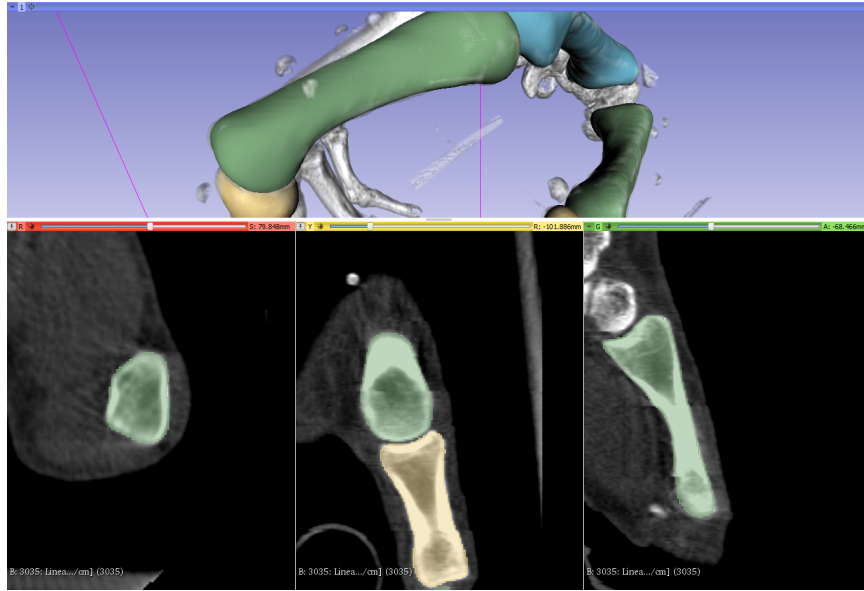
Figure 4.16: Segmentation of the phalanges and metacarpal bones from a CT scan of a hand. The colors green, blue, and tan indicate the segmented boundaries of the various bones.
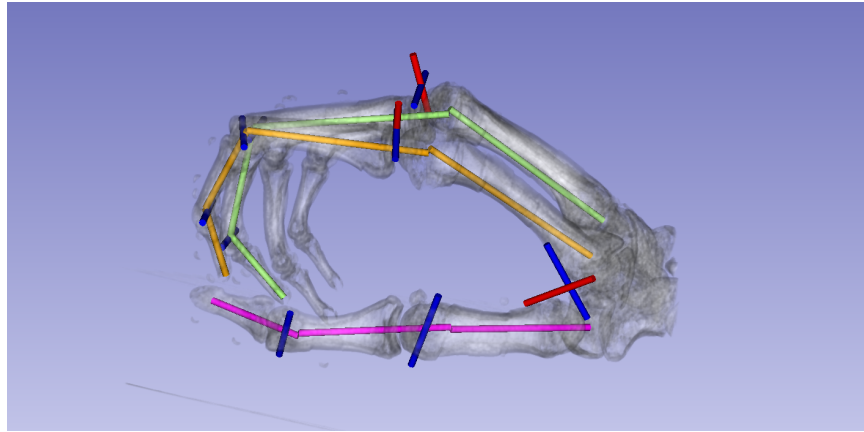
Figure 4.17: Overlay of the calculated long axes of the finger bones on a CT image set. The long axes of the thumb (pink), index (orange), and middle (green) fingers intersect near the axes of the IP and MCP joints.

Since noise exists in the CT measurement, the long axes of the two bones which make up a joint are unlikely to exactly intersect. Instead, we define the joint center as the center of the line which is mutually orthogonal to the long axes of both bones.
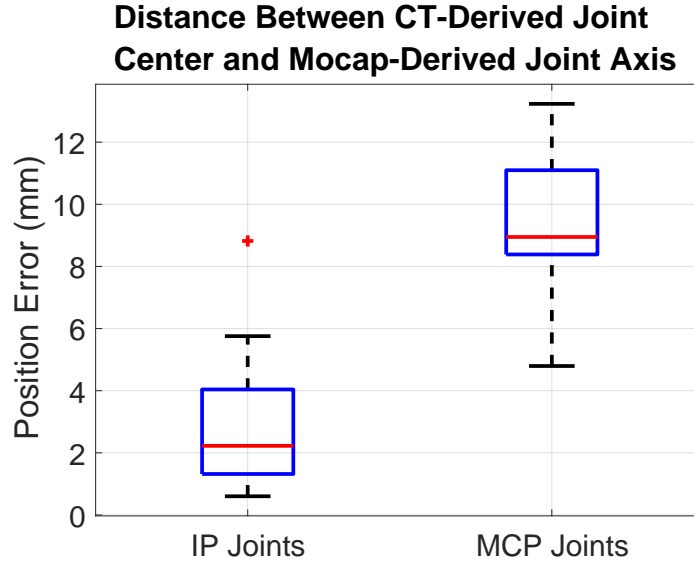
Figure 4.18: Calculated distance between CT scan derived joint centers and motion capture derived joint axes.

The distance between this joint center and the joint axis, as found using the motion capture data, was similarly defined as the length of a line, perpendicular to the motion capture axis, which connects the motion capture axis to the CT-derived joint center. We consider this distance to be the error of the motion capture method. These errors are summarized in Fig.4.18.

Error present in the IP joint fitting was about $2mm$ while the error for the MCP joint was about $9mm$. For the IP joints, the direction of this error did not appear systematic with the motion capture derived axes appearing both proximal and distal of the CT-derived joint center. For the MCP joint, we recognized a consistent trend that the flexion/extension axis appeared shifted distally from the anatomical center of the axis. This shift can be seen in Fig. 4.19. Skin motion was thought to be a probable cause of this so we checked for distortion of the motion capture data

indicative of skin motion. To do this we plotted the 2-D data for each marker in a plane orthogonal to the FE axis and normalized the position of the data to the average radius between the marker and the joint center. This, shown in Fig. 4.20, indicates that the marker path is highly circular. This systematic error is a potential area of future research, but was deemed acceptable as-is for use in the finger tracking and torque calculations of Sections 4.3 and 4.4.
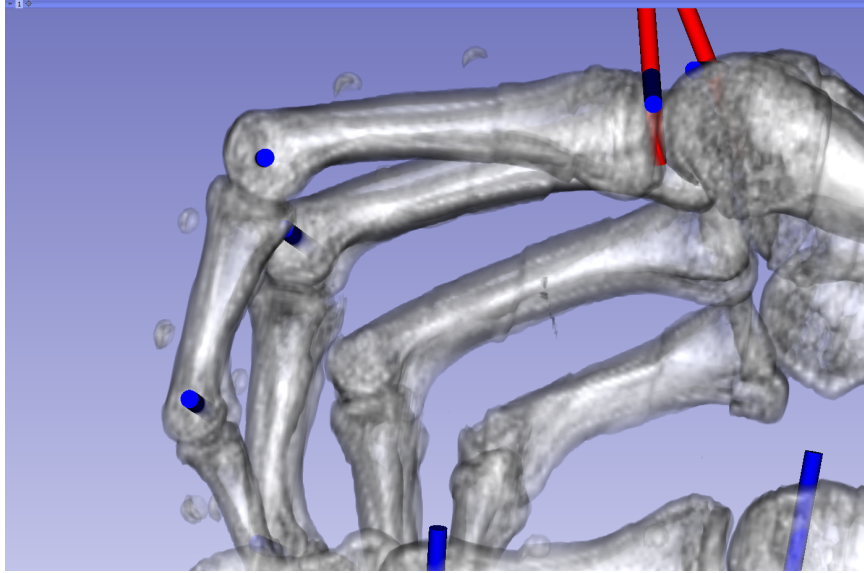
Figure 4.19: Depiction of the alignment between motion captured-derived joint axes with the anatomical axes of the index finger. Alignment of the interphalangeal joints with the anatomical axis is accurate to $3mm$. The MCP joint was seen to be shifted distally from the expected anatomical axis by about $10mm$.

Normalized Measured MCP Marker Positions
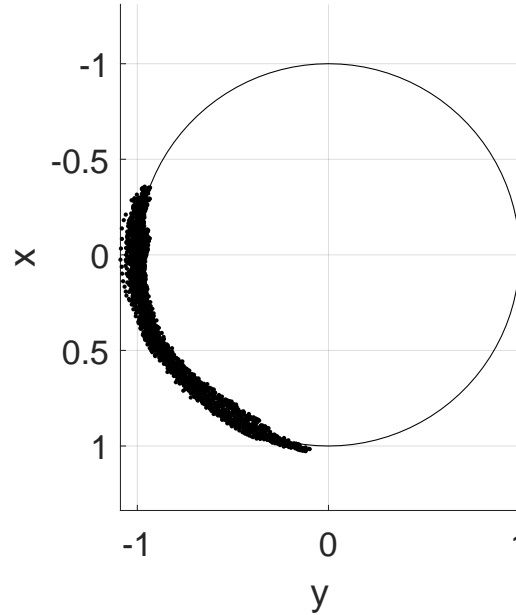
Figure 4.20: Normalized MCP marker positions. When normalized to the average radius from the flexion/extension axis, the markers used to fit the MCP joint follow a generally circular path.

4.3 Measurement of Grasping Forces and Torques in Activities of Daily Living

Most work in physical deign of hand orthoses can be summed up by the following overarching goal: optimization through minimizing size and weight of physical components without sacrificing relevant function. This statement, while short, is difficult to define objectively. Interpretations of an "optimal" design or "relevant" function will be very much open to interpretation. This gray area, however, should not discourage rigorous approaches to characterizing these metrics. In hand orthosis design,

lack of quantitative definitions of what constitutes relevant function have lead to evaluation of device performance on questionably relevant metrics. The definition of "grip force" is an example of this approach to device evaluation. A single value for the grip force that a device is capable of producing does little to characterize its performance, however, it is a common metric offered in published works. The force is measured assuming no addition or resistance of force from the user's joints, which as we established in Section 2.1.1, is a poor assumption for individuals with UMN. In addition to lacking relevance, the means by which it is evaluated are by no means standardized. It is not uncommon to see grip force characterized by fully extending one of the device's finger linkages, or actuators, and pressing the tip of the linkage against a load cell [17,19,20]. Considering that the pose of the linkage will effect the way in which it applies forces to the fingers [18], and that individuals typically do not use their fingers to apply forces with their joints fully extended, it is difficult to objectively consider the characterization relevant.

The main hindrance to relevant evaluation of a device's "grip force" is a lack of thoroughly characterized grasping data which can directly be applied to orthosis design. Due to this gap in the literature, engineers are left trying to interpret tangentially related or incomplete studies on grasping to size actuators and to design linkages of the devices. Measurement of grip strength as a diagnostic tool is common, using purpose built pinch gages and dynamometers to assess the maximal isometric strength of differing populations [142]. These clinical tools, however, have limited

use in informing engineering design. While some data on grasping during activities of daily living (**ADL**) does exist [143–146], studies which either focus on tasks that wouldn't benefit from an orthosis, allow subjects to use dexterity irreproducible by an orthosis, or simply lack measurement of kinematic data leave engineers to make imperfect assumptions.

To address the shortcomings in applying current grasping research to the optimization of orthotic devices, accurate measurements of reaction forces and skeletal kinematics during activities of daily living (**ADL**) using 9 minimally modified household objects was conducted. During the study, subjects were limited exclusively to the lateral and three-jaw-chuck grasps shown in Fig. 4.21, grasps likely to be achievable by a basic orthosis.

4.3.1 Instrumentation of Household Objects

Nine household objects were instrumented with high-precision load cells (LLB130, FUTEK Advanced Sensor Technology, Inc., Irvine, CA, USA) so as to accurately measure the forces which the subject applied to them. The objects were chosen through discussion with several occupational therapists based on their relevance to daily life, a need to exert grip strength with minimal dexterity when using the object, and a practical consideration of their ability to be instrumented with force sensors. The objects were chosen to be as common and representative as reasonably possible with most items selected from a best-sellers list provided by the web commerce site
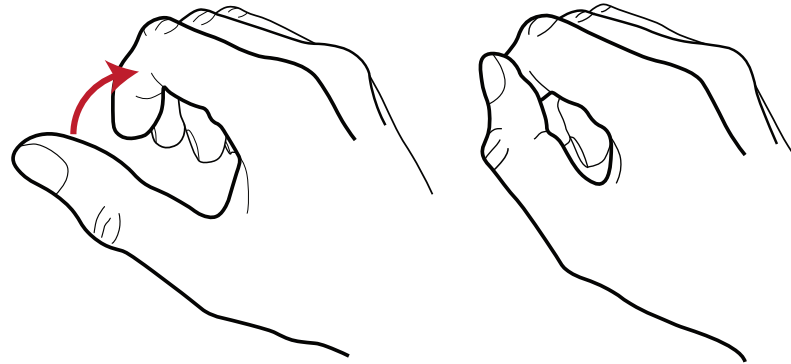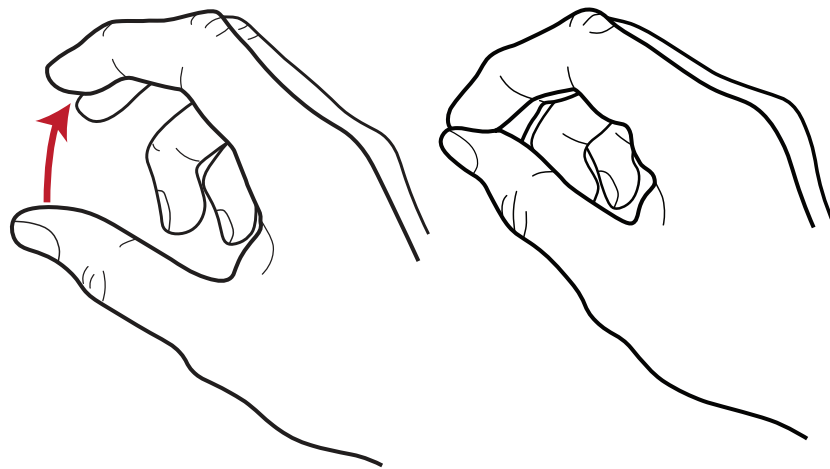
(a) Lateral Grasp

(b) Three Jaw Chuck Grasp

Figure 4.21: Depiction of three-jaw-chuck and lateral grasps used in measuring forces during activities of daily living.

Amazon. The items chosen were as follows:

- **Doorknob** (Brinks^{TM} Bell Knob model 2101-109, Hampton Products Intl. Corp)

- **Deadbolt** (Schilage^{TM} model B60N 619, Allegion plc.)

- **Coffee Cup** (Dixie^{TM} Perfect Touch 12oz. paper cup, Georgia Pacific)

- **Fork** (Mainstays^{TM} Swirl dinner forks model 0805A002, Wal-Mart Stores, Inc)

- **Steak Knife** (Eversharp^{TM} 5" model 35197-100, J.A. Henckels International)

- **Sweatpants** (Champion^{TM} Authentic, Hanesbrands Inc.)

- **Zipper** (YKK^{TM} #5 molded plastic separating zipper, YKK Corporation)

- **Toothbrush** (Colgate^{TM} Premiere Clean, Colgate-Palmolive Company)

- **Medicine Bottle** (Ezy Dose^{TM} 16 dram with push & turn cap, Apothecary Products, LLC.)

The doorknob, deadbolt, fork, zipper, cup, and medicine bottle were all modified with cutouts to contain the load cells. The toothbrush and knife handle were replicated in Solidworks and modified in CAD to contain spaces for the load cells. The tootbrush handle was 3D printed on a polyjet printer (Objet Connex 260, Stratasys) using an acrylic material for the handle and a rubber-like material for the textured

146

griping pads. The knife handle was printed from ABS plastic on a fused deposition modeling (**FDM**) machine. The constructed objects are shown in Fig. 4.22.

Loadcells for each object were amplified (AD620, Analog Devices, Inc., Norwood, MA, USA) to a sensitivity of $0.151\frac{V}{N}$ and recorded with a 12-bit analog input card (NI 9201, National Instruments, Austin, TX, USA) in an FPGA-based embedded controller (cRIO-9074, National Instruments). The data collection was synchronized to the motion capture system at 120hz sampling rate via an external trigger.

4.3.2   Protocol for Measurement of ADL Forces

After obtaining informed consent, participants in the study were instrumented with the motion capture marker set described in Section 4.1.1. Subjects then completed 8 activities using the objects described in Section 4.3.1. The tasks were specifically:

- Unlock and lock a deadbolt

- Turn a door knob, open a mock door, and close it

- Brush their teeth for approximately $20s$ periods

- Zip and unzip a fleece vest

- Hold a cup and pour sand into it

- Put on and take off a pair of sweatpants

- Remove and replace the lid of a pill bottle while it rests on a table

147

(a) Doorknob   (b) Deadbolt   (c) Toothbrush

(d) Zipper   (e) Steak Knife   (f) Fork

(g) Cup   (h) Sweatpants   (i) Medicine Bottle
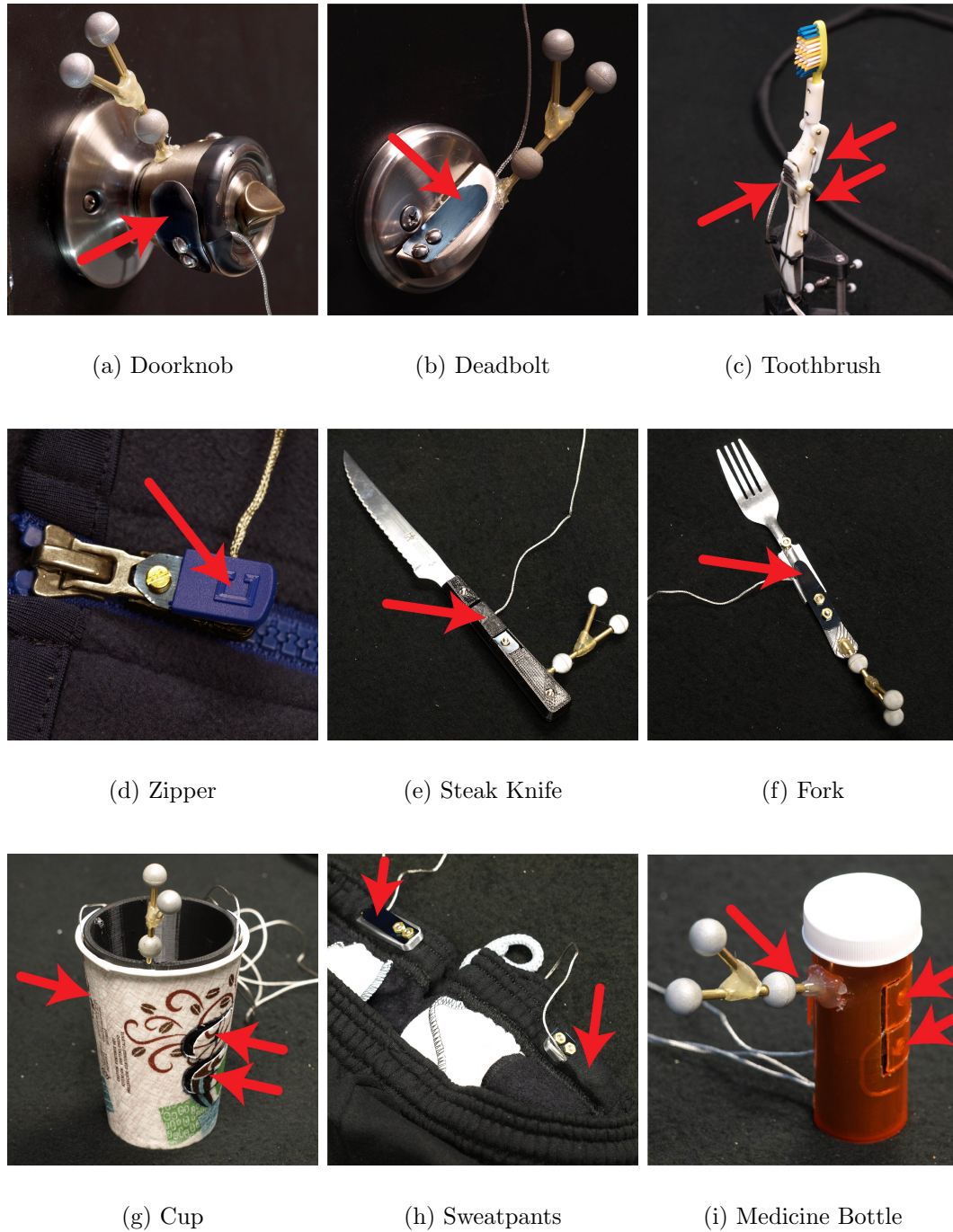
Figure 4.22: Instrumented objects used in the study of grip force in activities of daily living. Red arrows point to where subjects were instructed to grasp each object.

- Cut and eat pieces of steak using a fork and knife

Sand was used in place of liquid for the cup task to prevent interference with the electronic sensors. The steak came form a steak and frites meal prepared by a local restaurant. Small and large sized sweatpants were available depending upon the subject's size. Subjects were asked to wear a pair of light athletic shorts to the experiment in order to put the sweatpants on over top of.

The fork and knife were used together, with the fork in the left hand and the knife in the right hand. The sweatpants also used both hands, with each hand using a lateral grasp to pinch load cells embedded in the waist band. All other activities were completed exclusively with the right hand regardless of whether or not the subject was right hand dominant. This was decided because an individual may be impaired on their non-dominant side. Each subject completed 5 repetitions of each task.

Subjects were instructed specifically how and where to grasp each of these objects, using one of the two basic grasps shown in Fig. 4.21. This limited set of motions was used for two primary reasons. First, it allowed for complete and accurate force measurement with a limited set of sensors installed in each object. This small sensor set minimized the dimensional, inertial, and tactile differences between the instrumented object and a standard object. Changes to these properties would be expected to lead to modified grip force [147–150]. Secondly, this grasp set allows the study to maintain relevance to prosthetic and orthotic evaluation. Limited dexterity in these devices would prevent them from directly replicating the much more complex and variable

grasping taxonomy that subjects would naturally employ. For example, the commercially available MyoPro (Myomo, Inc.) exclusively assists with a three-jaw-chuck grasp.

The study was designed to include 2 separate sessions for each participant. In the first session, no instruction was given regarding the amount of strength with which to grip the objects. Subjects were only instructed on where to place their fingers and that they needed to complete each task. In the second session, subjects were instructed to try and use the minimal amount of grip force possible to complete the task. We here on refer to these two test conditions as the ***regular force*** and ***low force*** trials. A minimal force is thought to have more relevance to a functional performance threshold for an orthosis.

4.3.3 Subject Descriptions

Upon approval of the protocol from the Worcester Polytechnic Institute's IRB 10 subjects were recruited for the study, 5 male 5 female, 8 right hand dominant 2 left hand dominant, average age 23 ± 4.1 years ($mean \pm \sigma$), from the WPI student body. Each participant attended 2 data collections on different days to complete the "regular" and "low force" tests. Nine of the subjects completed the two sessions within 1 month of each other, with an average time between sessions of 18 ± 11 days. Due to scheduling issues, one subject attended the second session 6 months after the first. No subjects dropped out from the study.

4.3.4   Data Processing

The start and end of each repetition of a given task were manually segmented from inspection of the load cell data. Marker data for all subjects was manually labeled and had ghost markers removed. After deriving a kinematic hand model for the subject using the protocol of Section 4.1, marker data for each task was processed in Matlab to calculate the joint angles, load cell positions, and load cell vectors at each moment in time. If occluded data made it impossible to calculate the angles of a joint over any period, a linear interpolation was used to fill in the gap. The calculated joint angles were then low pass filtered with a $3Hz$ cutoff which preserved the data related to finger motion while smoothing out fluctuations related to motion capture measurement errors. The joint positions, joint orientations, load cell positions, and load cell orientations were then represented in a common reference frame. An example of the processed hand model is shown in Fig. 4.23.

Using this processed model, we could calculate the torque at each of the joints needed to maintain the finger posture against the measured force. We do this using Eq. 4.31 where $p_{LoadCell}$ and p_{Joint} are the positions of the load cell and joint in a common reference frame, $v_{LoadCell}$ and v_{Joint} are the vectors of the load cell and joint in a common reference frame, and $F_{LoadCell}$ is the magnitude of the measured force from the load cell.
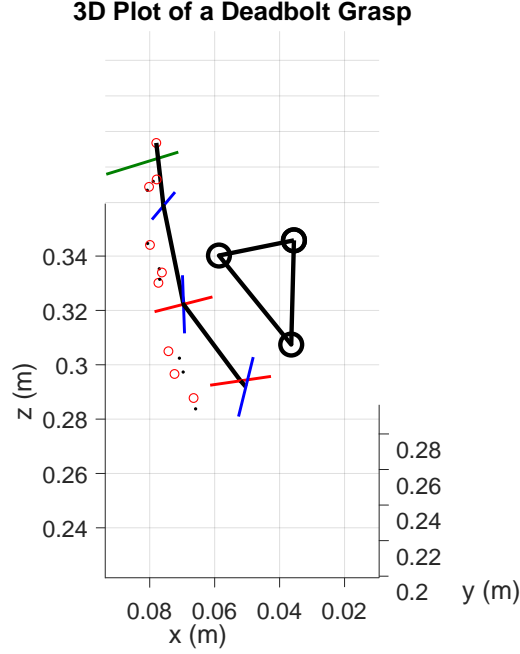
Figure 4.23: 3D Plot of the measured kinematic model and load cell vector for a dead-blot grasp. Blue lines indicate flexion/extension axes, red line abduction/adduction axes, black dots measured marker positions, red circles modeled marker positions, and the green line is the load cell vector.

$$\tau = \left[(p_{LoadCell} - p_{Joint}) \times F_{LoadCell}v_{LoadCell}\right] \cdot v_{Joint} \tag{4.31}$$

Eq. 4.31 is simply the cross product of the moment arm to the load cell and the load cell vector, of which only the torque about the joint axis is recorded. An example of applying the complete kinematic tracking, load cell tracking, and load cell measurement to the joint torque measurement of a repeated task is shown in Fig.

4.24. Here, the torque about the abduction/adduction axis of the thumb's CMC joint

is overlaid for the 5 repetitions. The joint torques for all tasks are summarized in

Section 4.3.5.
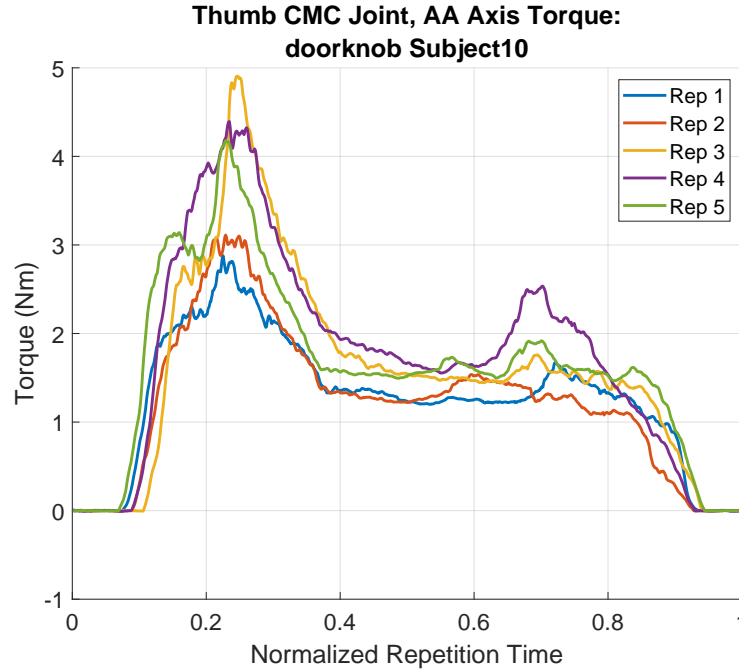
Figure 4.24: CMC joint torques measured from 5 repetitions of a subject opening a
door.

4.3.5   ADL Grasp Force Results

The results of the measured joint torques are summarized in Figs. 4.26 to 4.36. To

generate the box-plots in each of these figures, the maximum torques for each of

the 5 repetition for each joint of a given task were calculated for each subject. The

median value of these measurements were taken for each subject and combined to

form the box-plots. The plots are labeled with the joint name and the axis name,

with FE corresponding to the flexion/extension axis and AA corresponding to the abduction/adduction axis. Labels with "_LF" appended to them indicate data collected during the low force session. Similarly, the maximum load cell magnitudes are combined into the box-plot of Fig. 4.25. The for the sweatpants and zipper tasks the maximum force are reported exclusively as reliable tracking of the hand during these tasks was not possible due to total occlusion of the thumb.
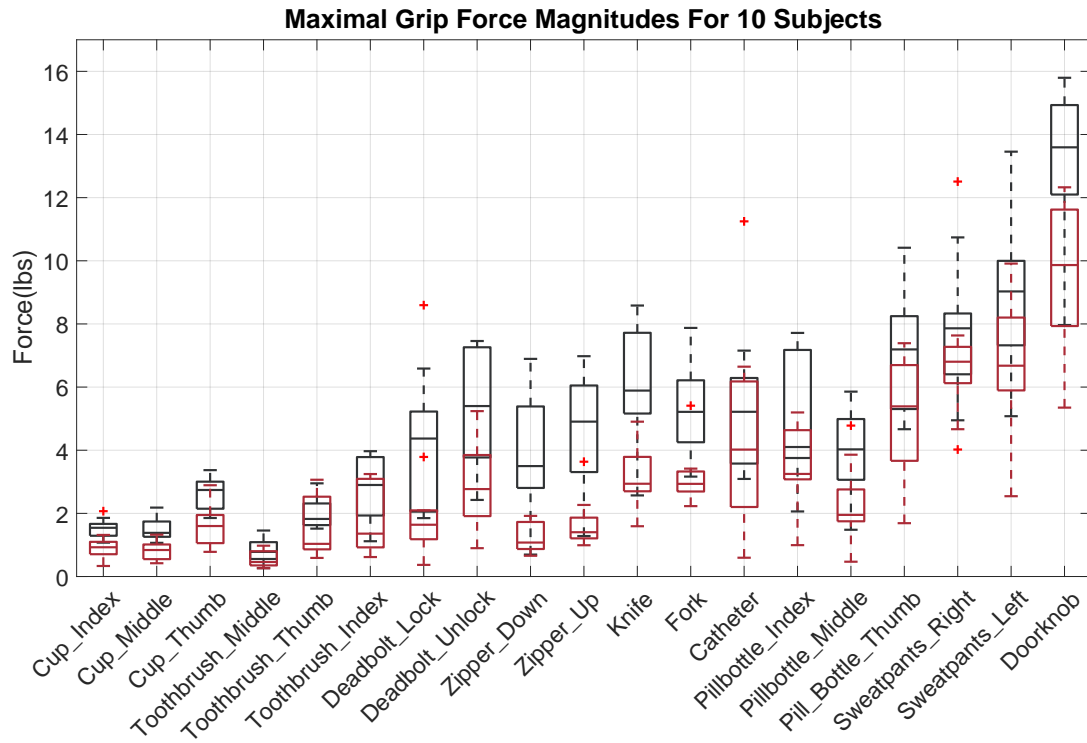
Figure 4.25: Summary of maximum finger tip forces recorded during nine activities of daily living. Grey boxes indicate measurements taken during the regular force sessions while red boxes indicate data taken during the low force sessions.

Figure 4.26: Index finger maximum joint torques during the pillbottle task.

Figure 4.27: Middle finger maximum joint torques during the pillbottle task.
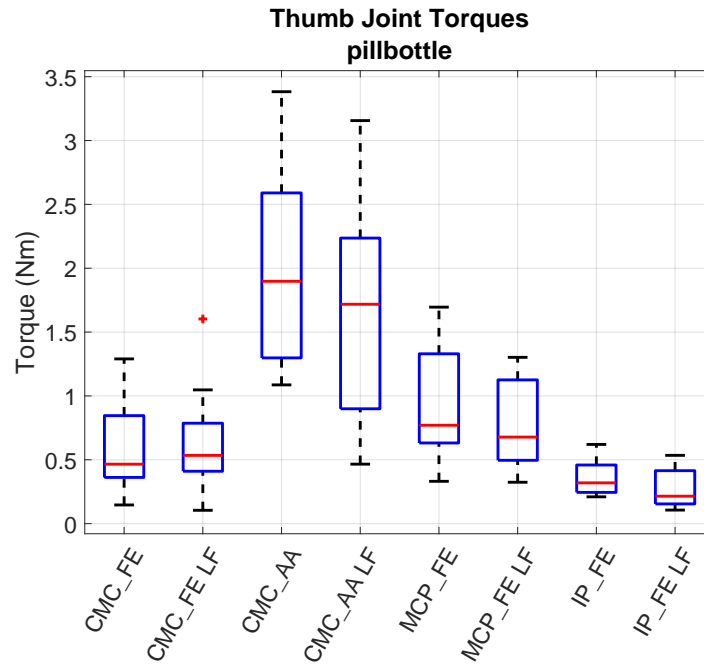
Figure 4.28: Thumb maximum joint torques during the pillbottle task.
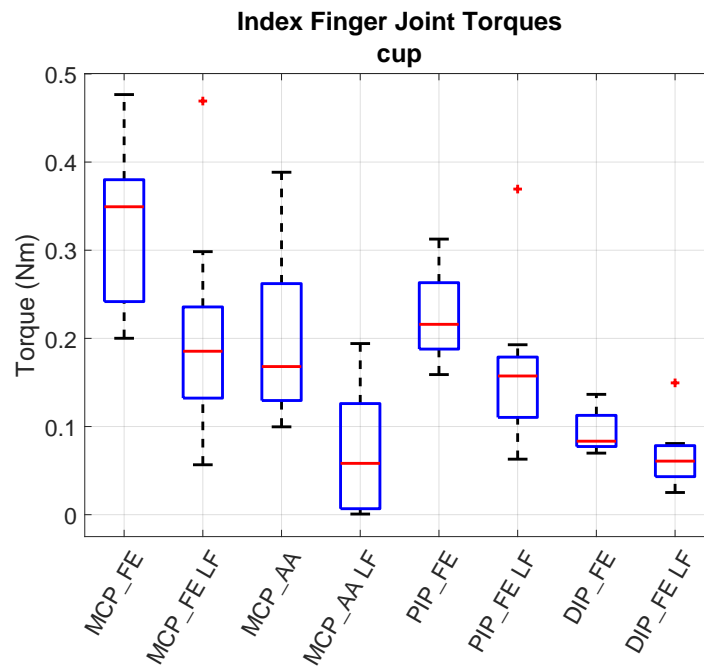
Figure 4.29: Index finger maximum joint torques during the cup task.
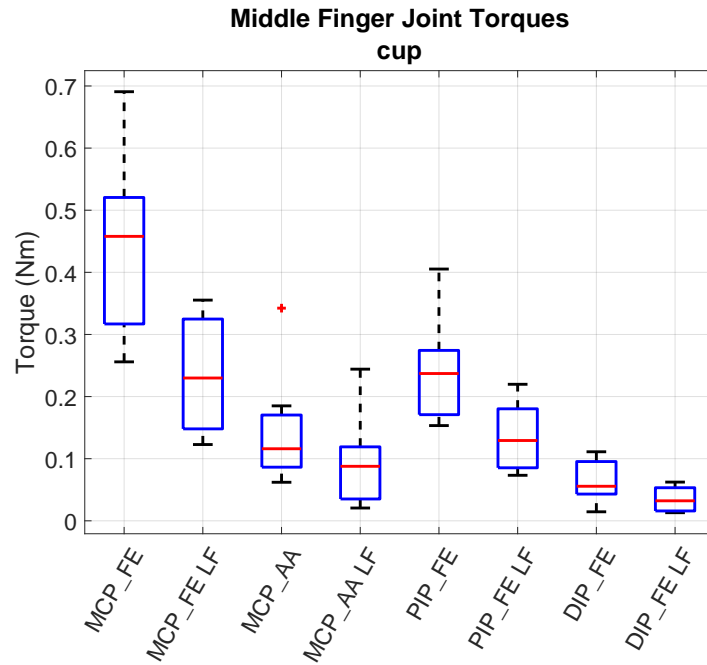
Figure 4.30: Middle finger maximum joint torques during the cup task.

Figure 4.31: Thumb joint torques during the cup task.

Figure 4.32: Thumb maximum joint torques during the doorknob task.

Figure 4.33: Thumb maximum joint torques during the deadbolt task.
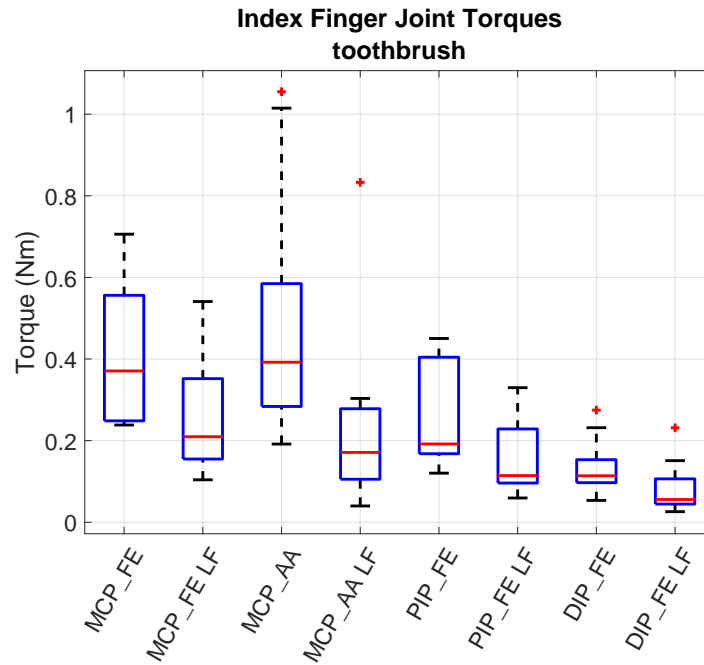
Figure 4.34: Index finger maximum joint torques during the tooth brushing task.
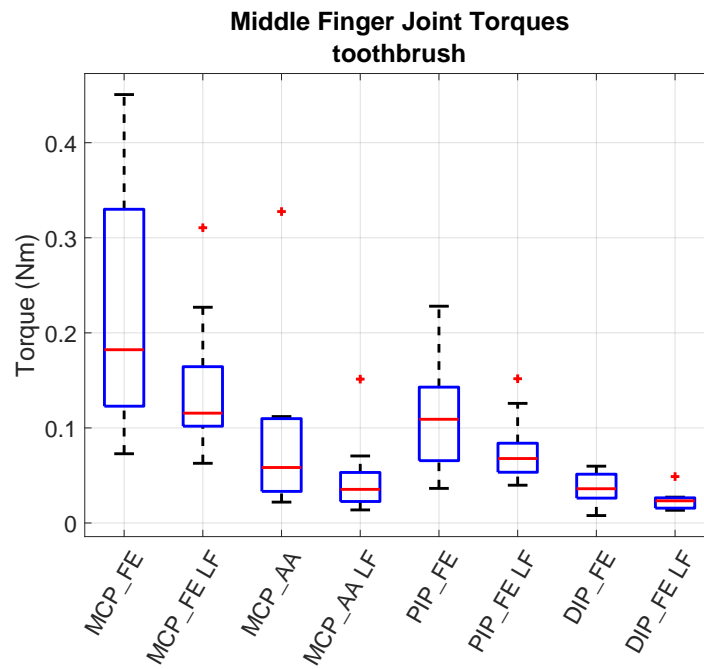
Figure 4.35: Middle finger maximum joint torques during the tooth brushing task.
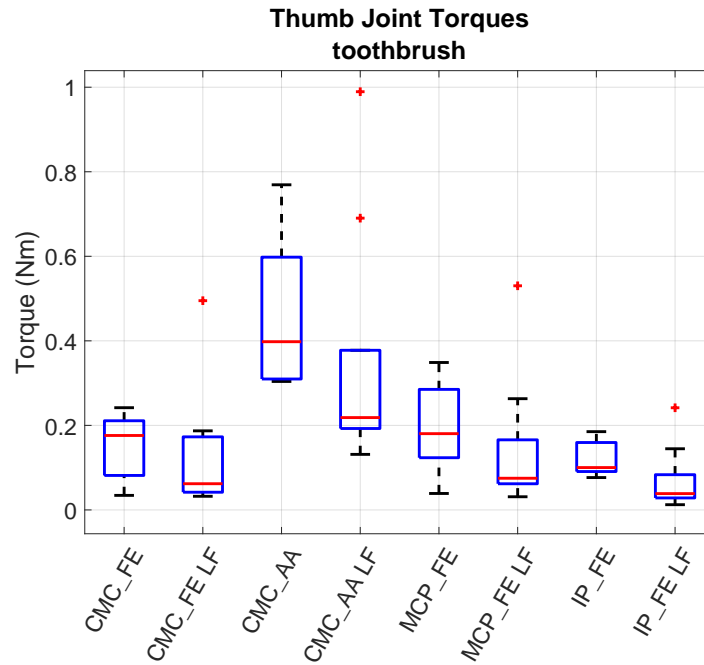
Figure 4.36: Thumb maximum joint torques during the tooth brushing task.
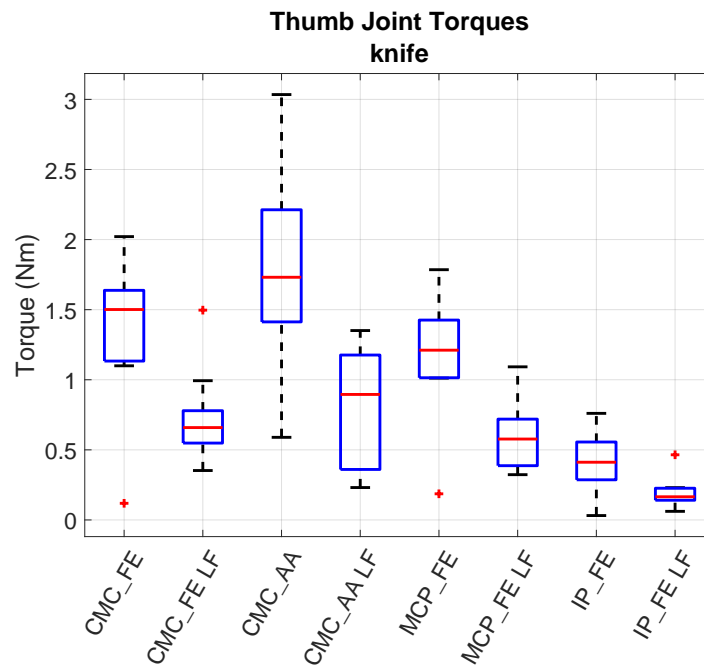
Figure 4.37: Thumb maximum joint torques during the knife task.

4.4 Measurement of Forces for Assisting Finger Extension of TBI Patients

As was described in Section 2.1.1, individuals suffering from UMN do not exclusively present with muscle weakness. A resting flexed hand brought on by increases in muscle tone and spasticity is not uncommon among these patients. Considering the poor extension performance of the devices presented in Chapter 3, we sought to better understand the requirements of an orthosis which performs well in extension. In this section we seek to better understand the following questions: How much extension torque at each joint is needed to assist the hand of an individual with increased flexor tone due to UMN? How consistent is the extension torque needed to attain a given finger posture? And how do these torque profiles change when these patients are asked to attempt volitional extension of their hands?

4.4.1 Subject Descriptions

Upon approval of our protocol by the Worcester Polytechnic Institute's institutional review board, subjects were recruited from the population of stroke and TBI patients at Pine Bush Physical Therapy. Inclusion criteria required subjects to have increased flexor tone in the fingers, be greater than 3 months post injury, and be capable of giving informed consent. Of the 12 stroke and TBI patients in the population, 3 with

chronic motor deficits as a result of TBI met the inclusion criteria. One female and
two males were tested, average age 35.7 ± 19.7 years, who were 1, 2, and 22 years
post injury. All subjects were right-hand dominant with unilateral impairment; two
with dominant hand impairment and one with non-dominant impairment. A typical
resting hand posture of these subjects is shown in Fig. 4.38.
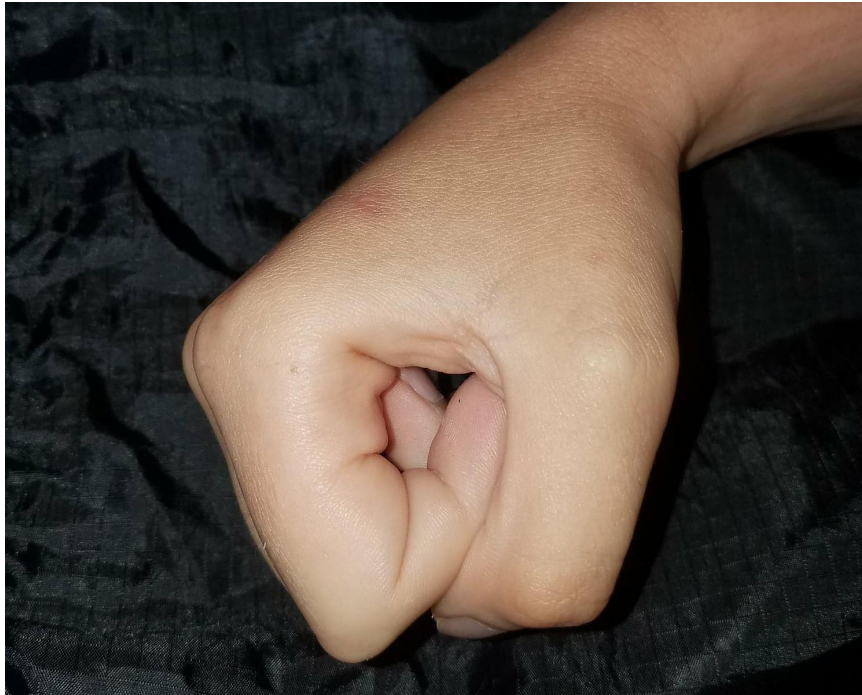
Figure 4.38: The resting hand posture of a TBI patient recruited for a study on
measuring forces for assisting finger extension. An increase in muscle tone keeps the
hand in a resting flexed posture. The degree of resting tone is highly variable and is
dependent on factors such as posture, stress, and recent physical activity.

4.4.2   Study Protocol

Forces were applied to the index finger and thumb using two load cells. A 25lb tension
load cell (LSB200, FUTEK Advanced Sensor Technology, Inc., Irvine, CA, USA) was

attached to the tip of the finger being tested using a Kevlar string. A 10lb compression load cell (LLB130, FUTEK, Inc.) was used to push on the proximal phalanx of the index finger against the direction of motion. The fixtures containing these load cells, and a demonstration of how they were used to apply forces to the fingers, are shown in Fig. 4.39. Load cells were amplified (AD620, Analog Devices, Inc., Norwood, MA, USA) to a sensitivity of $0.063\frac{V}{N}$ and recorded with a 12-bit analog input card (NI 9201, National Instruments, Austin, TX, USA) in an FPGA-based embedded controller (cRIO-9074, National Instruments). Load cell vectors were tracked by the attachment of rigid triangular marker frames and a one-time calibration measurement. Data was logged during the experiment at 120Hz with load cell data synced to the motion capture system via an external trigger.

Subjects were seated in an armchair and positioned with their elbow flexed at approximately 90°, wrist neutrally pronated, and wrist neutrally flexed. The subject's forearm was strapped to the arm of the chair to maintain this position and one researcher held the palm of the hand to maintain the wrist position throughout the experiment. The amount of assistance required to extend the index finger and thumb for each subject was evaluated under two test conditions. In the first condition, subjects were instructed to relax their hand while a licensed physical therapist (**PT**) applied forces to extend the finger currently instrumented. Immediately following this, subjects were instructed to attempt volitional extension of their fingers with the PT assisting them to achieve full extension on the instrumented finger. To avoid
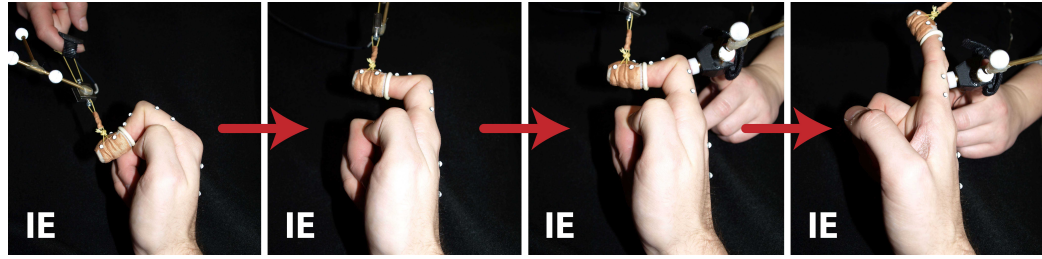
(a)
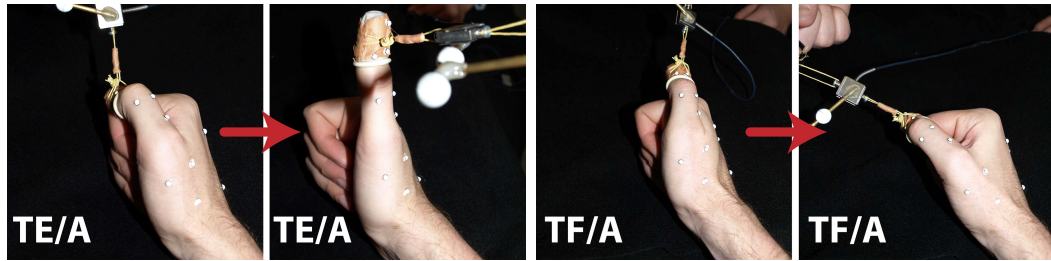
(b)   (c)

Figure 4.39: Assisted motions of the index finger and thumb. (a) The physical ther-
apist extends the MCP joint fully by pulling on the distal phalanx through a tension
load cell, they then stabilize the MCP by pushing on the proximal phalanx with a
compression load cell while extending the IP joints fully. (b) The thumb is extended
and abducted and (c) the thumb is flexed and abducted by pulling on the distal
phalanx through a tension load cell.

velocity-dependent increases in tone, a generally slow rate of extension was used

lasting up to 12s. The PT used their experience performing passive stretching of TBI

patients to adjust speed as necessary and avoid these spastic effects.

The index finger was instrumented first and followed an extension pattern which

has relevance to opening the hand prior to grasp. The PT first extended the MCP joint

by pulling on the distal phalanx through the tension load cell, they then stabilized

the MCP joint by pushing on the proximal phalanx with the compression load cell,

finally they extended the proximal and distal interphalangeal (**PIP** and **DIP**) joints by continuing to pull on the distal phalanx. This index extension (**IE**) was repeated 10 times for each test condition and the pattern is shown in Fig. 4.39(a).

For the thumb, the PT assisted two motion patterns independently of each other. First, the thumb was extended and abducted (**TE/A**) by pulling on the distal phalanx through the tension load cell bringing the IP and MCP joints into full extension and abducting the CMC joint. This motion has relevance to positioning for a functional key-grasp and is shown in Fig. 4.39(b). Following this, the thumb's CMC joint was flexed and abducted (**TF/A**), which has relevance to positioning for a three jaw chuck grasp and is shown in Fig. 4.39(c). Each of these patterns was repeated 10 times.

4.4.3   TBI Measurement Results

The 10 repetitions of each test condition were segmented for plotting and analysis. Only the extension portion of each joint motion was segmented, which was defined as the period from when the joint's angle begins monotonically extending up until the time where full extension is reached at all joints. An example of a joint extension pattern for the index finger is shown in Fig. 4.40. In this example, the initial MCP extension causes flexion of the PIP joint. Once the MCP reaches full extension, further torque needs to be applied to maintain the MCP position as the PIP is extended. MCP segmentation starts prior to the PIP but ends when the PIP reaches

full extension to capture the peak torque.
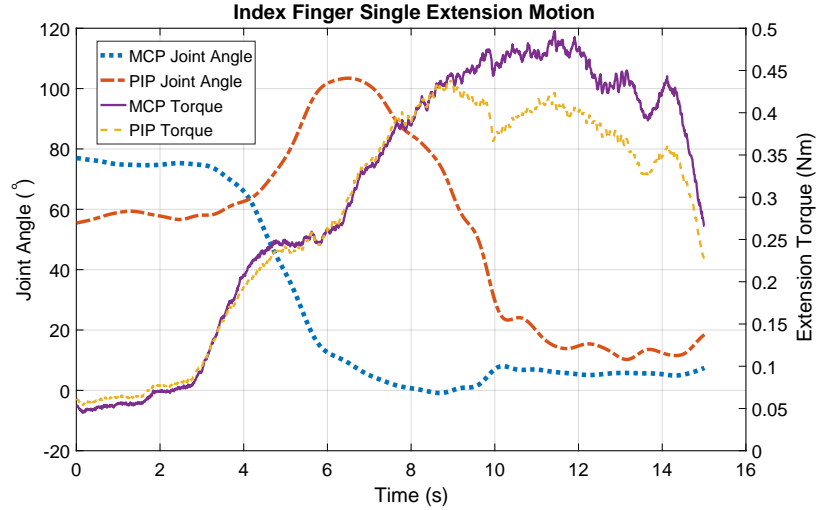
Figure 4.40: Data from a single extension motion of the index finger PIP and MCP
joints for TBI Subject01 while relaxed. The initial MCP extension causes flexion of
the PIP, even as extension torque applied to the joint increases.

Segmented torque vs joint angle data was resampled at a fixed joint angle incre-
ment to generate an average extension profile for each subject and test condition.
Fig. 4.41 shows these profiles and their standard deviations for motions where a re-
peatable relationship between torque and joint angle was observed. Plots of the index
finger DIP were omitted as subjects had a resting posture in which the joint was fully
extended and moved little during the assisted motion. A peak value, which serves
as a bound on the torque preventing flexion brought on by motion of the PIP and
MCP, is provided in Table 4.1. The motion profiles of thumb flexion and abduction
also did not provide repeatable relationships between torque and joint angle, and are
thus represented solely in their table. Their values quantify the torque necessary to

move the joint through its range of motion, but an inability to coordinate that motion

was a limitation of our experimental setup. The peak torques measured at all joints

are also given with those for index extension, **IE**, in Table 4.1, thumb extension and

abduction, **TE/A**, in Table 4.2, and thumb flexion and abduction, **TF/A**, in Table

4.3. Fig. 4.42 provides a physical interpretation of the reported data.

Table 4.1: Index extension, **IE**, assistance applied at each joint in order to achieve full finger extension. Subject initially relaxed their hand while being repeatedly assisted, followed by attempted volitional extension while being repeatedly assisted.

	Peak MCP Torque Relaxed (Nm $\pm\sigma$)	Peak MCP Torque Vol. Extension (Nm $\pm\sigma$)	Peak PIP Torque Relaxed (Nm $\pm\sigma$)	Peak PIP Torque Vol. Extension (Nm $\pm\sigma$)	Peak DIP Torque Relaxed (Nm $\pm\sigma$)	Peak DIP Torque Vol. Extension (Nm $\pm\sigma$)
Subject 1	0.43 ± 0.06	0.62 ± 0.08	0.37 ± 0.05	0.75 ± 0.07	0.18 ± 0.02	0.21 ± 0.03
Subject 2	0.36 ± 0.05	0.75 ± 0.19	0.25 ± 0.03	0.46 ± 0.08	0.08 ± 0.02	0.24 ± 0.04
Subject 3	0.22 ± 0.08	0.68 ± 0.22	0.12 ± 0.05	0.44 ± 0.19	0.07 ± 0.03	0.26 ± 0.08

Table 4.2: Thumb extension and abduction, **TE/A**, assistance applied at each joint to achieve full finger extension. Subjects initially relaxed their hand while being assisted, followed by attempted volitional extension while being assisted.

	Peak CMC Torque Relaxed (Nm $\pm\sigma$)	Peak CMC Torque Vol. Extension (Nm $\pm\sigma$)	Peak MCP Torque Relaxed (Nm $\pm\sigma$)	Peak MCP Torque Vol. Extension (Nm $\pm\sigma$)	Peak IP Torque Relaxed (Nm $\pm\sigma$)	Peak IP Torque Vol. Extension (Nm $\pm\sigma$)
Subject 1	0.53 ± 0.07	0.67 ± 0.14	0.38 ± 0.05	0.44 ± 0.08	0.17 ± 0.02	0.23 ± 0.05
Subject 2	1.06 ± 0.12	1.83 ± 0.20	0.71 ± 0.08	1.35 ± 0.13	0.19 ± 0.03	0.32 ± 0.06
Subject 3	0.17 ± 0.03	0.70 ± 0.18	0.29 ± 0.06	1.24 ± 0.29	0.13 ± 0.03	0.72 ± 0.22
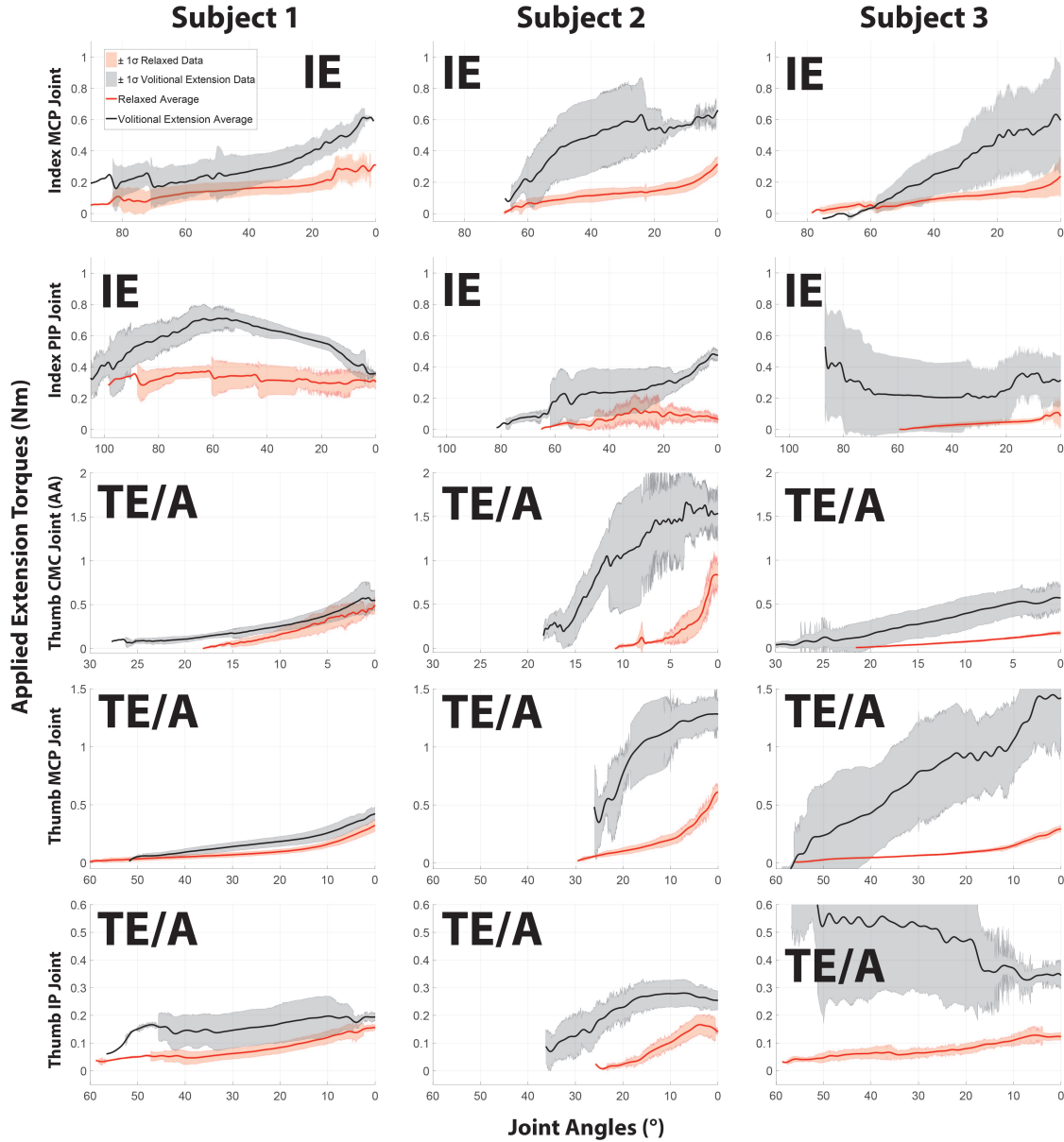
Figure 4.41: Torques applied to assist finger extension of 3 TBI patients. The red lines and shaded regions show the torque when the subject was relaxed. The black lines and gray regions show the assisting torque when the subject was asked to attempt volitional extension. Plots are labeled IE, TE/A, and TF/A corresponding to the motions in Fig.**??**. The results indicate that it became harder to extend the fingers of each subject after they had been asked to aid in the extension.
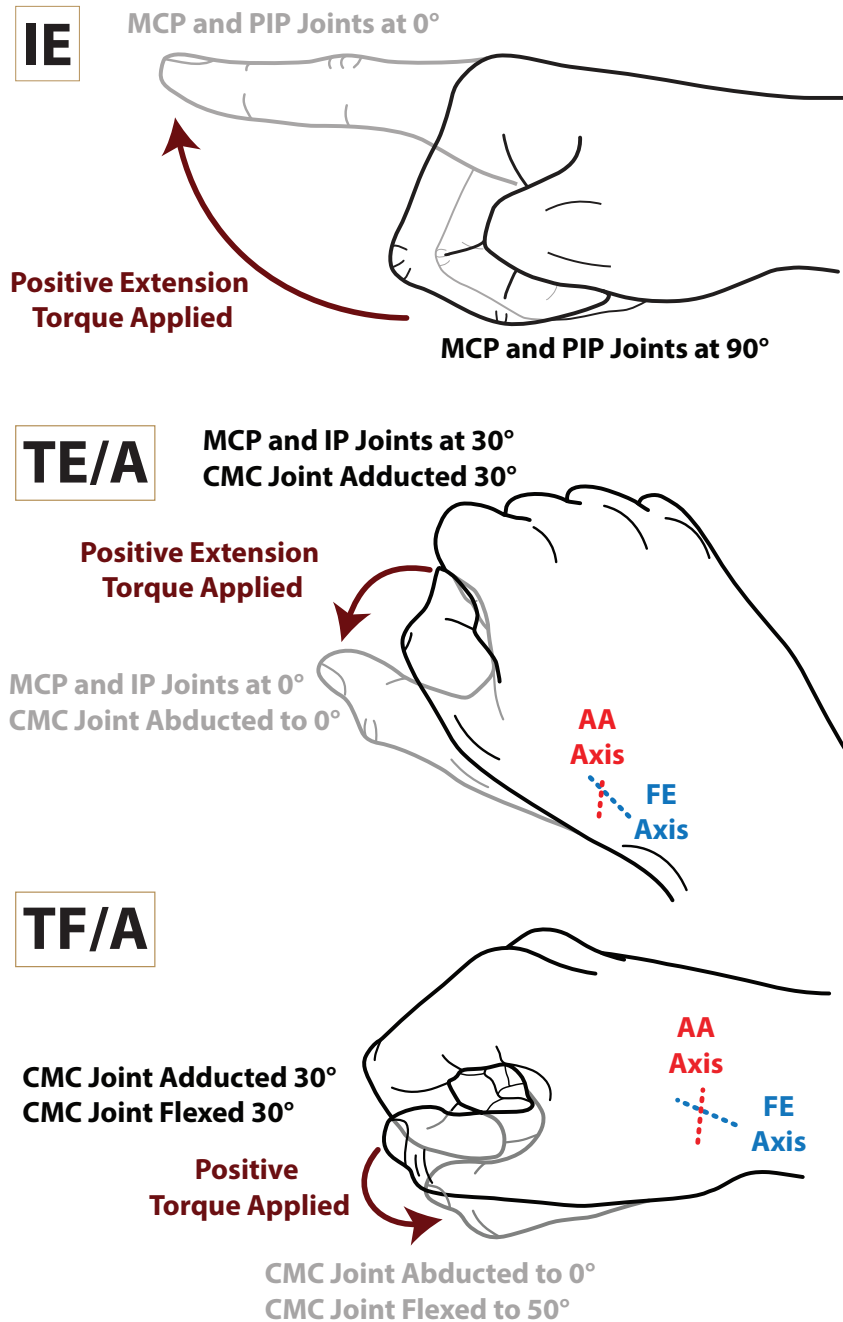
Figure 4.42: Physical description of the motions described by the data collected on
TBI subjects.

Table 4.3: Thumb flexion and abduction, $\boldsymbol{TF/A}$, assistance applied at each joint to achieve full finger extension. Subjects initially relaxed their hand while being assisted, followed by attempted volitional extension while being assisted.

	Years Since In-jury (yrs.)	Hand with Motor Deficit	Peak CMC AA Torque Relaxed (Nm $\pm\sigma$)	Peak CMC AA Torque Vol. Extension (Nm $\pm\sigma$)	Peak CMC FE Torque Relaxed (Nm $\pm\sigma$)	Peak CMC FE Torque Vol. Extension (Nm $\pm\sigma$)
Subject 1	1	Right	0.21 ± 0.06	0.61 ± 0.13	0.09 ± 0.04	0.13 ± 0.08
Subject 2	21	Right	0.63 ± 0.10	2.23 ± 0.33	0.29 ± 0.03	0.41 ± 0.24
Subject 3	2	Left	0.35 ± 0.09	0.33 ± 0.12	0.15 ± 0.04	0.33 ± 0.08

The results indicate that when subjects were asked to attempt volitional extension of their fingers it commonly required more effort from the PT to assist that extension. This behavior was observed qualitatively during testing and is supported by the measurements in Fig. 4.41. In no cases was a subject able to fully, or partially, extend their fingers without therapist assistance. The average amount of torque required to extend the index finger MCP joint of a given subject ranged from $0.22 \pm 0.08 Nm$ up to $0.75 \pm 0.19 Nm$. Peak torques above 1.0Nm at the MCP were measured during single index finger extensions of Subjects 2 and 3. The range of MCP measurements agree with prior work which indicated 0.5Nm was required to extend one individual's MCP joint [26]. The data presented expands on this prior work, characterizing how the resting tone may vary for a given individual along with measuring torque at all joints of the index finger and thumb.

Limitations of this study included leaving control of extension speed and joint

coordination to the assisting physical therapist as well as testing the subjects in a single arm and body posture. Depending on the specifics of each subject's condition, these variables are likely to play a factor in the measured torques at each of the joints. The study is also limited by the small sample size meaning the results cannot be taken as a comprehensive characterization of the TBI population. However, the data serves as a case-study of three potential hand orthosis users whose motor impairments were not deemed by the assisting clinician to be unusual for TBI.

4.5 Discussion and Conclusions

This chapter has provided a method for characterizing the forces which must be applied to the hand of individuals with impairment due to UMN in order to assist in the completion of daily tasks. The measurement of both joint torques needed to assist in extension and flexion can aid in optimizing the design of hand orthoses. Components such as motors, linkages, batteries, and transmissions are directly related to these torques. Furthermore, providing protocols and analys tools for orthotic engineers to make needed measurements on their own which are directly relevant to their device's function can have the further impact of better informing orthosis designs. The measurements made here will be applied to one particular design in Chapter 5, but have relevance to orthosis design in general.

CHAPTER 5

Cable-Actuated Orthosis to Aid Finger Extension

In order to rectify some of the shortcomings of the orthoses evaluated in Chapter 3, here, we apply the measurements made in Chapter 4 to the design of a cable based orthosis for aiding finger extension of individuals with increased flexor tone associated with the upper motor neuron syndrome (***UMN***). Much focus has already been paid to the design and evaluation of orthoses on their ability for assisting finger flexion [6,15,17–19,98,105], but relatively little has been given to assisting extension against moderate to severe increases in muscle tone. The work of Fischer et al. [5] is one of the few examples found where the researchers focused primarily on finger extension, however with the application focused on rehabilitation rather than assistance. The work of Gasser et al. is clearly capable of assisting extension given the description of a patient used in pilot testing as having "considerable flexor tone", who when unassisted "spent most of the trial trying to work the bottle into his closed fist" [100]. While Gasser's design was able to assist extension, little is said by the author about

specific design considerations for accommodating extension [10,100]. In this work, we consider the design aspects of a cable-actuated glove meant to assist the traumatic brain injury (**TBI**) patients tested in Section 4.4. The specific contributions are as follows:

- **Contribution 1**

  Demonstration of how the measurements made in Chapter 4 can be applied to better design an orthosis. Actuators are sized by calculating the power needed to assist the extensions performed in Section 4.4. The tendon path, motor gearing, and ball-screw selection are also designed around the requisite forces.

- **Contribution 2**

  Construction of an orthosis, it's actuation unit, and software interfaces for aiding finger extension. We sought to develop a capable research platform that is not far removed from a practical assistive orthosis. The device is designed to be well-packaged, portable, and reasonably lightweight. This work will enable future clinical studies of an orthosis which assists extension.

The broader impact of this chapter is in applying new methods for the design of assistive orthoses that are possible due to better characterized design criteria from Chapter 4. The work also establishes a design and prototype for future testing of orthosis concepts. We believe that assisting extension of individulas with hypertonia has been under-represented by the robotics community and that this orthosis will
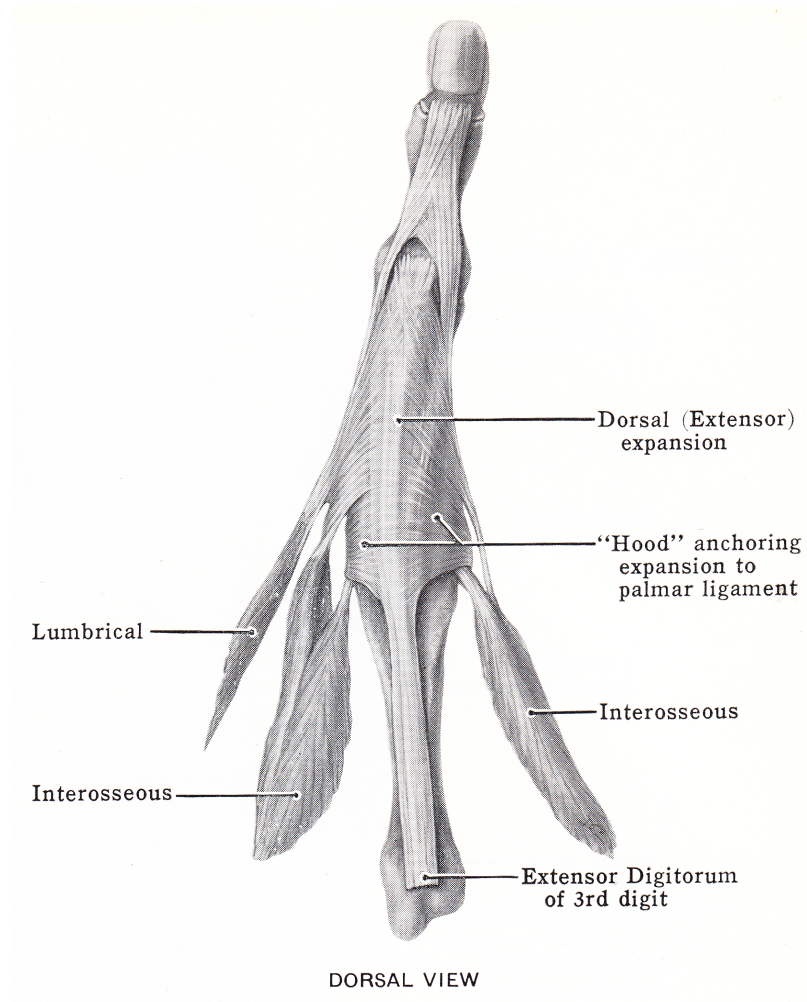
Figure 5.1: Anatomy of the extensor hood. Reproduced from [151].

provide a means to evaluate the effectiveness of robotics for this application.

5.1 Orthosis Design

To rectify some of the extension deficits associated with the work presented in Chapter 3, we looked to the anatomy of the hand, shown in fig 5.1, as well as the anatomically

correct robotic hands of Deshpande et al. [115] and Xu et al. [117]. We noticed that lacking from the single cable extension of the glove developed by Delph et al. [11] was the function of the intrinsic muscles of the hand, specifically the interossei. These muscles feed into the lateral bands of the extensor hood regulating torques at the DIP and PIP joints [117] and controlling abduction and adduction of the MCP joints. This element of the design would provide stability to the MCP joint which was an issue with Delph's design. The human anatomy also includes a sagittal band, which wraps around the dorsal aspect of the MCP joint and stabilizes the tendon of the extrinsic extensor. These ligaments constrain the tendons to the midline of the MCP and prevent it from lifting away in hyperextension as was seen with the glove of Delph. While these features of the human anatomy explain the deficiencies in the previously evaluated design, mimicking the extensor hood directly was found to be impractical as cables would need to be routed across the palm to reproduce the function of the interossei and through the palm to directly mimic the sagittal ligaments. Furthermore, based on our experience in Chapter 3, inclusion of more than one motor per finger, as would be needed to accurately mimic the interossei, would lead to impractically sized devices. Xu et al. used a passive spring to mimic the intrinsic muscles in their anatomically correct robotic hand [117], however, we did not want to pursue this design as the spring would impede the user's ability to flex their fingers. While we don't mimic the extensor hood directly, we incorporate new design elements into a cable-actuated orthosis which are inspired by the anatomical
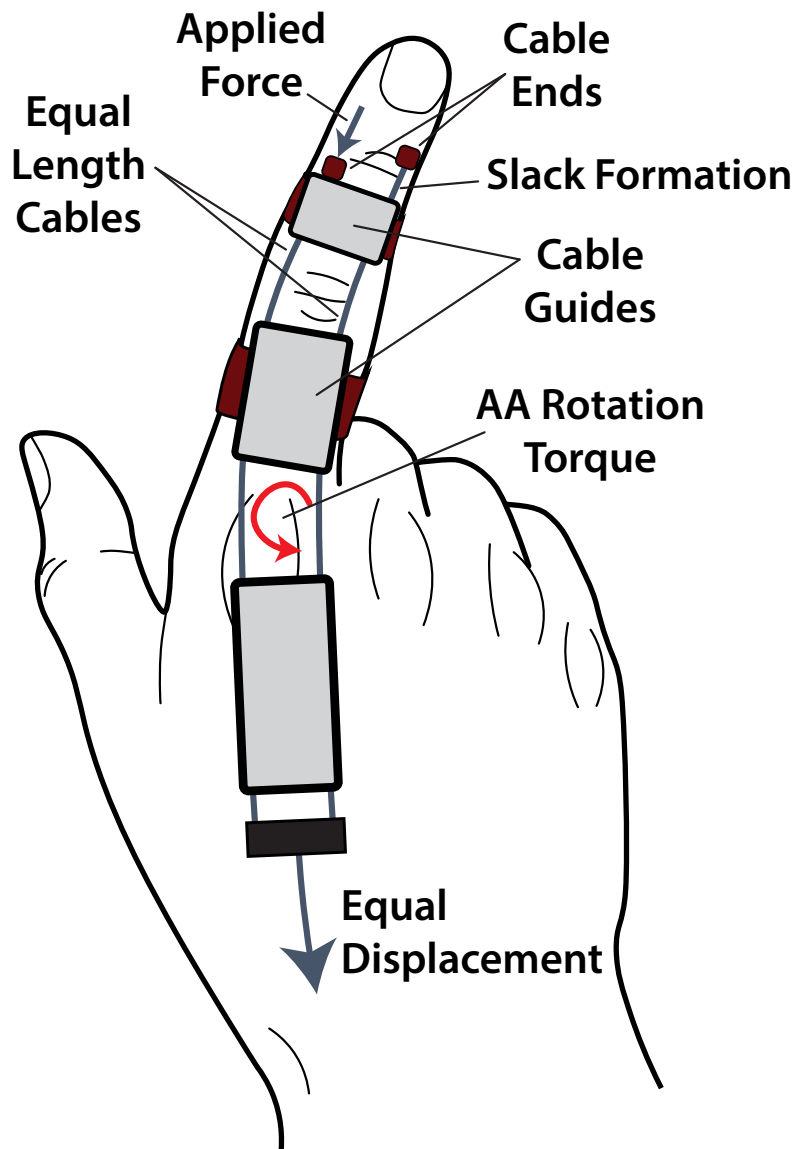
Figure 5.2: Self regulating abduction/adduction rotation using two cables for finger extension. Due to a constant path length for both cables and an equal displacement imposed by the actuation unit, slack forms between the cable guide on the inside radius and the terminal cable guide. This causes an imbalance in tension between the two cables which creates a moment that seeks to re-center the abduction/adduction axis of the MCP joint.

extensor to stabilize the MCP joint and better constrain the cable path.

176

To passively stabilize the MCP joints, we split each extension cable so that two cables run in parallel along the length of each finger. The use of two cables for extension self-regulates a neutral abduction/adduction ($\boldsymbol{AA}$) rotation so as to avoid the irregular postures seen with the single cable orthosis in Fig. 3.3(d). This stability comes from passing one tendon to either side of the joint. The cables are constrained to a constant length and equal displacement is applied to each from the orthosis' actuation unit. A rotation of the MCP about the AA axis causes the cable nearer the center of the rotation to take a shorter path across the MCP, leading to slack formation between the cable end and the terminal cable guide. This increases the amount of tension in the cable on the outer radius of the MCP rotation, which produces a torque that tends to bring the joint back to center. This is illustrated in Fig. 5.2.

Another aspect of extension we sought to improve upon was a reduction in the cable tensions needed to produce a given torque. Large cable tensions in the design of Delph et al. [11] were found to deform the orthosis and apply painful pressure to the hand dorsum. These tensions also apply translational loads which must be supported by the user's joints. Reducing these loads is beneficial to user comfort and safety. Increasing the moment arm between cable and joint reduces the needed tension, but has trade-offs with device packaging. A thicker orthosis will feel more bulky and cumbersome to the user. Furthermore, increasing the moment arm requires the cable to travel further for a given rotation of the joint, increasing the stroke length of the needed actuators. It is the responsibility of the engineer to balance these trade-offs.
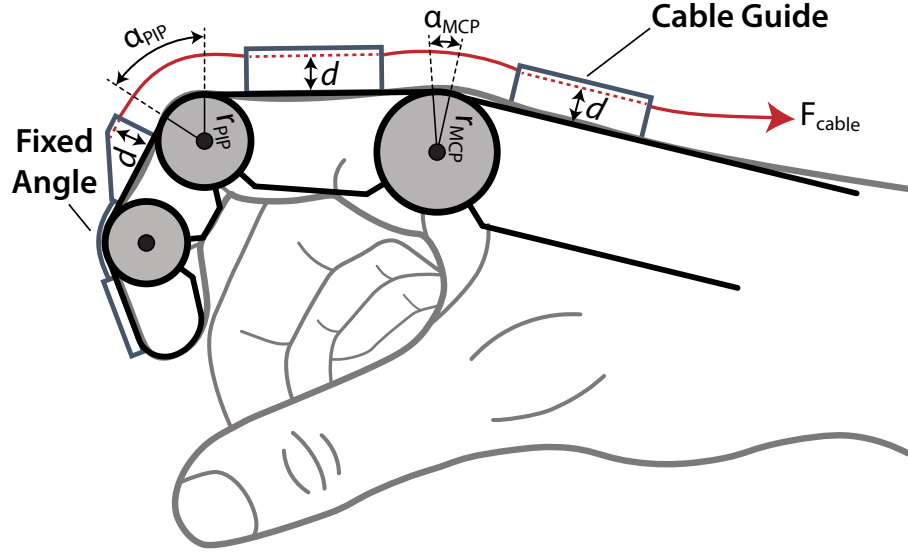
Figure 5.3: The cable path designed for the extension orthosis. Offsets are applied to increase the moment arm to each of the joints, reducing the needed tension to be supplied by the orthosis.

Given the experiments of Section 4.4 and the results presented in Table 4.1, we wanted to be able to extend the MCP joint against a resisting torque of $0.75Nm$. From our study of able body grasping, we were able to use the kinematic models generated for each subject to estimate the distance between the hand dorsum and the MCP axis which we consider r_{MCP} of Fig. 5.3. These radii are listed in Table 5.1. The median radius for the 10 subjects is $10.4mm$. We model the extension torque at each joint assuming the joint behaves as a pulley, where torque is equal to the tension in the cable multiplied by the pulley radius. We assume that the inertial properties of the fingers can be neglected, which is validated by the work of Sancho-Bru et al. who's model found inertia accounted for only $5N$ of tension in the extensor
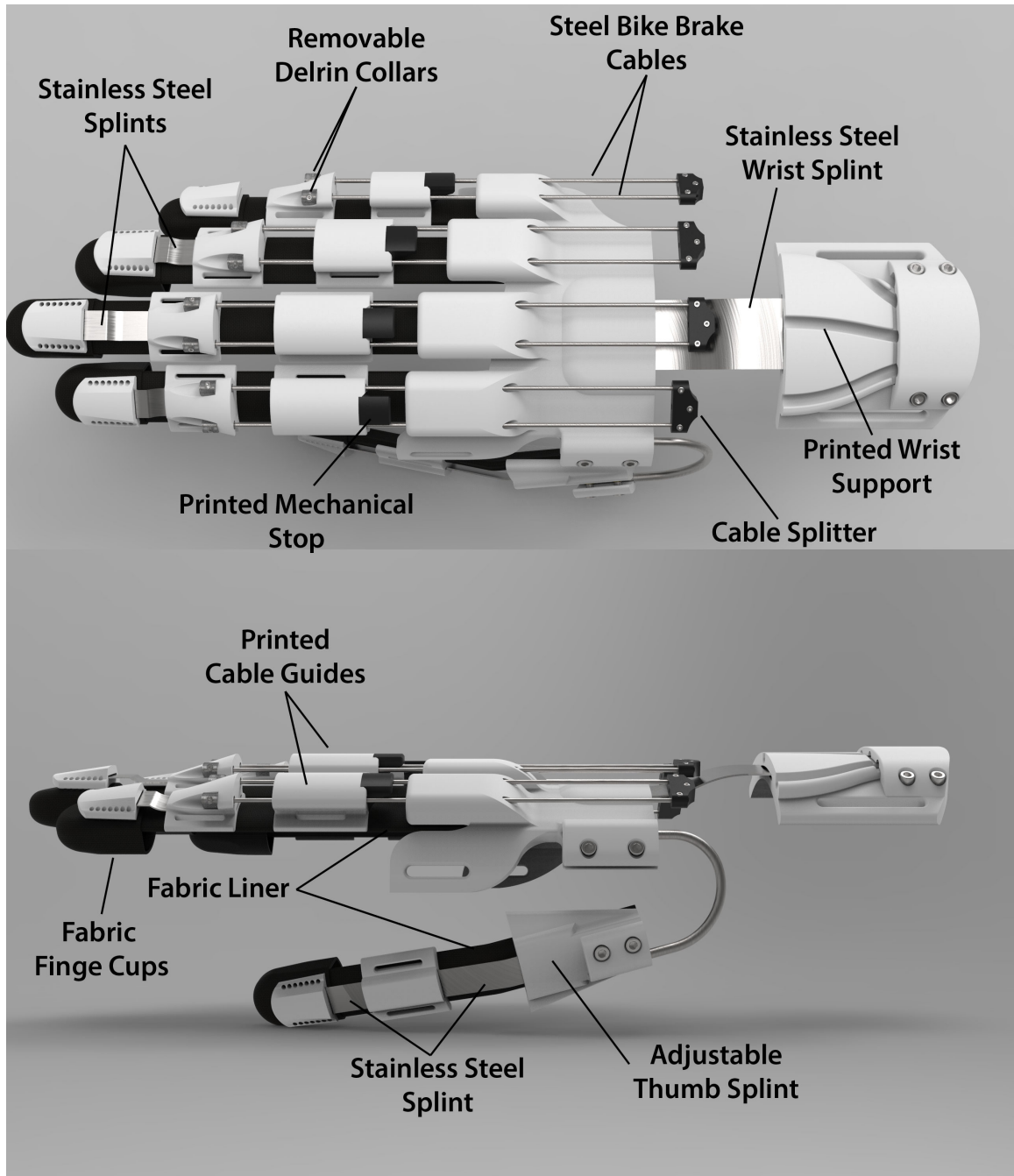
Figure 5.4: Annotated render of the designed cable-based extension orthosis.

Table 5.1: Index and middle finger extensor moment arms, r_x, for 10 able-bodied subjects. The values are the average of two kinematic model fits using the methods of Section 4.1. The median MCP radius is $10.4mm$, median PIP radius $6.9mm$, and median DIP radius $4.4mm$.

.

Subject	Index Finger Joints				Middle Finger Joints		
	r_{MCP} (mm)	r_{PIP} (mm)	r_{DIP} (mm)		r_{MCP} (mm)	r_{PIP} (mm)	r_{DIP} (mm)
01	7.3	6.2	3.7		8.3	6.8	4.7
02	11.2	6.7	3.8		9.4	7.4	4.4
03	11.7	6.9	4.3		10.2	6.8	4.6
04	10.0	7.7	5.0		9.2	9.2	4.4
05	9.1	5.3	4.4		11.1	7.4	5.1
06	11.3	6.7	4.5		11.9	6.5	5.5
07	10.4	8.4	5.3		12.0	9.2	7.1
08	10.4	6.7	3.8		9.7	7.0	4.2
09	10.8	7.6	3.5		9.2	6.7	4.0
10	11.0	7.9	3.6		11.4	8.2	4.8

digitorum communis muscle during fast finger extensions of $0.2s$ [152]. With these assumptions, $72N$ of tension would be needed to apply $0.75Nm$ of extension assistance to the MCP. Adding a $10mm$ offset to our cable path would reduce this by half to $37N$ of tension. This offset value was considered a moderate increase in orthosis thickness, with larger increases likely to become obtrusive. For comparison, this a similar thickness to previously presented pneumatic and hydraulic gloves [12, 17–19] while being slimmer than some rigid designs [9, 33]. A $10mm$ offset for both the MCP and PIP joints would also increase the minimum stroke length of the needed linear actuator from about $27mm$ to $58mm$. Stroke length is approximated using

Eq. 3.10 from Chapter 3 incorporating the cable offset into the radius. Doing a preliminary design of an actuation unit capable of providing $75mm$ of stroke, which leaves a comfortable margin for errors related to user fitment, indicated the actuation unit would be approximately $175mm$ long, similar in length to the actuation unit presented in Section 3.2. Increasing the actuation unit beyond this size was not desired. It should be noted that the selection of the $10mm$ offset was the result of an iterative design process that found it to be a compromise of actuation unit size, orthosis size, and cable tension. Further refinement of this offset incorporating user feedback regarding the ergonomic factors of various sizes would lead to a more optimal value.

Combining these elements, we designed the orthosis shown in Fig. 5.4. The four fingers are actuated from four independent Bowden cables. The housing for each Bowden cable terminates in a plastic wrist support. Each Bowden cable is then split where it passes over the hand dorsum. The split cables for each finger pass through teflon-lined plastic cable guides on the hand dorsum and the proximal phalanx. These cable guides apply the $10mm$ offset to the joint radius and distribute the forces of the cables through the soft tissues of the hand, preventing the painful pressure found in the tendon actuated glove of Chapter 3. The thumb is fixed in place using an adjustable brace, a design we adopted from the work of Gasser et al. [100]. Fixing the thumb in opposition allows for performing several functional grasps while simplifying the orthosis design. Based on our experience with the TBI subjects in Section 4.4,
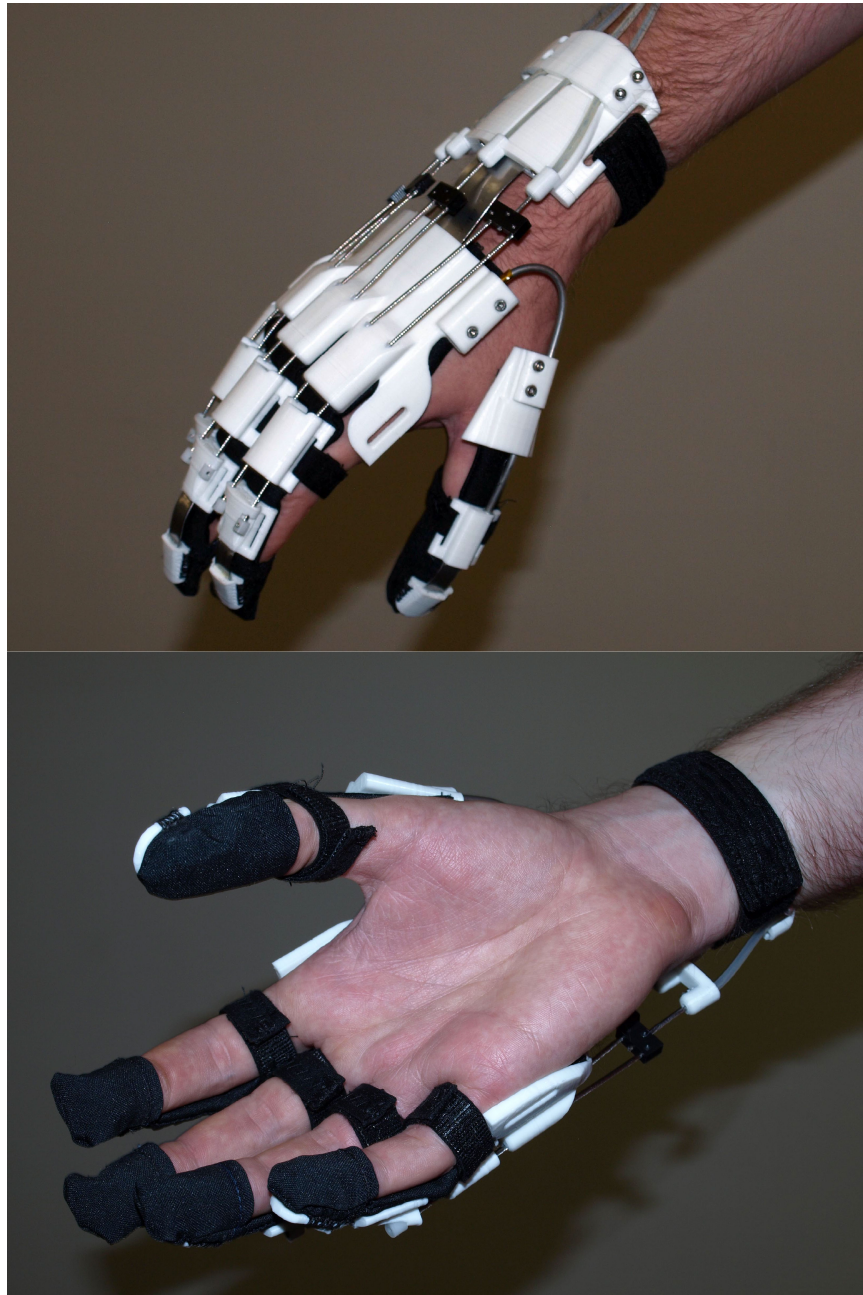
Figure 5.5: Palmar and dorsal views of a cable actuated extension orthosis being worn by a user. Fabric cups at each of the fingertips along with straps at the wrist and proximal phalanges secure the device to the user.

coordinated extension of the PIP and DIP joints was challenging as extending one joint would be expected to cause flexion of the other due to coupling from the tendon of the flexor digitorum profundus. Coordinating this motion with an under-actuated, non-rigid design did not seem practical and we decided to splint the DIP joint in a partially flexed pose. We also included a brace to keep the wrist in a neutral pose, although control of the wrist is important for successful completion of ADLs and should be a focus of future work. The constructed orthosis is shown in Fig. 5.5.

5.2   Actuator Design

Work conducted in Chapter 4 can now be used to optimize motor size to meet the desired function of the cable-actuated extension orthosis. While it should be noted that the conditions we consider "optimal" are still left to some interpretation, Section 4.4 now provides an understanding of the torques which must be applied to rotate a joint though its range of motion, information that is critical for proper motor selection.

An important parameter, directly related to motor size, is the maximum mechanical power required to extend a finger through its range of motion. The power to extend each joint is equal to the torque applied, τ, times the angular speed, ω. The power for a finger is equal to the sum of the power at the individual joints as described in Eq. 5.1.

$$P_{extend}(t) = \tau_{MCP}(t)\omega_{MCP}(t) + \tau_{PIP}(t)\omega_{PIP}(t) + \tau_{DIP}(t)\omega_{DIP}(t) \qquad (5.1)$$

In practice, each torque profile $\tau(t)$ will be dependent on a number of factors such as the extension speed, the individual's current muscle tone, and the coordination between joints. Using the average torque profiles for both test conditions of each subject from Section 4.4, however, should provide an estimate of the range of needed power.

We define the velocity profile, $\omega(t)$, of Eq. 5.1 based on the desired performance of the device. An ideal velocity profile would smoothly extend the finger from it's fully flexed position to full extension in a desired amount of time. Typically, the ability to fully flex or extend the finger in $1s$ is used as a design parameter. For comparison, the data-sets used for fitting the kinematic models to the able-bodied subjects in Section 4.3 indicated that people would regularly complete a cycle of flexion and extension in about $1s$ if asked to rhythmically make this motion, as shown in Fig. 5.2. A $1s$ extension time provided by the orthosis would therefore be about one half the speed an able-bodied individual would choose to move their finger. To achieve an ideally smooth $1s$ extension profile, we used a quintic polynomial trajectory to approximate the joint angle, α. The extension velocity of a quintic position profile can be seen in Fig. 5.2 to reasonably represent the joint motion of an able bodied subject when they extend their MCP.

To determine the motor power needed to extend the fingers of the TBI patients in
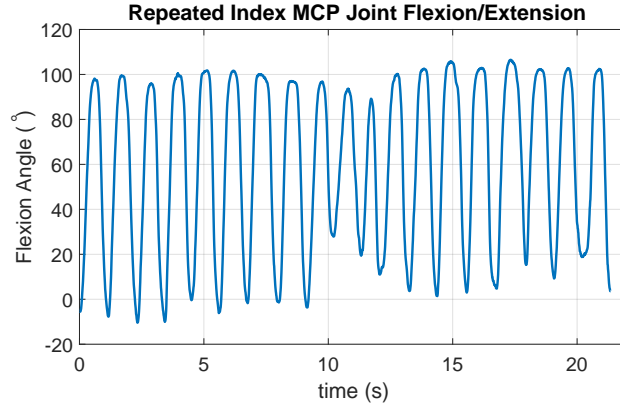
(a) Joint angle for 19 flexion/extension motions
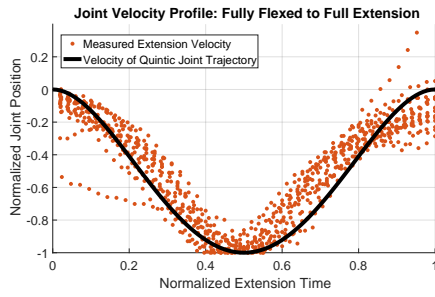
(b) 19 Overlaid joint velocity measurements normalized to their maximum velocity.
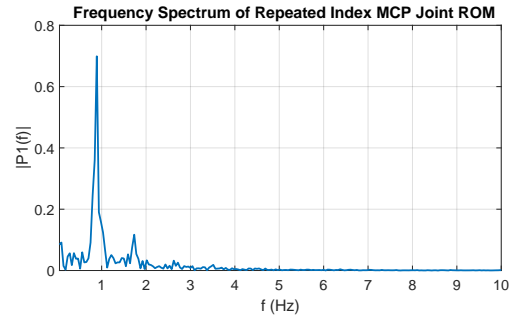
(c) FFT of rhythmic MCP flexion/extension for estimation of time to complete one cycle.

Figure 5.6: The joint trajectory of a subject asked to repeatedly flex their MCP joint through it's range of motion (a). In overlaying the extension portions, the velocity of a quintic joint trajectory is seen to reasonably approximates the observed data with an R-square value of 0.82 (b). The frequency spectrum of the data shows the individual repeats the flexion/extension cycle consistently at a frequency of slightly less than *1hz* (c).

Section 4.4 along this $1s$ quintic joint profile, we needed to also account for transmission losses between the motor and hand. For this design, the Bowden cable and the conversion from rotary to linear motion are the two primary contributors to losses

185

in efficiency. A major limitation of the design presented in Section 3.2 was low mechanical efficiency in the linear actuator. Peak mechanical power of those actuators, the Firgelli L12-30-100-6P, was stated by the manufacturer as 31N at 7mm/s which equates to $0.217W$. The electrical power input to produce this is stated to be $230mA$ at $6V$, or $1.38W$, indicating a peak efficiency of 16%. The major contributor to this poor efficiency is a result of the Firgelli motor using a sliding lead screw for linear motion, which typically have poor efficiencies of less than 30% as indicated in Fig. 5.7. This combined with a typical efficiency for a DC motor of this size of about 80% and gearhead efficiency of about 90% explain the total 16% efficiency of the Firgelli motor. To improve upon this, we decided to use a ball screw for conversion between rotational and linear motion. Ball screws can have efficiencies of about 90%, as indicated by Fig. 5.7, with the tradeoff that ballscrews are more expensive than sliding leadscrews.

Bowden cable efficiency was measured on a newly designed cable constructed for this orthosis which is smaller in diameter than that used in the actuation unit of Section 3.2. The need to support cable compression necessitates the larger Bowden cable housing in that design. Here, we use a $1.5mm$ steel bike brake cable inside a Teflon cable housing with $2mm$ inner diameter and $3.2mm$ outer diameter. Lithium grease (No. 620-AA, Lubriplate Lubricants, Newark, NJ), a general purpose lubricant, was used to reduce friction within the housing. Two grease caps were attached at either end of the housing to prevent the loss of lubricant over time. Using two
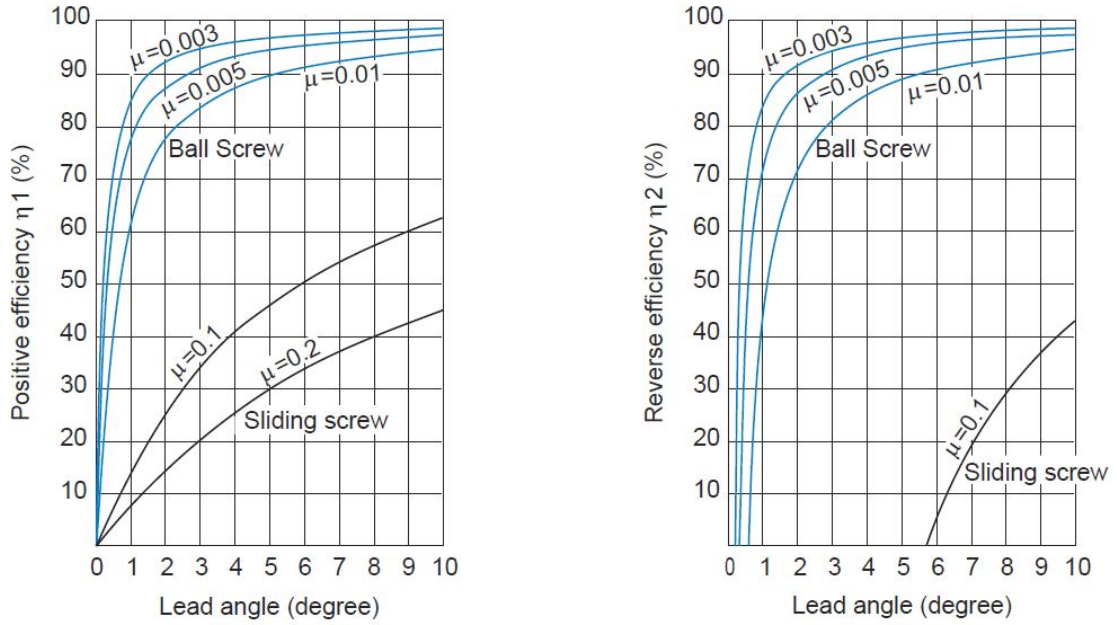
Figure 5.7: Approximate efficiencies of ball screw and sliding lead screw linear motion devices.Reproduced from THK CO., LTD, available: `tech.thk.com/en/products/pdf/en_b15_006.pdf`

$25lbs$ load cells (LSB200, Futek Advanced Sensor Technology Inc.), we measured the efficiency of the constructed cable under static loading up to an input of $20lbs$ with the cable housing bent 180°. The results of this test are shown in Fig. 5.8 and indicate the Bowden cable to be 70% efficient.

Combining ballscrew and Bowden cable losses, a transmission efficiency of 63% was assumed for the orthosis. Using this efficiency, the $1s$ quintic joint profile, and the average torque profiles of the TBI subjects in Section 4.4 we calculated the power needed from a motor to extend each subject's finger. The results are shown in Fig. 5.9. Peak power of around $4W$ is seen for each subject. The highest power is needed during the tests where subjects were asked to attempt volitional extension of their
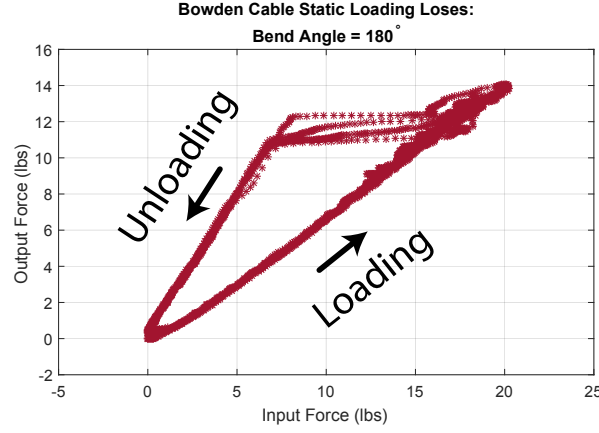
Figure 5.8: Efficiency of constructed pull-type Bowden cable. A hysteresis loop is evident between loading and unloading due to the friction in the cable.

fingers. Subjects 2 and 3 both required less than $1W$ peak power when relaxed while subject 1 required about $2.5W$. We chose to design to the higher power, $4-5W$, condition as input from the assisting clinician during the study suggested the resistance experienced while they were attempting volitional extension was more representative of what would be experienced during daily activities than the relaxed and resting condition.

This power calculation lead us to choose a DC motor rated for $3W$ of continuous mechanical power output (DCX14L EB SL 6V, Maxon Precision Motors, inc., Sachseln, Switzerland). Design guidelines provided by the motor manufacturer, Maxon, suggest that over-driving the motors by up to 2 times their power rating for several seconds is permissible within normal operation. The rated torque for the motor is $6.23mNm$, again with permissible intermittent over-driving of up to 2 times the nominal rating. We paired this motor to a high-efficiency ballscrew. The driving torque, τ, required to obtain a thrust force, F_a, on a ball screw with lead, Ph, and efficiency
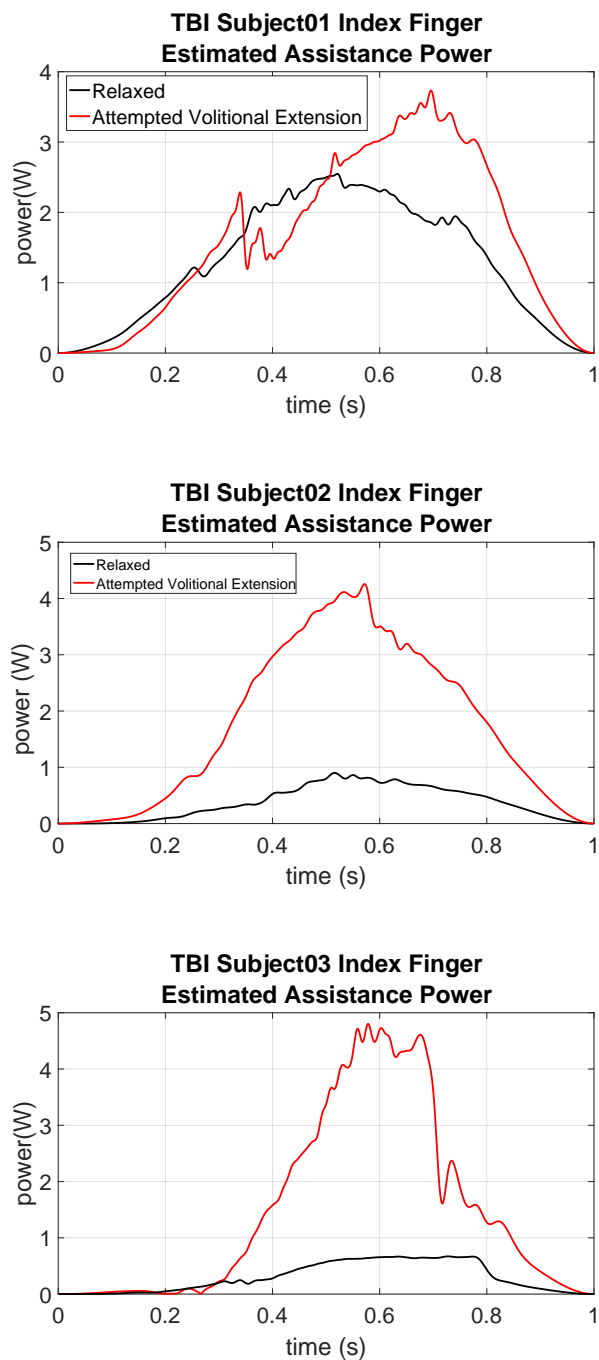
Figure 5.9: Motor power required to assist extension of the index fingers of TBI patients. The power is estimated using the average torque profiles found in Fig. 4.41 and an assumed 1s extension of both joints.

η is given by Eq. 5.2 [153]. Given the rated torque of the motor, the required $37N$ of tension needed at the fingers, the 70% Bowden cable efficiency, and an assumed efficiency of 90% for the ballscrew, a pitch of $0.67mm$ would provide the needed cable tension. Based on this, we selected a $6mm$ diameter ballscrew with a $1mm$ pitch (MTF-0601, THK) which when over-driven with a torque 1.5 times the motor rating, will provide the necessary maximum cable tension. As maximum cable tension is anticipated for only short intermittent periods, this over-driving is acceptable as per the manufacturer.

$$\tau = \frac{F_a l}{2\pi\eta} \tag{5.2}$$

Finally, the linear motion of the leadscrew is supported by a linear slide (ML 5 carriage and LWL 5 R120 B track, IKO International, Inc.) which connects to the cable and ballscrew nut via a custom made aluminum coupler. Thrust bearings and radial bearings support the end of the ballscrew where it is paired to the motor via a small spur gear. The construction of the linear actuator assembly is shown in Fig. 5.10.

5.3   Actuation Unit System Design

A refinement of the system architecture used for the remote-actuation unit presented in Section 3.2.1 was implemented for a new actuation unit for the cable-actuated
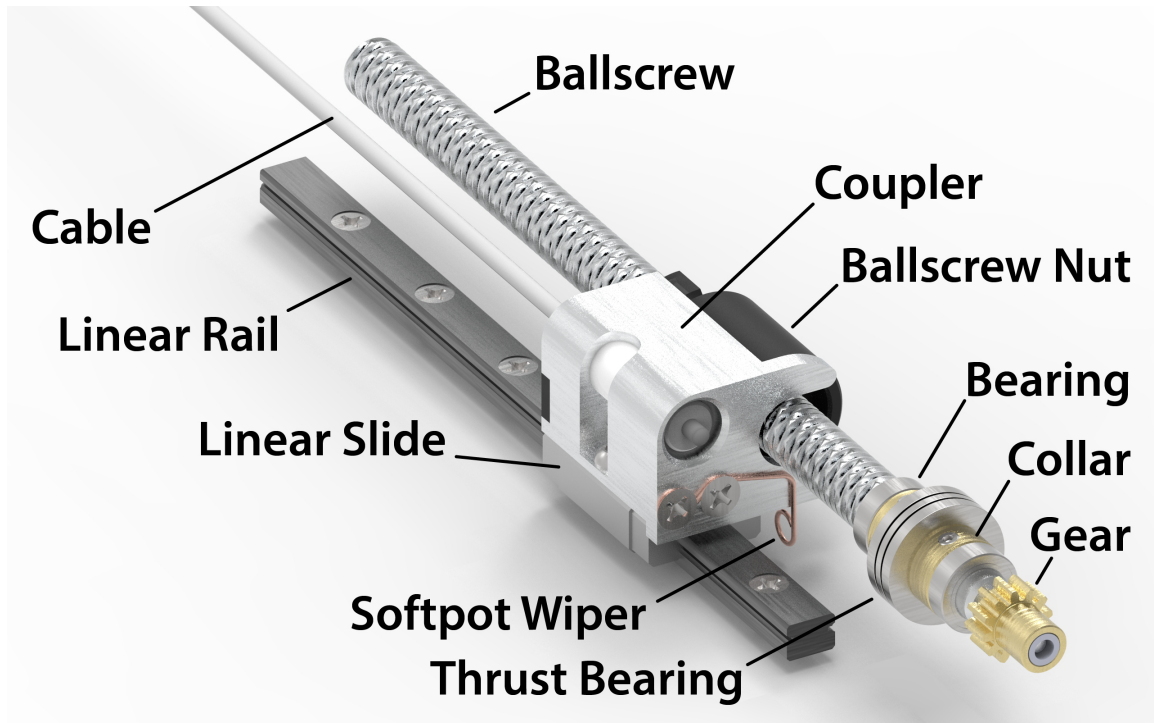
Figure 5.10: Ballscrew-based linear actuator designed for providing cable tension to an orthosis for extension against moderate to severe increases in muscle tone.

extension orthosis. A central microcontroller sets the voltage output of 4 motor drivers based on readings from analog sensors and user input provided wirelessly from a computer or tablet. An updated microcontroller, motor drivers, and the addition of EMG electrodes differentiates this design from the one presented in Section 3.2.1.

Improvements were made to the user interface for controlling and communicating with the actuation unit. Streaming of all 10 sensor inputs at an update rate of $50Hz$ was included to allow for monitoring device operation and RMS filtered EMG signals. The user is able to select between two control modes for the orthosis, either direct control of the motor position via slide bars on the UI or via the EMG sensors. The user is able to specify thresholds for the EMG controller which are sent to the orthosis

Figure 5.11: System architecture of the orthosis for aiding finger extension. A similar architecture is used to the one employed for the sliding spring exoskeleton used in Section 3.2. The dashed lines indicate features which the central processor is compatible with, but were not implemented on the extension orthosis.

either by wired or wireless serial communication. All data from the UI is recorded and saved along with a session log for error tracking. The User interface is shown in Fig. 5.12.

5.3.1 Control Board Design

The commercial microcontroller development board used in Section 3.2 was chosen for its simplicity, support, and ease of programming. It was not, however, an energy efficient, computationally powerful, or efficiently packaged solution. To rectify these issues, an improved implementation of the central actuation unit controller was developed for this orthosis. A more capable ARM Cortex-M3 32bit microcontroller (ATSAM3X8EA, Microchip Technology, Chandler, Arizona) was used in place

Figure 5.12: System architecture of the orthosis for aiding finger extension. A similar architecture is used to the one employed for the sliding spring exoskeleton used in Section 3.2.

of the 8bit Atmega processor of the previous implementation. The processor was chosen because of its low power consumption and adequate number of serial ports, PWM channels, analog inputs, and digital I/O for the application. The processor is also used a in popular development board, the Arduino Due, meaning it is well documented and supported. This microcontroller was incorporated into a single custom circuit board containing the motor drivers (DRV8834RGER, Texas Instruments, Dallas, TX), wireless communication (XB24CZ7PIS-004, Digi International, Minnetonka, MN), wired communication (FT232RQ, Future Technology Devices International (FTDI), Glasgow, UK), and analog inputs detailed in Fig. 5.11. The microcontroller is programmed to run at a fixed control loop period of $2ms$ which is maintained using an interrupt. The bottleneck of the control loop is the wireless

communication module, which requires a $400\mu s$ delay between bytes sent to it. The controller is programmed to send one 3 byte packet per loop execution. Each packet contains data and for a single analog channel along with a start byte and an identification of the analog channel number. The constructed circuit board is shown in Fig. 5.13. A flow chart of the main control loop implemented for the prototype is shown in Fig. 5.14.
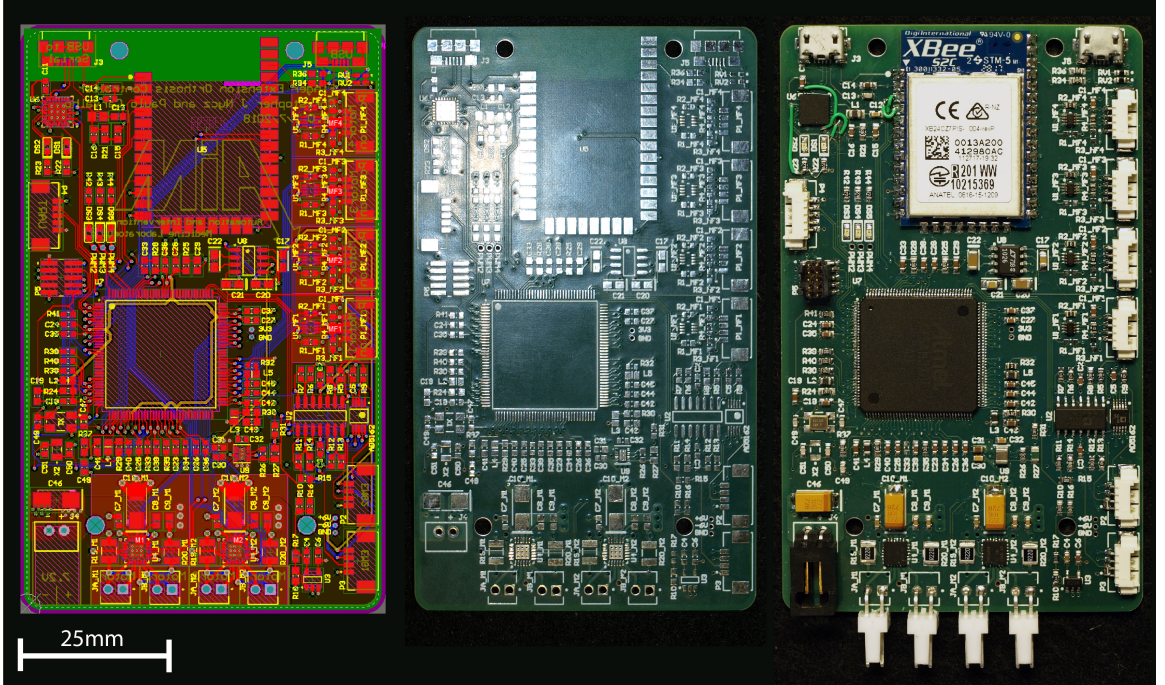
Figure 5.13: Constructed extension orthosis control board. (Left) PCB layout, (Center) printed circuit board, (Right) populated circuit board.

5.3.2 EMG Electrodes

The inclusion of electromyography, **EMG**, electrodes is common among prosthetic and orthotic devices as a way for the user to interface with, and provide input to, the
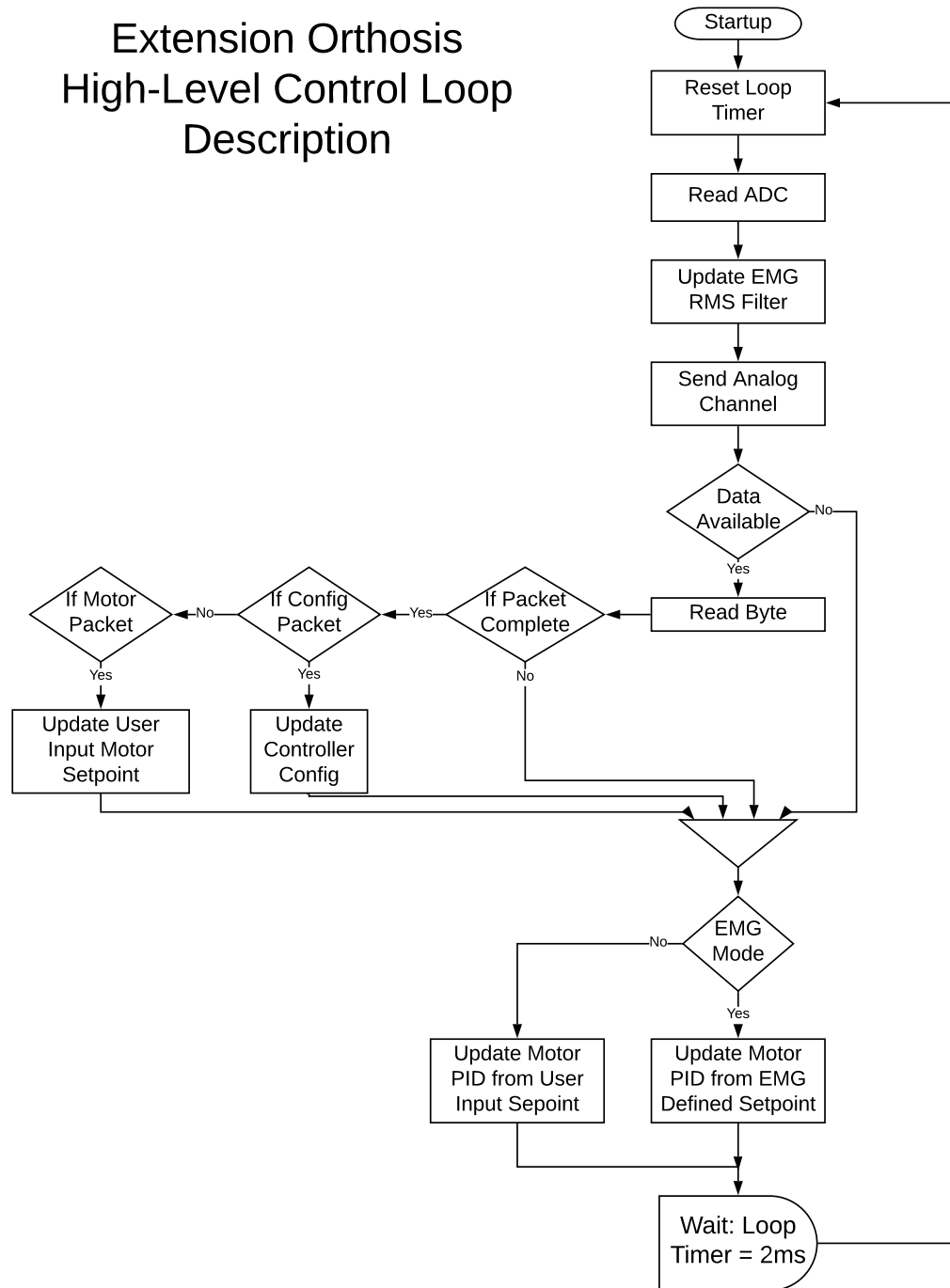
Figure 5.14: High level control loop description for a cable-based extension orthosis.

device controllers. Inclusion of EMG sensors for this specific application was done on the recommendation of clinicians who posited that requiring the user to exercise their extensors in order to operate the device could aid in re-learning, adding a therapeutic quality to the assistive device.

Suitable EMG electrodes for this application were not readily available. Commercial options exist mostly as either low quality hobby amplifiers requiring single use Ag/AgCl electrodes, such as the MyoWare^{TM} from Advancer^{TM} Technologies and the EMG sensor from Bitalino^{TM}, or as part of high end laboratory instrumentation, such as those offered by Delsys^{TM}, Inc. A reusable dry electrode, similar to the Delsys^{TM} DE-2.1 sensor, is desirable for device applications due to their ease of use.

The EMG signal is typically of frequency $25hz$ to a few kilohertz and of magnitude $.1mV$ to $90mV$ [154]. Active electrodes, those in which amplification occurs at the electrode itself, typically precondition the signal with a bandpass filter and amplification. A passband with a high pass cutoff of 10-20hz and low pass cutoff of 200-500hz is typical [155] and is what is used by the Delsys^{TM} DE-2.1 sensor. For our application, a passband from 15-480hz was designed for. A differential gain of 200 was selected from within a recommended range of 10-2000 [155] due to it being high enough to prevent signal loss during transmission but low enough to avoid saturating in most conditions. The implemented a sensor, based on the design of Clancy [155], is briefly described here.

The pre-amp stage shown in Fig. 5.15 acts as a high pass filter with a capacitor
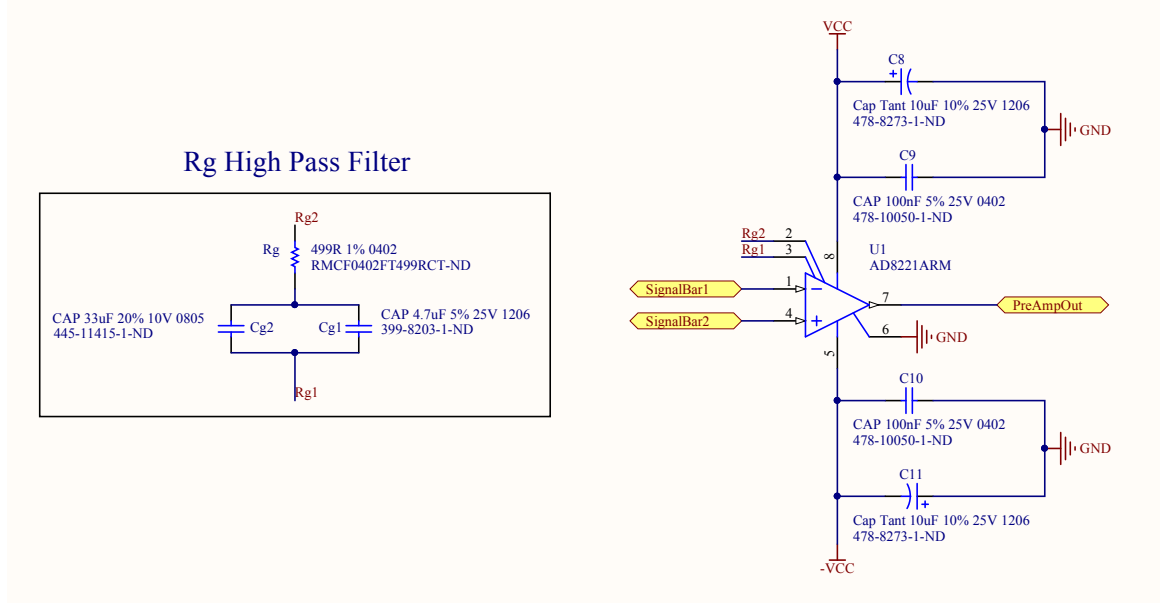
Figure 5.15: Pre-amp stage of the EMG electrode. This stage provides initial high pass filtering and amplification of the differential signal picked up by the two electrodes.

placed in series with the gain resistor. This filter removes high-amplitude low frequency signals, such as those arising from motion artifact and any DC offset between the two electrodes, prior to amplification. The gain of the pre-amp is described by Eq. 5.3.

$$G_{pa}(s) = \frac{(49400 + R_g)(C_{g1}C_{g2})s + 1}{(C_{g1} + C_{g2})R_g s + 1} \tag{5.3}$$

The active high pass filter shown in Fig. 5.16 is a typical second order filter with the transfer function of Eq. 5.4. Similarly, the active low pass filter shown in Fig. 5.16 is a typical second order filter with transfer function of Eq. 5.5. The output of the active filters is AC-coupled to the senor output using the passive high pass filter described by Eq. 5.6. The transfer function of the complete EMG electrode is the
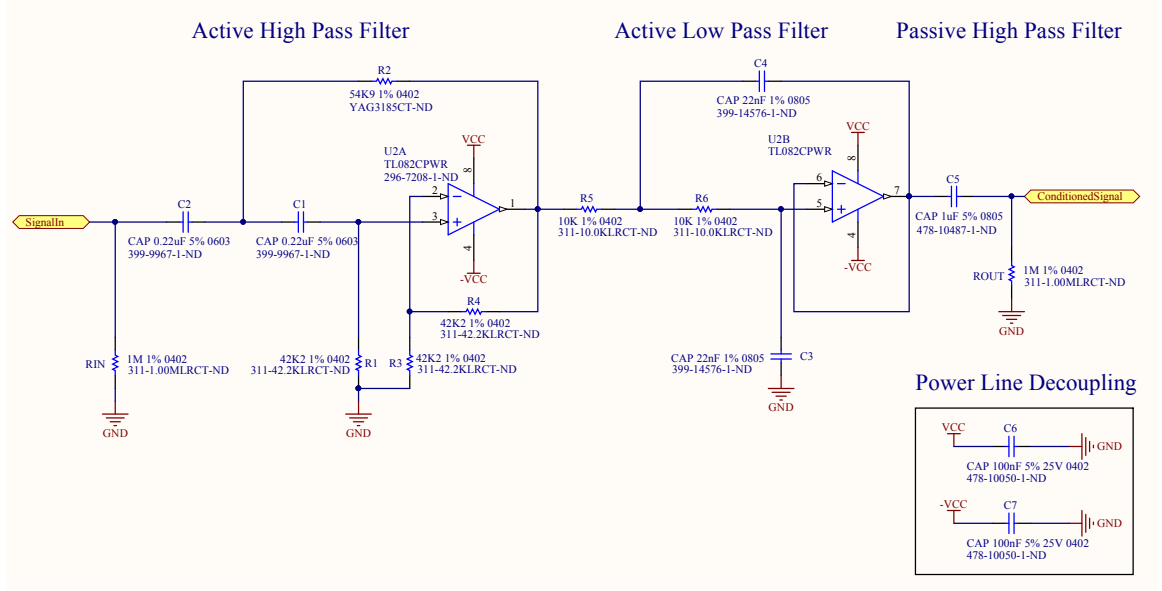
Figure 5.16: Signal conditioning of the EMG electrode. The output of the pre-amp stage is passed through active high and low pass filters before being ac-coupled to the sensor output through a passive high pass filter.

product of the component transfer functions, as given by in Eq. 5.7

$$G_{ahp}(s) = \frac{(R_3 + R4)R_1 R_2 C_1 C_2 s^2}{R_1 R_2 R_3 C_1 C_2 s^2 + (R_1 R_3 C_1 - (R_3 + R_4)R_1 C_1 + R_2 C_1 + R_2 C_2)s + R_3}$$

(5.4)

$$G_{alp}(s) = \frac{1}{R_5 R_6 C_3 C_4 s^2 + (R_5 + R_6)C_3 s + 1}$$

(5.5)

$$G_{php}(s) = \frac{R_{OUT}C_5 s}{R_{OUT}C_5 s - 1}$$

(5.6)

$$G_{EMG}(s) = G_{pa}G_{ahp}G_{alp}G_{php}$$

(5.7)

Physical components were chosen with narrow tolerance bands to improve electrode-to-electrode repeatability. All resistors were readily available in 0402 package size

(a) Designed Performance

(b) Measured Performance
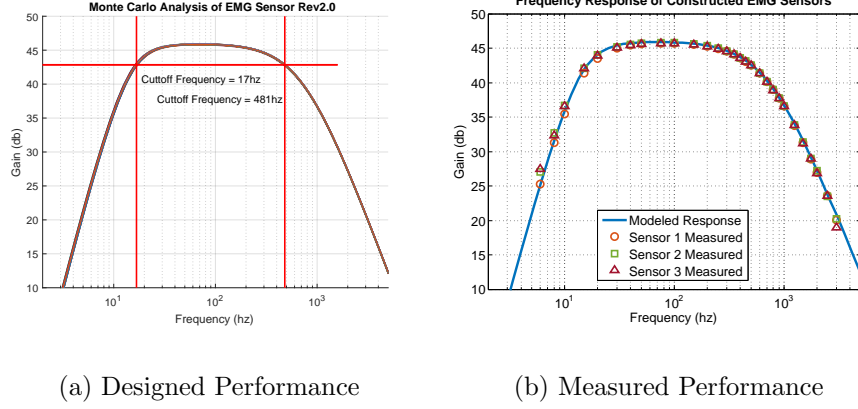
Figure 5.17: Monte Carlo analysis of the electrode with specified components (a) and the measured performance of 3 constructed electrodes (b). A bandpass nominally from 17-480hz and 46db gain is achieved.

with $\pm 1\%$ tolerances. Surface mount ceramic capacitors were mostly available with $\pm 5\%$ tolerances, but in larger package sizes. The chosen components are labeled in Fig. 5.16 and Fig. 5.15. A 1000 iteration Monte Carlo analysis was performed with the selected components, assuming components were normally distributed about their nominal value with tolerance bands covering $\pm 3\sigma$. The results of the analysis are shown in Fig. 5.3.2 which show little expected deviation of the constructed electrodes from the nominal response.

Three electrodes were constructed, as shown in Fig. 5.18 with one intended for initial testing and two intended for the final exoskeleton. The frequency response of each electrode was measured using a National Instruments cRIO-9074. Each electrode was powered with $\pm 12V$ and it's sensor inputs connected to a 16-bit analog output card (NI-9264, National Instruments). An 80mV peak-to-peak sine wave was swept
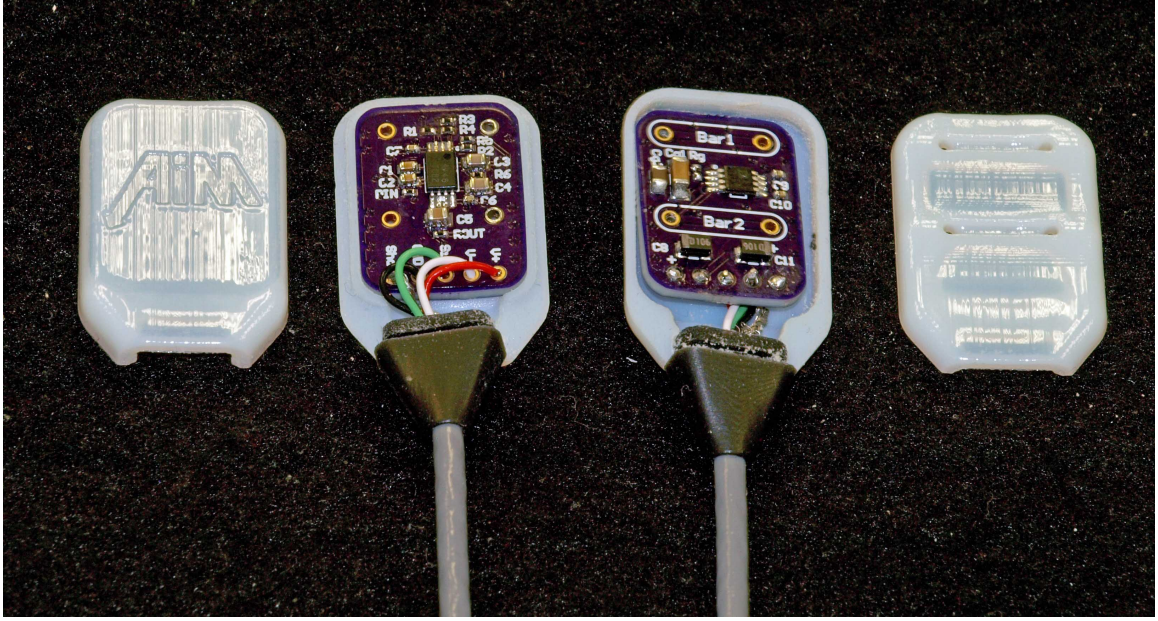
Figure 5.18: Two assembled EMG electrodes showing the two sides of assembled circuit board and plastic casing. The skin facing side of the casing (right) and outward facing side of the casing (left) have been removed to show the circuit board assembly. The casings are sealed together using a quick-set epoxy.

from 6hz-2khz and the electrode's output read using a 12-bit analog input card (NI-9201, National Instruments) sampled at 20khz. For each frequency, 10,000 samples were acquired. In Matlab, the periods of each frequency were separated, overlaid, and averaged. The peak-to-peak output signal was calculated at each frequency and divided by the input signal magnitude to attain the gain. The results of the hardware tests for the 3 sensors are shown in Fig. 5.3.2 and indicate little variation between the constructed sensors.

Using the constructed electrodes we implement a simple EMG processing algorithm based on applying thresholds to windowed average values of the rectified signals from electrodes placed on the flexor digitorum profundus ($\boldsymbol{FDP}$) and extensor digi-
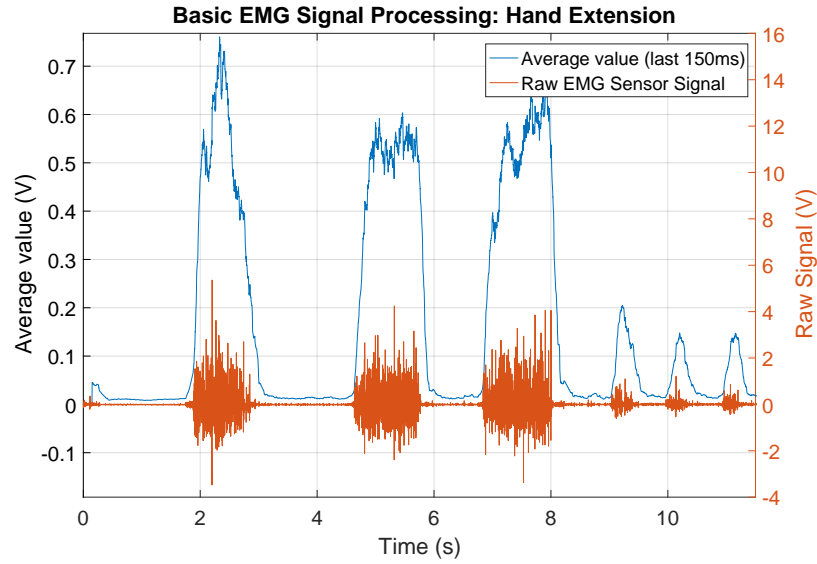
Figure 5.19: EMG RMS filter performance on an able-bodied subject with constructed sensors. Three maximal contractions of the extensor digitorum communis are followed by three un-resisted extensions.

torum communis ($\textbf{EDC}$) muscles [155, 156]. On the microcontroller, the windowed average is implemented with a circular buffer. On each execution of the control loop, the oldest value in the buffer is subtracted from the EMG average value, the newest sample is added to the EMG average value, and the newest sample is placed into the buffer at the index of the oldest value. An example of the raw EMG signal for the EDC, as measured with the constructed electrodes, and its corresponding average value are shown in Fig. 5.19. In the user interface, the operator can specify if they wish to control the motors from the EMG signals, and specify the thresholds associated with flexion and extension of the orthosis. If EMG control is specified, and if the average value of the EMG window for flexion is above its threshold, then the position setpoints for all motors increment a specified amount each execution of the
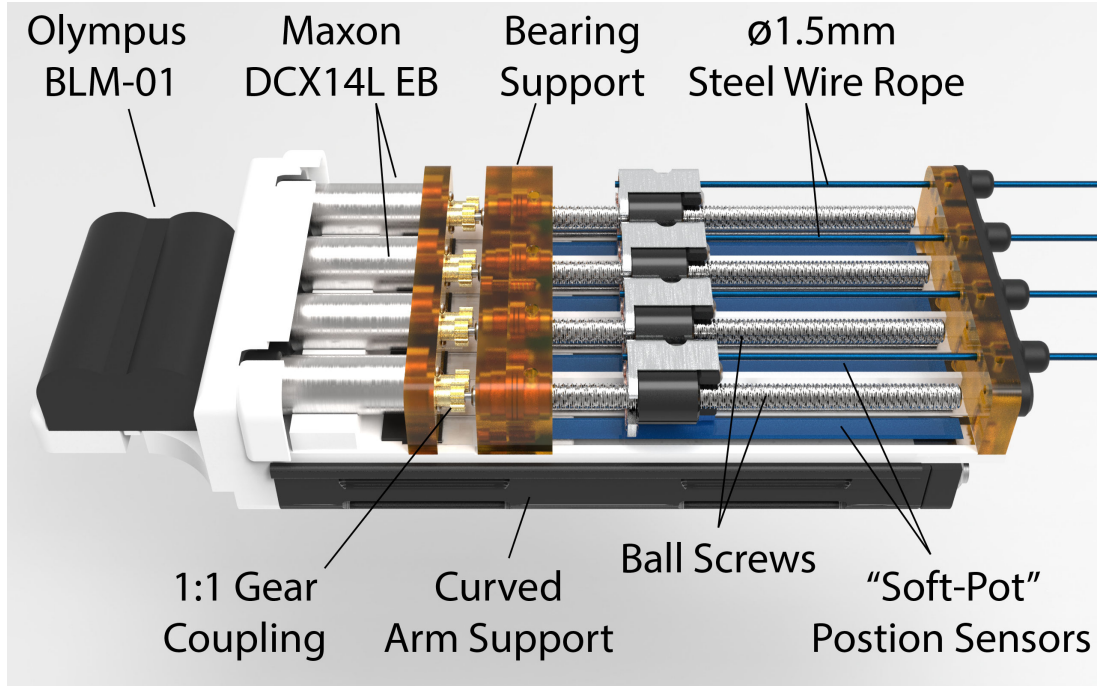
Figure 5.20: Annotated render of the revised actuation unit.

control loop. Conversely, if the average value of the EMG window for extension is above its threshold, then the position setpoints for all motors decrement a specified amount each execution of the control loop.

5.4 Actuation Unit Implementation

As opposed to the back-pack design of the actuation unit presented in Section 4, the updated actuation unit was designed to strap to the upper arm. This was made possible by the improved packaging of the electronics, allowing for the control board to be mounted on top of the actuators as opposed to a separate electronics box. Mounting on the upper arm reduces the amount of bending that the Bowden cables
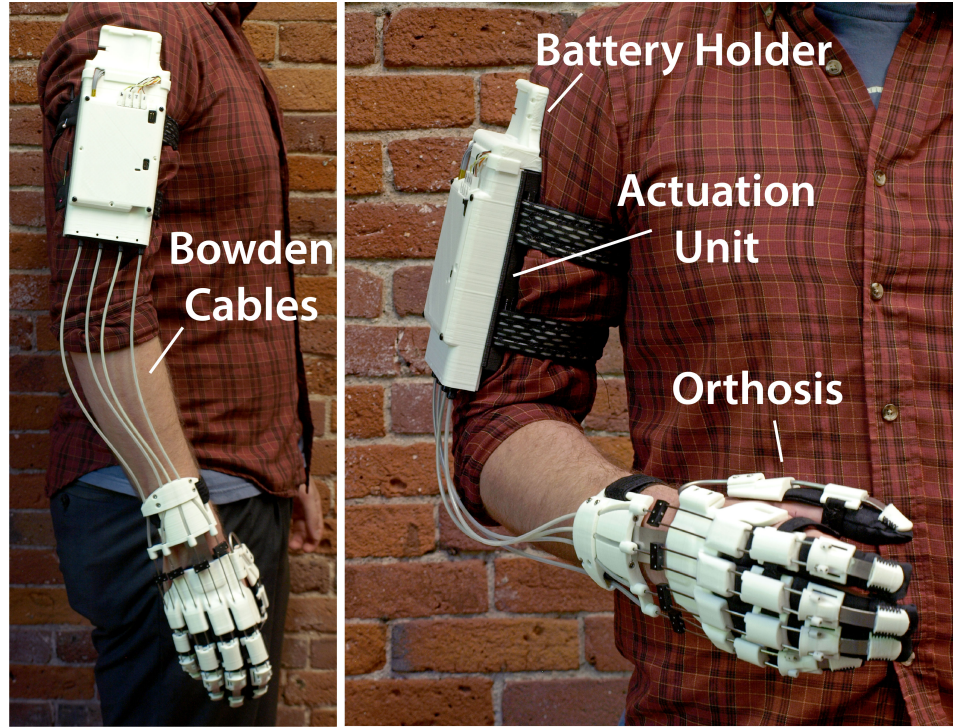
Figure 5.21: A user wearing the constructed orthosis with exposed actuation unit internals.

are subjected to, increasing efficiency. Mounting on the upper arm, as opposed to the back, also prevents interference when sitting back in a chair. The trade-off is that the shoulder must now bear the weight of the actuation unit. The packaging of the actuators within the actuation unit is shown in Fig. 5.20. The constructed actuation unit being worn by a user is shown in Fig. 5.21.

5.5 Extension Orthosis Phantom Testing

To test the performance of the extension orthosis, we constructed the hand phantom shown in Fig. 5.22. The phantom is constructed using the CT scans and motion
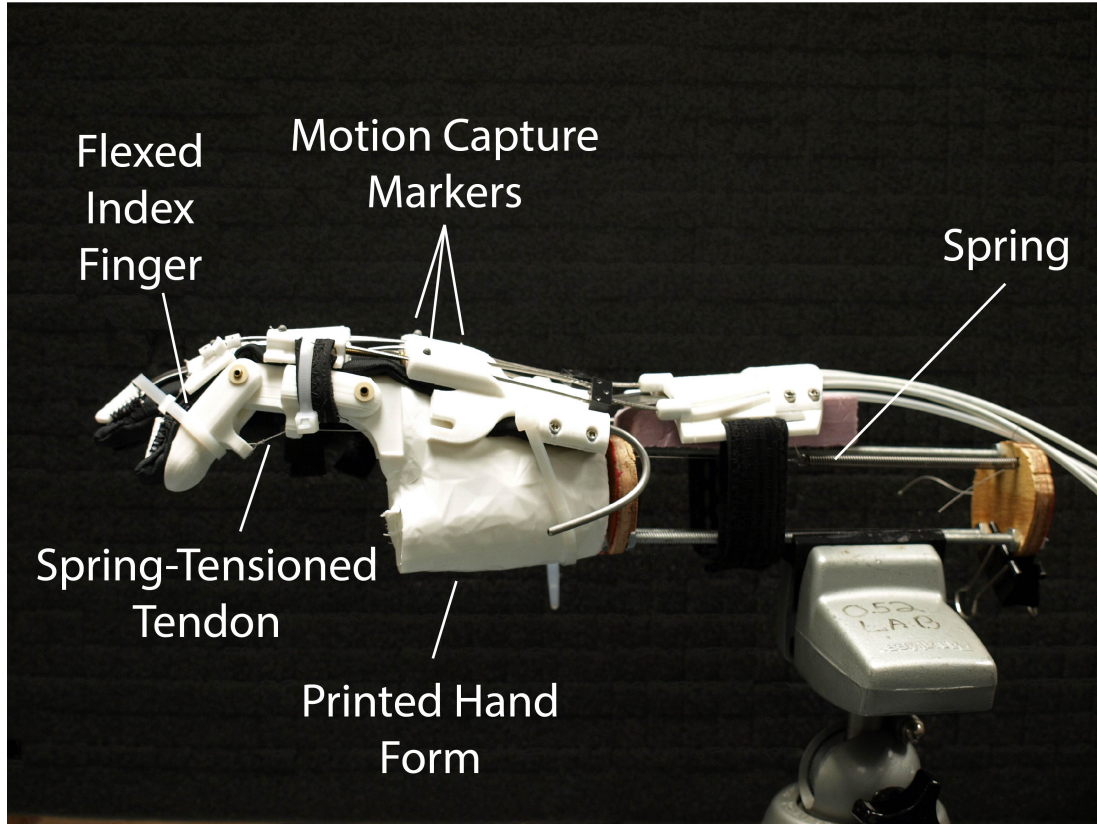
Figure 5.22: Testing setup used for validating an extension orthosis. A hand phantom containing an index finger spring-tensioned into flexion is fit with the orthosis. Motion capture is used to track the joint movement as the actuation unit extends the finger against the spring resistance.

capture data of an average-sized male subject from the study in Section 4.2. The palm of the hand is 3D printed from a segmentation of the CT images. An articulating index finger is 3D printed with the PIP and MCP joints positioned and oriented as indicated by the motion capture data for that subject. A single tendon, tensioned by a $320\frac{N}{m}$ spring, is included to flex the PIP and MCP joints, mimicking muscle tone in the flexor digitorum profundus. The tendon passes through guides $17mm$ below the joint axes. Using Eqs. 3.2-3.5, we calculated that extending the finger would stretch the spring $52mm$ providing $15.6N$ of tension. We included an additional $10mm$ of
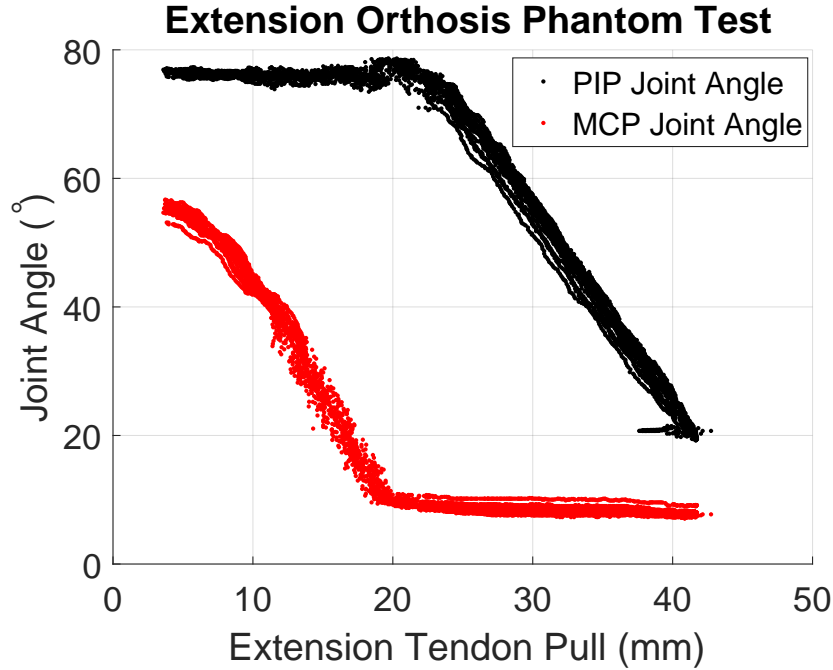
Figure 5.23: Motion of index finger phantom extended by repeatedly by a cable-actuated extension orthosis. The MCP joint is extended first followed by the PIP joint. The extension cable is pulled by $42mm$ to fully extend the finger.

pre-tension in the spring equating to a total maximum tension of $18.8N$. Assuming frictional losses of 70% through the cable guides, as has been shown to be typical of our Bowden cables, this setup will resist with approximately $0.5Nm$ of torque at the MCP and PIP joints. This resistance is similar to what was seen with the TBI subjects of Section 4.4.

We tested the ability of the orthosis to repeatedly extend the index finger of the constructed phantom from a fully flexed position. Each pull was programmed to take about $2s$ to complete. Using the optical tracking setup described in Chapter 4, we measured the motion of the PIP and MCP joints during the extensions. Using the setup shown in Fig. 5.22, we extended the phantom finger 15 times. The resulting

measured motions of the MCP and PIP joints are reported in Fig. 5.23. The results show that, for a fixed resistance, the orthosis provides a consistent extension of the finger. The MCP joint is extended first, followed by the PIP joint, with neither hyper-extending as was seen with the entirely soft glove of Section 3.1.

5.6   Discussion and Conclusions

This chapter detailed the process taken to design an orthosis for aiding finger extension against moderate to severe increases in muscle tone. Measurements taken in Chapter 4 were applied to directly calculate the mechanical power that needed to be provided by the motors to assist finger extension. Focusing on the power required to move the fingers is important for assisting extension of individuals suffering from UMN as their fingers need to be moved through a resistance. This is in contrast to assisting grasp in a weak or flaccid hand where a static application of force is required only after the hand comes into contact with an object. In this case motor torque, not power, is the critical design parameter.

We also presented a complete prototype of the designed orthosis and demonstrated it's ability to extend a finger phantom which mimicked a hand with flexor muscle tone. The constructed prototype will serve as a useful research platform for future studies regarding the assistance of individuals with UMN. Although intended as a research platform, the prototype was designed so as not to be far removed from what could be

considered a practical product. The entire device is wearable, battery powered, and packaged to be a reasonable size and weight. With further refinement, such a device has the potential to be a useful assistive aid during daily activities for individuals with UMN.

CHAPTER **6**

Conclusions and Future Work

"Today I walked down a street I

used to wander..."

John Prine

The work presented in this thesis explored the use of portable robotic hand orthoses for assisting individuals with hand impairments associated with the upper motor neuron syndrome (***UMN***). Our early experience with devices indicated a need for better characterization of design criteria in order to improve upon their performance. In particular, we could qualitatively observe deficits in the extension performance of a tendon-actuated glove and the flexion performance of a sliding spring orthosis, however, we could not quantify to what extent nor could we model the expected behavior of a hand wearing such a device with much confidence. We therefore presented a method for measuring the torques about the finger joints of subjects using optical

motion capture methods. We used this developed process to measure grasping torques during activities of daily living, and extension torques required to assist individuals suffering from UMN. We then applied what was learned extending the fingers of UMN patients to the design of a new orthosis for finger extension. This work has provided generalizable insight into the assistance of impaired hand function as well as design aspects of various orthosis concepts.

6.1 Summary of Work and Contributions

The contributions of this work are in providing an understanding of the design process related to assistive hand orthoses. We accomplished this through application experience in the development of several hand orthoses with vastly different design concepts, through the study of the forces needed grasp objects during activities of daily living, and through the study of forces needed to extend the fingers of impaired individuals against increases in muscle tone. Our work with many different devices has led us to be able to directly compare the relative merits of each. This work also provided the experience necessary to design biomechanic studies which specifically adressed gaps in published data needed for optimization of orthosis designs. We approached these studies in a manner which was generic, which did not incorporate the use of a specific orthosis or tailor the measurements to any one particular design concept. In focusing on studies of what an orthosis should do, as opposed to studies which evalu-

ate a particular orthosis, we believe we've provided a more general understanding of orthosis design. Regardless of actuator type or mechanical design, the measurements made during the conducted studies on grasping and assisting finger extension are of relevance to orthotic engineers working to assist finger motion.

6.2 Impact

The development of methods to assist impaired hand function is a valuable pursuit as they have the potential to impact well over a million people in the United States. However, powered hand orthoses have reached very few individuals who would benefit from their use. While this work may not provide a direct solution to the problem, the lessons learned and the designs presented will help contribute to improvements in the function and design of these devices. The measurements made during our studies will allow engineers to be more targeted in their selection of components and their design of the devices. Improving the function and reducing the size of these devices will lead to their greater use and greater benefit to those who need them.

6.3 Future Work

While this work presented an improved understanding of orthosis performance and design criteria, it exposed many other questions along the way. The final device is by no-means a perfect and complete solutions. Here we list potential directions of future

research which we believe will benefit

- **Clinical Testing on Diverse UMN Population**

  While we presented studies conducted on TBI patients and the development of devices to meet the criteria derived from these studies, we stopped short of testing these devices on a disabled population. Future work should conduct rigorous evaluation of these orthoses on a diverse population of individuals with hand impairments. The work should seek to quantify the ability to assist impaired individuals, identify the types of impairments best treated by specific orthosis designs, and evaluate the potential for a long term rehabilitative benefit in using the devices.

- **Modification of the Extension Orthosis to Provide Flexion as Well**

  While extension was the focus of the work performed in Chapter 5, both flexion and extension are likely needed for a device to be useful to a larger population of people. Accomplishing this with minor modification to the orthosis presented in Chapter 5 may in fact be possible. The semi-rigid cables used in the orthosis will support a certain amount of compression and in testing the device it was noticed that pushing against these cables would support a moderate amount of flexion assistance. More rigorous design and evaluation, applying the grasping measurements made in Chapter 4, should be conducted in future work to modify the design to be capable of clinically relevant flexion assistance.

- **Advanced User Interfaces**

  User interfaces were not discussed in great depth in this work, with implementations mostly simple prototypes focused on testing mechanical function and not deployable solutions. While EMG interfaces were implemented in Chapter 5 which were representative of EMG algorithms implemented by commercial devices such as Myomo's Myopro, it is expected that these algorithms will not perform well. Our testing with TBI patients indicated that an involuntary co-contraction of the flexor muscles occurred when subjects were asked to extend their hands, which would complicate the detection of desired extension. The work of Thielbar et al. found the use of EMG on stroke patients to be unreliable requiring addition of a voice command to switch between flex and extend modes [96]. Intuitive and simple to use solutions are currently lacking and would greatly benefit the abilities of hand orthoses.

- **Improved Ergonomics**

  A limiting factor to the design presented in Chapter 5 is the difficulty associated with donning and doffing the device. Since the orthoses need to apply substantial forces to the user, they must be well-secured. We accomplished this by including one strap per finger, a cup around each finger tip, a palm strap, and a wrist strap. The process of independently donning the device on can be cumbersome even for an able-bodied individual. Ergonomics are a diffi-

cult to address topic as objectively quantifying and modeling the performance of a design concept is difficult prior to user testing. Addressing the issues in research labs are further limited by the need to manufacture concepts, which typically require expertise in textiles work. Addressing these challenges and improving upon the ergonomics is a valuable area of future research as it will greatly improve the practicality of the orthoses.

References

[1] N. Norouzi-Gheidari, P. S. Archambault, and J. Fung, "Effects of robot-assisted therapy on stroke rehabilitation in upper limbs: systematic review and meta-analysis of the literature," *Journal of rehabilitation research and development*, vol. 49, no. 4, p. 479, 2012.

[2] J. M. Veerbeek, A. C. Langbroek-Amersfoort, E. E. H. van Wegen, C. G. M. Meskers, and G. Kwakkel, "Effects of robot-assisted therapy for the upper limb after stroke: A systematic review and meta-analysis," *Neurorehabilitation and Neural Repair*, vol. 31, no. 2, pp. 107–121, 2017, pMID: 27597165.

[3] H. T. Peters, S. J. Page, and A. Persch, "Giving them a hand: Wearing a myoelectric elbow-wrist-hand orthosis reduces upper extremity impairment in chronic stroke," *Archives of Physical Medicine and Rehabilitation*, vol. 98, no. 9, pp. 1821 – 1827, 2017.

[4] S. J. Page, V. Hill, and S. White, "Portable upper extremity robotics is as efficacious as upper extremity rehabilitative therapy: a randomized controlled pilot trial," *Clinical Rehabilitation*, vol. 27, no. 6, pp. 494–503, 2013, pMID: 23147552.

[5] H. C. Fischer, K. M. Triandafilou, K. O. Thielbar, J. M. Ochoa, E. D. C. Lazzaro, K. A. Pacholski, and D. G. Kamper, "Use of a portable assistive glove to facilitate rehabilitation in stroke survivors with severe hand impairment," *IEEE Transactions on Neural Systems and Rehabilitation Engineering*, vol. 24, no. 3, pp. 344–351, March 2016.

[6] P. Polygerinos, K. C. Galloway, E. Savage, M. Herman, K. O. Donnell, and C. J. Walsh, "Soft robotic glove for hand rehabilitation and task specific training,"

in *2015 IEEE International Conference on Robotics and Automation (ICRA)*, May 2015, pp. 2913–2919.

[7] P. Staubli, T. Nef, V. Klamroth-Marganska, and R. Riener, "Effects of intensive arm training with the rehabilitation robot ARMin II in chronic stroke patients: four single-cases," *Journal of neuroengineering and rehabilitation*, vol. 6, no. 1, p. 46, 2009.

[8] E. B. Brokaw, D. Nichols, R. J. Holley, and P. S. Lum, "Robotic therapy provides a stimulus for upper limb motor recovery after stroke that is complementary to and distinct from conventional therapy," *Neurorehabilitation and Neural Repair*, vol. 28, no. 4, pp. 367–376, 2014, pMID: 24297763.

[9] Y. Yun, S. Dancausse, P. Esmatloo, A. Serrato, C. A. Merring, P. Agarwal, and A. D. Deshpande, "Maestro: An EMG-driven assistive hand exoskeleton for spinal cord injury patients," in *2017 IEEE International Conference on Robotics and Automation (ICRA)*, May 2017, pp. 2904–2910.

[10] B. W. Gasser and M. Goldfarb, "Design and performance characterization of a hand orthosis prototype to aid activities of daily living in a post-stroke population," in *2015 37th Annual International Conference of the IEEE Engineering in Medicine and Biology Society (EMBC)*, Aug 2015, pp. 3877–3880.

[11] M. A. Delph, S. A. Fischer, P. W. Gauthier, C. H. M. Luna, E. A. Clancy, and G. S. Fischer, "A soft robotic exomusculature glove with integrated semg sensing for hand rehabilitation," in *2013 IEEE 13th International Conference on Rehabilitation Robotics (ICORR)*, June 2013, pp. 1–7.

[12] H. K. Yap, B. W. K. Ang, J. H. Lim, J. C. H. Goh, and C. H. Yeow, "A fabric-regulated soft robotic glove with user intent detection using emg and rfid for hand assistive application," in *2016 IEEE International Conference on Robotics and Automation (ICRA)*, May 2016, pp. 3537–3542.

[13] H. In, B. B. Kang, M. Sin, and K. J. Cho, "Exo-glove: A wearable robot for the hand with a soft tendon routing system," *IEEE Robotics Automation Magazine*, vol. 22, no. 1, pp. 97–105, March 2015.

REFERENCES

[14] D. Popov, I. Gaponov, and J. H. Ryu, "Portable exoskeleton glove with soft structure for hand assistance in activities of daily living," *IEEE/ASME Transactions on Mechatronics*, vol. 22, no. 2, pp. 865–875, April 2017.

[15] J. Arata, K. Ohmoto, R. Gassert, O. Lambercy, H. Fujimoto, and I. Wada, "A new hand exoskeleton device for rehabilitation using a three-layered sliding spring mechanism," in *2013 IEEE International Conference on Robotics and Automation*, May 2013, pp. 3902–3907.

[16] M. Cempini, M. Cortese, and N. Vitiello, "A powered finger-thumb wearable hand exoskeleton with self-aligning joint axes," *IEEE/ASME Transactions on Mechatronics*, vol. 20, no. 2, pp. 705–716, April 2015.

[17] P. Polygerinos, Z. Wang, K. C. Galloway, R. J. Wood, and C. J. Walsh, "Soft robotic glove for combined assistance and at-home rehabilitation," *Robotics and Autonomous Systems*, vol. 73, no. Supplement C, pp. 135 – 143, 2015, wearable Robotics.

[18] S. S. Yun, B. B. Kang, and K. J. Cho, "Exo-glove PM: An easily customizable modularized pneumatic assistive glove," *IEEE Robotics and Automation Letters*, vol. 2, no. 3, pp. 1725–1732, July 2017.

[19] P. Polygerinos, S. Lyne, Z. Wang, L. F. Nicolini, B. Mosadegh, G. M. Whitesides, and C. J. Walsh, "Towards a soft pneumatic glove for hand rehabilitation," in *2013 IEEE/RSJ International Conference on Intelligent Robots and Systems*, Nov 2013, pp. 1512–1517.

[20] T. Noritsugu, H. Yamamoto, D. Sasakil, and M. Takaiwa, "Wearable power assist device for hand grasping using pneumatic artificial rubber muscle," in *SICE 2004 Annual Conference*, vol. 1, Aug 2004, pp. 420–425 vol. 1.

[21] L. Saharan, A. Sharma, M. J. de Andrade, R. H. Baughman, and Y. Tadesse, "Design of a 3D printed lightweight orthotic device based on twisted and coiled polymer muscle: iGrab hand orthosis," in *Proc. SPIE 10164, Active and Passive Smart Structures and Integrated Systems*, 2017. [Online]. Available: http://dx.doi.org/10.1117/12.2260266

REFERENCES

[22] C. J. Nycz, M. A. Delph, and G. S. Fischer, "Modeling and design of a tendon actuated soft robotic exoskeleton for hemiparetic upper limb rehabilitation," in *2015 37th Annual International Conference of the IEEE Engineering in Medicine and Biology Society (EMBC)*, Aug 2015, pp. 3889–3892.

[23] C. J. Nycz, T. Btzer, O. Lambercy, J. Arata, G. S. Fischer, and R. Gassert, "Design and characterization of a lightweight and fully portable remote actuation system for use with a hand exoskeleton," *IEEE Robotics and Automation Letters*, vol. 1, no. 2, pp. 976–983, July 2016.

[24] C. B. Ivanhoe and T. A. Reistetter, "Spasticity: the misunderstood part of the upper motor neuron syndrome," *American journal of physical medicine & rehabilitation*, vol. 83, no. 10, pp. S3–S9, 2004.

[25] M. N. H., E. Alberto, and C. M. K., "Common patterns of clinical motor dysfunction," *Muscle & Nerve*, vol. 20, no. 6, pp. 21–35, 1997.

[26] D. G. Kamper, H. C. Fischer, E. G. Cruz, and W. Z. Rymer, "Weakness is the primary contributor to finger impairment in chronic stroke," *Archives of Physical Medicine and Rehabilitation*, vol. 87, no. 9, pp. 1262 – 1269, 2006.

[27] C. J. Nycz, T. B. Meier, P. Carvalho, G. Meier, and G. S. Fischer, "Design criteria for hand exoskeletons: Meaurement of forces needed to assis finger extension in traumatic brain injury patients," *IEEE Robotics and Automation Letters*, accepted June 2018.

[28] J. G. Colebatch and S. Gandevia, "The distribution of muscular weakness in upper motor neuron lesions affecting the arm," *Brain*, vol. 112, no. 3, pp. 749–763, 1989.

[29] H. K. Graham and P. Selber, "Musculoskeletal aspects of cerebral palsy," *Bone & Joint Journal*, vol. 85-B, no. 2, pp. 157–166, 2003.

[30] B. Dellon and Y. Matsuoka, "Prosthetics, exoskeletons, and rehabilitation [Grand Challenges of Robotics]," *IEEE Robotics Automation Magazine*, vol. 14, no. 1, pp. 30–34, March 2007.

[31] H. M. Van der Loos, D. J. Reinkensmeyer, and E. Guglielmelli, *Rehabilitation and Health Care Robotics*. Springer International Publishing, 2016, pp. 1685–1728. [Online]. Available: https://doi.org/10.1007/978-3-319-32552-1_64

[32] E. J. Koeneman, R. S. Schultz, S. L. Wolf, D. E. Herring, and J. B. Koeneman, "A pneumatic muscle hand therapy device," in *The 26th Annual International Conference of the IEEE Engineering in Medicine and Biology Society*, vol. 1, Sept 2004, pp. 2711–2713.

[33] N. S. K. Ho, K. Y. Tong, X. L. Hu, K. L. Fung, X. J. Wei, W. Rong, and E. A. Susanto, "An emg-driven exoskeleton hand robotic training device on chronic stroke subjects: Task training system for stroke rehabilitation," in *2011 IEEE International Conference on Rehabilitation Robotics*, June 2011, pp. 1–5.

[34] M. F. Rotella, K. E. Reuther, C. L. Hofmann, E. B. Hage, and B. F. BuSha, "An orthotic hand-assistive exoskeleton for actuated pinch and grasp," in *2009 IEEE 35th Annual Northeast Bioengineering Conference*, April 2009, pp. 1–2.

[35] A. M. Dollar and H. Herr, "Lower extremity exoskeletons and active orthoses: Challenges and state-of-the-art," *IEEE Transactions on Robotics*, vol. 24, no. 1, pp. 144–158, Feb 2008.

[36] T. Yan, M. Cempini, C. M. Oddo, and N. Vitiello, "Review of assistive strategies in powered lower-limb orthoses and exoskeletons," *Robotics and Autonomous Systems*, vol. 64, no. Supplement C, pp. 120 – 136, 2015.

[37] S. L. Colby and J. M. Ortman, "Projections of the size and composition of the US population: 2014 to 2060," *Current Population Reports*, no. P25-1143, 2014.

[38] E. J. Benjamin *et al.*, "Heart disease and stroke statistics—2017 update: A report from the American Heart Association," *Circulation*, vol. 135, no. 10, pp. e146–e603, 2017.

[39] C. R, S. S, B. A, and et al, "Trends in incidence, lifetime risk, severity, and 30-day mortality of stroke over the past 50 years," *JAMA*, vol. 296, no. 24, pp. 2939–2946, 2006.

REFERENCES

[40] R. Bonita and R. Beaglehole, "Recovery of motor function after stroke." *Stroke*, vol. 19, no. 12, pp. 1497–1500, 1988.

[41] E. S. Lawrence *et al.*, "Estimates of the prevalence of acute stroke impairments and disability in a multiethnic population," *Stroke*, vol. 32, no. 6, pp. 1279–1284, 2001.

[42] M. M. Adams and A. L. Hicks, "Spasticity after spinal cord injury," *Spinal cord*, vol. 43, no. 10, p. 577, 2005.

[43] C. Cans, J. D. la Cruz, and M.-A. Mermet, "Epidemiology of cerebral palsy," *Paediatrics and Child Health*, vol. 18, no. 9, pp. 393 – 398, 2008.

[44] C. L. Arneson *et al.*, "Prevalence of cerebral palsy: autism and developmental disabilities monitoring network, three sites, United States, 2004," *Disability and health journal*, vol. 2, no. 1, pp. 45–48, 2009.

[45] J. A. Langlois, W. Rutland-Brown, and M. M. Wald, "The epidemiology and impact of traumatic brain injury: a brief overview," *The Journal of head trauma rehabilitation*, vol. 21, no. 5, pp. 375–378, 2006.

[46] D. J. Thurman, C. Alverson, K. A. Dunn, J. Guerrero, and J. E. Sniezek, "Traumatic brain injury in the United States: a public health perspective," *The Journal of head trauma rehabilitation*, vol. 14, no. 6, pp. 602–615, 1999.

[47] J. D. Cassidy *et al.*, "Incidence, risk factors and prevention of mild traumatic brain injury: results of the WHO Collaborating Centre Task Force on Mild Traumatic Brain Injury," *Journal of rehabilitation medicine*, vol. 36, no. 0, pp. 28–60, 2004.

[48] A. W. Selassie, E. Zaloshnja, J. A. Langlois, T. Miller, P. Jones, and C. Steiner, "Incidence of long-term disability following traumatic brain injury hospitalization, United States, 2003," *The Journal of head trauma rehabilitation*, vol. 23, no. 2, pp. 123–131, 2008.

[49] E. Zaloshnja, T. Miller, J. A. Langlois, and A. W. Selassie, "Prevalence of long-term disability from traumatic brain injury in the civilian population of the

United States, 2005," *The Journal of head trauma rehabilitation*, vol. 23, no. 6, pp. 394–400, 2008.

[50] W. C. Walker and T. C. Pickett, "Motor impairment after severe traumatic brain injury: A longitudinal multicenter study," *Journal of Rehabilitation Research and Development*, vol. 44, no. 7, pp. 975–82, 2007.

[51] M. M. Goldenberg, "Multiple sclerosis review," *Pharmacy and Therapeutics*, vol. 37, no. 3, p. 175, 2012.

[52] P. Dilokthornsakul, R. J. Valuck, K. V. Nair, J. R. Corboy, R. R. Allen, and J. D. Campbell, "Multiple sclerosis prevalence in the United States commercially insured population," *Neurology*, vol. 86, no. 11, pp. 1014–1021, 2016.

[53] I. Kister *et al.*, "Natural history of multiple sclerosis symptoms," *International Journal of MS Care*, vol. 15, no. 3, pp. 146–156, 2013.

[54] S. L. Foad, C. T. Mehlman, and J. Ying, "The epidemiology of neonatal brachial plexus palsy in the United States," *The Journal of Bone & Joint Surgery*, vol. 90, no. 6, pp. 1258–1264, 2008.

[55] S. K. Doumouchtsis and S. Arulkumaran, "Are all brachial plexus injuries caused by shoulder dystocia?" *Obstetrical & gynecological survey*, vol. 64, no. 9, pp. 615–623, 2009.

[56] S. P. Chauhan, S. B. Blackwell, and C. V. Ananth, "Neonatal brachial plexus palsy: Incidence, prevalence, and temporal trends," *Seminars in Perinatology*, vol. 38, no. 4, pp. 210 – 218, 2014.

[57] A. O. Narakas, "The treatment of brachial plexus injuries," *International Orthopaedics*, vol. 9, no. 1, pp. 29–36, Jun 1985.

[58] N. Smania *et al.*, "Rehabilitation of brachial plexus injuries in adults and children," *European journal of physical and rehabilitation medicine*, vol. 48, no. 3, p. 483506, September 2012.

[59] J. Rankine, "Adult traumatic brachial plexus injury," *Clinical Radiology*, vol. 59, no. 9, pp. 767 – 774, 2004.

[60] M. Arner, A.-C. Eliasson, S. Nicklasson, K. Sommerstein, and G. Hgglund, "Hand function in cerebral palsy. Report of 367 children in a population-based longitudinal health care program," *The Journal of Hand Surgery*, vol. 33, no. 8, pp. 1337 – 1347, 2008.

[61] R. T Katz and W. Rymer, "Spastic hypertonia: Mechanisms and measurement," in *Archives of physical medicine and rehabilitation*, vol. 70, pp. 144–55, 03 1989.

[62] S. A. Sahrmann and B. J. Norton, "The relationship of voluntary movement to spasticity in the upper motor neuron syndrome," *Annals of Neurology*, vol. 2, no. 6, pp. 460–465, 1977.

[63] G. Sheean, "The pathophysiology of spasticity," *European Journal of Neurology*, vol. 9, pp. 3–9, 2002.

[64] S. Jacob, C. Francone, and W. Lossow, *Structure and function in man*. Philidelphia, PA: W.B. Saunders Company, 1978.

[65] (2017) Hypertonia information page. [Online]. Available: https://www.ninds. nih.gov/Disorders/All-Disorders/Hypertonia-Information-Page

[66] T. D. Sanger, M. R. Delgado, D. Gaebler-Spira, M. Hallett, and J. W. Mink, "Classification and definition of disorders causing hypertonia in childhood," *Pediatrics*, vol. 111, no. 1, pp. e89–e97, 2003.

[67] J. A. Beres-Jones, T. D. Johnson, and S. J. Harkema, "Clonus after human spinal cord injury cannot be attributed solely to recurrent muscle-tendon stretch," *Experimental Brain Research*, vol. 149, no. 2, pp. 222–236, Mar 2003.

[68] P. Brown, "Pathophysiology of spasticity." *Journal of neurology, neurosurgery, and psychiatry*, vol. 57, no. 7, p. 773, 1994.

[69] E. Lundstrm, A. Ternt, and J. Borg, "Prevalence of disabling spasticity 1 year after first-ever stroke," *European Journal of Neurology*, vol. 15, no. 6, pp. 533–539, 2008.

[70] C. L. Watkins, M. J. Leathley, J. M. Gregson, A. P. Moore, T. L. Smith, and A. K. Sharma, "Prevalence of spasticity post stroke," *Clinical Rehabilitation*, vol. 16, no. 5, pp. 515–522, 2002, pMID: 12194622.

[71] D. K. Sommerfeld, E. U.-B. Eek, A.-K. Svensson, L. W. Holmqvist, and M. H. von Arbin, "Spasticity after stroke," *Stroke*, vol. 35, no. 1, pp. 134–139, 2004.

[72] N. J. O'Dwyer, L. Ada, and P. D. Neilson, "Spasticity and muscle contracture following stroke," *Brain*, vol. 119, no. 5, pp. 1737–1749, 1996.

[73] R. J. Greenwood, T. M. McMillan, M. P. Barnes, and C. D. Ward, *Handbook of neurological rehabilitation*. Psychology Press, 2005, ch. 47, pp. 663–694.

[74] J. L. Giuffre, S. Kakar, A. T. Bishop, R. J. Spinner, and A. Y. Shin, "Current concepts of the treatment of adult brachial plexus injuries," *Journal of Hand Surgery*, vol. 35, no. 4, pp. 678–688, 2010.

[75] R. W. Evans, *Neurology and trauma*. Oxford University Press, 2006.

[76] D. J. Gladstone, C. J. Danells, and S. E. Black, "The fugl-meyer assessment of motor recovery after stroke: A critical review of its measurement properties," *Neurorehabilitation and Neural Repair*, vol. 16, no. 3, pp. 232–240, 2002.

[77] J.-H. Lin, M.-J. Hsu, C.-F. Sheu, T.-S. Wu, R.-T. Lin, C.-H. Chen, and C.-L. Hsieh, "Psychometric comparisons of 4 measures for assessing upper-extremity function in people with stroke," *Physical Therapy*, vol. 89, no. 8, pp. 840–850, 2009.

[78] S. J. Page, G. D. Fulk, and P. Boyne, "Clinically important differences for the upper-extremity Fugl-Meyer scale in people with minimal to moderate impairment due to chronic stroke," *Physical Therapy*, vol. 92, no. 6, pp. 791–798, 2012.

[79] S. L. Wolf, P. A. Catlin, M. Ellis, A. L. Archer, B. Morgan, and A. Piacentino, "Assessing wolf motor function test as outcome measure for research in patients after stroke," *Stroke*, vol. 32, no. 7, pp. 1635–1639, 2001.

[80] C. E. Lang, D. F. Edwards, R. L. Birkenmeier, and A. W. Dromerick, "Estimating minimal clinically important differences of upper-extremity measures early after stroke," *Archives of Physical Medicine and Rehabilitation*, vol. 89, no. 9, pp. 1693 – 1700, 2008.

[81] R. W. Bohannon and M. B. Smith, "Interrater reliability of a modified ashworth scale of muscle spasticity," *Physical Therapy*, vol. 67, no. 2, pp. 206–207, 1987.

[82] C. Collin, D. T. Wade, S. Davies, and V. Horne, "The barthel adl index: A reliability study," *International Disability Studies*, vol. 10, no. 2, pp. 61–63, 1988, pMID: 3403500.

[83] K. J. Ottenbacher, Y. Hsu, C. V. Granger, and R. C. Fiedler, "The reliability of the functional independence measure: a quantitative review," *Archives of physical medicine and rehabilitation*, vol. 77, no. 12, pp. 1226–1232, 1996.

[84] P. W. Duncan, D. Wallace, S. M. Lai, D. Johnson, S. Embretson, and L. J. Laster, "The stroke impact scale version 2.0," *Stroke*, vol. 30, no. 10, pp. 2131–2140, 1999.

[85] N. Hogan, H. I. Krebs, J. Charnnarong, P. Srikrishna, and A. Sharon, "MIT-MANUS: a workstation for manual therapy and training. I," in *[1992] Proceedings IEEE International Workshop on Robot and Human Communication*, Sep 1992, pp. 161–165.

[86] H. I. Krebs *et al.*, "Rehabilitation robotics: pilot trial of a spatial extension for MIT-MANUS," *Journal of NeuroEngineering and Rehabilitation*, vol. 1, no. 1, p. 5, Oct 2004.

[87] S. E. Fasoli, H. I. Krebs, J. Stein, W. R. Frontera, and N. Hogan, "Effects of robotic therapy on motor impairment and recovery in chronic stroke," *Archives of physical medicine and rehabilitation*, vol. 84, no. 4, pp. 477–482, 2003.

[88] B. T. Volpe, D. Lynch, A. Rykman-Berland, M. Ferraro, M. Galgano, N. Hogan, and H. I. Krebs, "Intensive sensorimotor arm training mediated by therapist or robot improves hemiparesis in patients with chronic stroke,"

Neurorehabilitation and Neural Repair, vol. 22, no. 3, pp. 305–310, 2008, pMID: 18184932.

[89] A. C. Lo *et al.*, "Robot-assisted therapy for long-term upper-limb impairment after stroke," *New England Journal of Medicine*, vol. 362, no. 19, pp. 1772–1783, 2010, pMID: 20400552.

[90] P. S. Lum, C. G. Burgar, M. Van der Loos, P. C. Shor, M. Majmundar, and R. Yap, "Mime robotic device for upper-limb neurorehabilitation in subacute stroke subjects: A follow-up study," *Journal of rehabilitation research & development*, vol. 43, no. 5, pp. 631–643, 2006.

[91] G. Rosati, P. Gallina, and S. Masiero, "Design, implementation and clinical tests of a wire-based robot for neurorehabilitation," *IEEE Transactions on Neural Systems and Rehabilitation Engineering*, vol. 15, no. 4, pp. 560–569, Dec 2007.

[92] S. Masiero, M. Armani, G. Ferlini, G. Rosati, and A. Rossi, "Randomized trial of a robotic assistive device for the upper extremity during early inpatient stroke rehabilitation," *Neurorehabilitation and Neural Repair*, vol. 28, no. 4, pp. 377–386, 2014, pMID: 24316679.

[93] L. Dovat, O. Lambercy, R. Gassert, T. Maeder, T. Milner, T. C. Leong, and E. Burdet, "Handcare: A cable-actuated rehabilitation system to train hand function after stroke," *IEEE Transactions on Neural Systems and Rehabilitation Engineering*, vol. 16, no. 6, pp. 582–591, Dec 2008.

[94] O. Lambercy, L. Dovat, H. Yun, S. K. Wee, C. W. Kuah, K. S. Chua, R. Gassert, T. E. Milner, C. L. Teo, and E. Burdet, "Effects of a robot-assisted training of grasp and pronation/supination in chronic stroke: a pilot study," *Journal of NeuroEngineering and Rehabilitation*, vol. 8, no. 1, p. 63, Nov 2011.

[95] M. Mihelj, T. Nef, and R. Riener, "ARMin II - 7 DoF rehabilitation robot: mechanics and kinematics," in *Proceedings 2007 IEEE International Conference on Robotics and Automation*, April 2007, pp. 4120–4125.

[96] K. O. Thielbar, K. M. Triandafilou, H. C. Fischer, J. M. OToole, M. L. Corrigan, J. M. Ochoa, M. E. Stoykov, and D. G. Kamper, "Benefits of using a voice

and emg-driven actuated glove to support occupational therapy for stroke survivors," *IEEE Transactions on Neural Systems and Rehabilitation Engineering*, vol. 25, no. 3, pp. 297–305, March 2017.

[97] E. B. Brokaw, I. Black, R. J. Holley, and P. S. Lum, "Hand spring operated movement enhancer (handsome): A portable, passive hand exoskeleton for stroke rehabilitation," *IEEE Transactions on Neural Systems and Rehabilitation Engineering*, vol. 19, no. 4, pp. 391–399, Aug 2011.

[98] B. B. Kang, H. Lee, H. In, U. Jeong, J. Chung, and K. J. Cho, "Development of a polymer-based tendon-driven wearable robotic hand," in *2016 IEEE International Conference on Robotics and Automation (ICRA)*, May 2016, pp. 3750–3755.

[99] Myopro 2 general FAQs. [Online]. Available: http://myomo.com/wp-content/uploads/2017/11/MyoPro-2-General-FAQs-PN25239-Rev7.pdf

[100] B. W. Gasser, D. A. Bennett, C. M. Durrough, and M. Goldfarb, "Design and preliminary assessment of vanderbilt hand exoskeleton," in *2017 International Conference on Rehabilitation Robotics (ICORR)*, July 2017, pp. 1537–1542.

[101] A. Chiri, F. Giovacchini, N. Vitiello, E. Cattin, S. Roccella, F. Vecchi, and M. C. Carrozza, "Handexos: Towards an exoskeleton device for the rehabilitation of the hand," in *2009 IEEE/RSJ International Conference on Intelligent Robots and Systems*, Oct 2009, pp. 1106–1111.

[102] F. Zhang, L. Hua, Y. Fu, H. Chen, and S. Wang, "Design and development of a hand exoskeleton for rehabilitation of hand injuries," *Mechanism and Machine Theory*, vol. 73, pp. 103 – 116, 2014.

[103] I. Filip, M. A. D., S. R. F., C. Xin, and W. G. M., "Soft robotics for chemists," *Angewandte Chemie International Edition*, vol. 50, no. 8, pp. 1890–1895, 2011.

[104] P. Panagiotis, C. Nikolaus, M. S. A., M. Bobak, O. C. D., P. Kirstin, C. Matteo, T. M. T., and S. R. F., "Soft robotics: Review of fluiddriven intrinsically soft devices; manufacturing, sensing, control, and applications in humanrobot interaction," *Advanced Engineering Materials*, vol. 19, no. 12, p. 1700016, May 2017.

[105] B. W. K. Ang and C. H. Yeow, "Print-it-yourself (piy) glove: A fully 3d printed soft robotic hand rehabilitative and assistive exoskeleton for stroke patients," in *2017 IEEE/RSJ International Conference on Intelligent Robots and Systems (IROS)*, Sept 2017, pp. 1219–1223.

[106] J. Maciejasz, Pawełand Eschweiler, K. Gerlach-Hahn, A. Jansen-Troy, and S. Leonhardt, "A survey on robotic devices for upper limb rehabilitation," *Journal of NeuroEngineering and Rehabilitation*, vol. 11, no. 1, p. 3, Jan 2014.

[107] P. Polygerinos, K. C. Galloway, S. Sanan, M. Herman, and C. J. Walsh, "Emg controlled soft robotic glove for assistance during activities of daily living," in *2015 IEEE International Conference on Rehabilitation Robotics (ICORR)*, Aug 2015, pp. 55–60.

[108] L. Randazzo, I. Iturrate, S. Perdikis, and J. d. R. Milln, "mano: A wearable hand exoskeleton for activities of daily living and neurorehabilitation," *IEEE Robotics and Automation Letters*, vol. 3, no. 1, pp. 500–507, Jan 2018.

[109] U. Jeong, H. In, H. Lee, B. B. Kang, and K. J. Cho, "Investigation on the control strategy of soft wearable robotic hand with slack enabling tendon actuator," in *2015 IEEE International Conference on Robotics and Automation (ICRA)*, May 2015, pp. 5004–5009.

[110] M. K. Burns, K. V. Orden, V. Patel, and R. Vinjamuri, "Towards a wearable hand exoskeleton with embedded synergies," in *2017 39th Annual International Conference of the IEEE Engineering in Medicine and Biology Society (EMBC)*, July 2017, pp. 213–216.

[111] D. D. Wilkinson, M. V. Weghe, and Y. Matsuoka, "An extensor mechanism for an anatomical robotic hand (icra)," in *2003 IEEE International Conference on Robotics and Automation*, vol. 1, Sept 2003, pp. 238–243 vol.1.

[112] M. V. Weghe, M. Rogers, M. Weissert, and Y. Matsuoka, "The ACT hand: design of the skeletal structure," in *Proceedings 2004 IEEE International Conference on Robotics and Automation (ICRA)*, vol. 4, April 2004, pp. 3375–3379 Vol.4.

[113] L. Y. Chang and Y. Matsuoka, "A kinematic thumb model for the ACT hand," in *Proceedings 2006 IEEE International Conference on Robotics and Automation (ICRA)*, May 2006, pp. 1000–1005.

[114] Z. Xu, E. Todorov, B. Dellon, and Y. Matsuoka, "Design and analysis of an artificial finger joint for anthropomorphic robotic hands," in *2011 IEEE International Conference on Robotics and Automation (ICRA)*, May 2011, pp. 5096–5102.

[115] A. D. Deshpande *et al.*, "Mechanisms of the anatomically correct testbed hand," *IEEE/ASME Transactions on Mechatronics*, vol. 18, no. 1, pp. 238–250, Feb 2013.

[116] Z. Xu, V. Kumar, Y. Matsuoka, and E. Todorov, "Design of an anthropomorphic robotic finger system with biomimetic artificial joints," in *2012 4th IEEE RAS EMBS International Conference on Biomedical Robotics and Biomechatronics (BioRob)*, June 2012, pp. 568–574.

[117] Z. Xu and E. Todorov, "Design of a highly biomimetic anthropomorphic robotic hand towards artificial limb regeneration," in *2016 IEEE International Conference on Robotics and Automation (ICRA)*, May 2016, pp. 3485–3492.

[118] S. J. Heithoff, L. H. Millender, and J. Helman, "Bowstringing as a complication of trigger finger release," *The Journal of Hand Surgery*, vol. 13, no. 4, pp. 567 – 570, 1988.

[119] H. In, H. Lee, U. Jeong, B. B. Kang, and K.-J. Cho, "Feasibility study of a slack enabling actuator for actuating tendon-driven soft wearable robot without pretension," in *2015 IEEE International Conference on Robotics and Automation (ICRA)*, May 2015, pp. 1229–1234.

[120] R. R., C. K. Andrews, M. W., and T. R.-D., "Deep pain thresholds in the distal limbs of healthy human subjects," *European Journal of Pain*, vol. 9, no. 1, pp. 39–48.

[121] J. D. Greenspan and S. L. B. McGillis, "Thresholds for the perception of pressure, sharpness, and mechanically evoked cutaneous pain: Effects of

laterality and repeated testing," *Somatosensory & Motor Research*, vol. 11, no. 4, pp. 311–317, 1994.

[122] A. Schiele, P. Letier, R. van der Linde, and F. van der Helm, "Bowden cable actuator for force-feedback exoskeletons," in *IEEE/RSJ International Conference on Intelligent Robots and Systems, 2006*.   IEEE, 2006, pp. 3599–3604.

[123] L. E. Carlson, B. D. Veatch, and D. D. Frey, "Efficiency of prosthetic cable and housing." *JPO: Journal of Prosthetics and Orthotics*, vol. 7, no. 3, pp. 96–99, 1995.

[124] K. Matheus and A. M. Dollar, "Benchmarking grasping and manipulation: Properties of the objects of daily living," in *2010 IEEE/RSJ International Conference on Intelligent Robots and Systems*, Oct 2010, pp. 5020–5027.

[125] S. L. Delp, F. C. Anderson, A. S. Arnold, P. Loan, A. Habib, C. T. John, E. Guendelman, and D. G. Thelen, "Opensim: Open-source software to create and analyze dynamic simulations of movement," *IEEE Transactions on Biomedical Engineering*, vol. 54, no. 11, pp. 1940–1950, Nov 2007.

[126] K. R. S. Holzbaur, W. M. Murray, and S. L. Delp, "A model of the upper extremity for simulating musculoskeletal surgery and analyzing neuromuscular control," *Annals of Biomedical Engineering*, vol. 33, no. 6, pp. 829–840, Jun 2005.

[127] K. Yamane and W. Takano, *Springer Handbook of Robotics*.   Springer International Publishing, 2016, ch. Human Motion Reconstruction, pp. 1819–1834. [Online]. Available: https://doi.org/10.1007/978-3-319-32552-1_68

[128] R. Nataraj and Z.-M. Li, "Robust identification of three-dimensional thumb and index finger kinematics with a minimal set of markers," *Journal of biomechanical engineering*, vol. 135, no. 9, p. 091002, 2013.

[129] L. Y. Chang* and N. S. Pollard, "Method for determining kinematic parameters of the in vivo thumb carpometacarpal joint," *IEEE Transactions on Biomedical Engineering*, vol. 55, no. 7, pp. 1897–1906, July 2008.

[130] F. L. Buczek, E. W. Sinsel, D. S. Gloekler, B. M. Wimer, C. M. Warren, and J. Z. Wu, "Kinematic performance of a six degree-of-freedom hand model (6dhand) for use in occupational biomechanics," *Journal of Biomechanics*, vol. 44, no. 9, pp. 1805 – 1809, 2011.

[131] P. Cerveri, N. Lopomo, A. Pedotti, and G. Ferrigno, "Derivation of centers and axes of rotation for wrist and fingers in a hand kinematic model: Methods and reliability results," *Annals of Biomedical Engineering*, vol. 33, no. 3, pp. 402–412, Jan 2005.

[132] L. Y. Chang and N. S. Pollard, "Constrained least-squares optimization for robust estimation of center of rotation," *Journal of Biomechanics*, vol. 40, no. 6, pp. 1392 – 1400, 2007.

[133] J. R. Cook, N. A. Baker, R. Cham, E. Hale, and M. S. Redfern, "Measurements of wrist and finger postures: A comparison of goniometric and motion capture techniques," *Journal of Applied Biomechanics*, vol. 23, no. 1, pp. 70–78, 2007.

[134] L.-C. Kuo, F.-C. Su, H.-Y. Chiu, and C.-Y. Yu, "Feasibility of using a video-based motion analysis system for measuring thumb kinematics," *Journal of Biomechanics*, vol. 35, no. 11, pp. 1499 – 1506, 2002.

[135] F. P. J. van der Hulst, S. Schtzle, C. Preusche, and A. Schiele, "A functional anatomy based kinematic human hand model with simple size adaptation," in *2012 IEEE International Conference on Robotics and Automation (ICRA)*, May 2012, pp. 5123–5129.

[136] G. Wu *et al.*, "ISB recommendation on definitions of joint coordinate systems of various joints for the reporting of human joint motion–Part II: shoulder, elbow, wrist and hand," *Journal of Biomechanics*, vol. 38, no. 5, pp. 981 – 992, 2005.

[137] A. Gustus, G. Stillfried, J. Visser, H. Jörntell, and P. van der Smagt, "Human hand modelling: kinematics, dynamics, applications," *Biological Cybernetics*, vol. 106, no. 11, pp. 741–755, Dec 2012.

[138] G. Stillfried, U. Hillenbrand, M. Settles, and P. van der Smagt, *The Human Hand as an Inspiration for Robot Hand Development.* Springer International

Publishing, 2014, ch. MRI-Based Skeletal Hand Movement Model, pp. 49–75. [Online]. Available: http://dx.doi.org/10.1007/978-3-319-03017-3_3

[139] A. Hollister, W. L. Buford, L. M. Myers, D. J. Giurintano, and A. Novick, "The axes of rotation of the thumb carpometacarpal joint," *Journal of Orthopaedic Research*, vol. 10, no. 3, pp. 454–460, 1992.

[140] S. S. H. U. Gamage and J. Lasenby, "New least squares solutions for estimating the average centre of rotation and the axis of rotation," *Journal of biomechanics*, vol. 35, no. 1, pp. 87–93, 2002.

[141] K. Halvorsen, M. Lesser, and A. Lundberg, "A new method for estimating the axis of rotation and the center of rotation," *Journal of Biomechanics*, vol. 32, no. 11, pp. 1221 – 1227, 1999.

[142] E. Y. Chao, *Biomechanics of the hand: a basic research study.* World Scientific, 1989.

[143] C. Pylatiuk, A. Kargov, S. Schulz, and L. Dderlein, "Distribution of grip force in three different functional prehension patterns," *Journal of Medical Engineering & Technology*, vol. 30, no. 3, pp. 176–182, 2006, pMID: 16772221.

[144] N. Smaby, M. E. Johanson, B. Baker, D. E. Kenney *et al.*, "Identification of key pinch forces required to complete functional tasks," *Journal of rehabilitation research and development*, vol. 41, no. 2, p. 215, 2004.

[145] M. S. Rice, C. Leonard, and M. Carter, "Grip strengths and required forces in accessing everyday containers in a normal population," *American Journal of Occupational Therapy*, vol. 52, no. 8, pp. 621–626, 1998.

[146] N. Fowler and A. Nicol, "Measurement of external three-dimensional interphalangeal loads applied during activities of daily living," *Clinical Biomechanics*, vol. 14, no. 9, pp. 646 – 652, 1999.

[147] R. S. Johansson and G. Westling, "Programmed and triggered actions to rapid load changes during precision grip," *Experimental Brain Research*, vol. 71, no. 1, pp. 72–86, Jun 1988.

[148] H. Forssberg, A. C. Eliasson, H. Kinoshita, R. S. Johansson, and G. Westling, "Development of human precision grip i: Basic coordination of force," *Experimental Brain Research*, vol. 85, no. 2, pp. 451–457, Jun 1991.

[149] R. S. Johansson, C. Häger, and R. Riso, "Somatosensory control of precision grip during unpredictable pulling loads," *Experimental Brain Research*, vol. 89, no. 1, pp. 192–203, Apr 1992.

[150] A.-C. Eliasson, H. Forssberg, K. Ikuta, I. Apel, G. Westling, and R. Johansson, "Development of human precision grip," *Experimental Brain Research*, vol. 106, no. 3, pp. 425–433, Jan 1995.

[151] J. C. B. Grant, *An atlas of anatomy: by regions...* Williams & Wilkins, 1962, vol. 1.

[152] J. Sancho-Bru, A. Prez-Gonzlez, M. Vergara-Monedero, and D. Giurintano, "A 3-d dynamic model of human finger for studying free movements," *Journal of Biomechanics*, vol. 34, no. 11, pp. 1491 – 1500, 2001.

[153] Features of the ball screw. [Online]. Available: https://tech.thk.com/en/products/pdf/en_b15_006.pdf

[154] J. Webster, *Medical instrumentation: application and design.* John Wiley & Sons, 2009, ch. 5, pp. 269–273.

[155] E. Clancy, E. Morin, and R. Merletti, "Sampling, noise-reduction and amplitude estimation issues in surface electromyography," *Journal of Electromyography and Kinesiology*, vol. 12, no. 1, pp. 1 – 16, 2002.

[156] V. T. Inman, H. Ralston, J. D. C. Saunders, M. B. Feinstein, and E. W. Wright, "Relation of human electromyogram to muscular tension," *Electroencephalography and Clinical Neurophysiology*, vol. 4, no. 2, pp. 187 – 194, 1952.